1-1-1972

Calorimetric Studies of Bulk Polymers.

Charles L. Beatty
University of Massachusetts Amherst

CALORIMETRIC STUDIES OF BULK POLYMERS

CHARLES L. BEATTY

CALORIMETRIC STUDIES OF BULK POLYMERS

A Dissertation Presented

by

Charles L. Beatty

Submitted to the Graduate School of the
University of Massachusetts in
partial fulfillment of the requirements for the degree of

DOCTOR OF PHILOSOPHY

August 1972

Major Subject Polymer Science and Engineering

CALORIMETRIC STUDIES OF BULK POLYMERS

A Dissertation

By

Charles L. Beatty

Approved as to style and content by:

(Chairman of Committee)

(Head of Department)

(Member)

(Member)

(Member)

August 1972

ACKNOWLEDGEMENTS

The author wishes to express his sincere appreciation to Professor Frank E. Karasz for his advice and guidance throughout the course of their association.

Special thanks are extended to Professors F. P. Price, R. S. Stein and R. S. Porter for their stimulating discussion and encouragement.

Special thanks are also extended to Judy M. Lewis for graciously typing this manuscript.

The generous financial support of this research by the Air Force Office of Scientific Research, the National Science Foundation and the Petroleum Research Fund is gratefully acknowledged.

DEDICATION

To my wonderful wife, whose patience and understanding as well as her assistance in data reduction and typing have been instrumental in the achievement of this attainment.

TABLE OF CONTENTS

Abstract		Page xiii
Introduction		Page xix
Chapter I	The Glass Transition of Linear Polyethylene	Page 1
Chapter II	Calorimetric Determination of the Sub-Glass Transition of Polycyclohexylmethacrylate	Page 40
Chapter III	Thermodynamic Classification of the Multiple Glass and Melting Transitions of Polydiethylsiloxane	Page 67
Chapter IV	Thermodynamic Properties of Poly ε Caprolactone	Page 88
Chapter V	Recommendations	Page 113
Chapter VI	Appendix	Page 118
	A. Operating Instructions for the High Precision Adiabatic Calorimeter	

LIST OF FIGURES

Abstract

Figure 1 - Heat Capacity of Polyethylenes of Various Degrees of Crystallinity — Page xiv

Figure 2 - Heat Capacity Difference Plot for the Glass Transition of Polyethylene — Page xiv

Figure 3 - Smectic Polypropylene Heat Capacity as a Function of Temperature and Transformation — Page xvi

Figure 4 - Low Temperature C_p Anomaly in Polycyclohexyl-methacrylate — Page xvi

Figure 5 - The Glass and Melting Transitions of Polydiethyl-siloxane — Page xvii

Figure 6 - The Heat Capacity of Poly-ε-caprolactone — Page xvii

Chapter I

Figure 1 - Small Angle Laser Light Scattering Pattern of Quenched Ultra-High Molecular Weight Linear Polyethylene — Page 8

Figure 2 - Schematic Diagram of Calorimeter Operation — Page 10

Figure 3 - The Low Temperature Heat Capacity of Linear Polyethylene of Low Crystallinity — Page 16

Figure 4 - Heat-Capacity Difference Plot — Page 18

Figure 5 - Polypropylene Data Obtained Immediately After the Polyethylene Measurements — Page 19

Figure 6 - The Heat Capacity of Three Crystallinities — Page 21

Figure 7 - Comparison of DSC and Adiabatic Calorimetrically Obtained Results for the 145°K Region — Page 24

Figure 8 - Heat Capacity Difference Plot Constructed by Linear Extrapolation of a Base Line from Below Tg — Page 27

Figure 9 - Variation of Encraty in the 240°K Region — Page 29

Figure 10 - Encraty of Quenched Eight Million Molecular Weight Linear Polyethylene for the 145°K Region — Page 30

Figure 11 - Heat Capacity Difference Plot Using the 80% Crystalline Curve for a Base Line — Page 31

Figure 12 - The Variation of Heat Capacity Difference at Tg With the Energy Required for Fusion — Page 33

Chapter II

Figure 1 - A Schematic Description of the Interconversion of the Chair Conformers — Page 43

Figure 2 - Heat Capacities of PCHMA and PMMA Via Adiabatic Calorimetry — Page 51

Figure 3 - Difference Cp Plot, Illustrating the Transition Breadth — Page 52

Figure 4 - Encraty of PCHMA and Various Tacticity PMMA's — Page 54

Figure 5 - Laue Photograph of PCHMA — Page 55

Figure 6 - Repeating Units of: a) Polycyclohexylmethacrylate and b) Polymethylmethacrylate — Page 57

Chapter III

Figure 1 - The Heat Capacity of Polydiethylsiloxane — Page 78

Figure 2 - The Variation of Low Temperature Peak With Crystallization and Annealing Conditions — Page 79

Figure 3 - X-ray Diffraction Scans of Polydiethylsiloxane at Two Temperatures Page 81

Chapter IV

Figure 1 - Overall Heat Capacity versus Temperature Results for Poly-ε-Caprolactone Page 97

Figure 2 - Heat Capacity Differences at Tg Due to Crystallinity Page 99

Figure 3 - Enthalpy versus Temperature Curve Page 100

Figure 4 - Entropy versus Temperature Page 101

Figure 5 - Wide-Angle X-ray Photograph of Poly-ε-caprolactone Page 102

Figure 6 - Encraty Differences at Tg Due to Different Crystallinities Page 109

Appendix

Figure A-1 - Schematic of Calorimeter and Heater Arrangement Page 123

Figure A-2 - Schematic Drawing of Apparatus for Extracting Sample from the Calorimeter Page 140

Figure A-3 - Schematic Drawing of Apparatus for Evacuating and Sealing Helium Inside the Calorimeter Page 144

Figure A-4 - Raw Data Sheet Used for Individual Runs Page 161

Figure A-5 - Schematic Description of Calorimeter Temperature Drift and Non-Adiabatic Conditions Page 166

Figure A-6 - First Page of Batch Program Listing for Sample Thermodynamic Computations Page 175

Figure A-7 - Second Page of Batch Program Listing for Sample Thermodynamic Computations Page 176

Figure A-8 - Third Page of Batch Program Listing for Sample Thermodynamic Computations Page 177

Figure A-9 - Listing of Batch Program Permanent, Semi-Permanent and Run Data — Page 179

Figure A-10 - Output of Permanent and Semi-Permanent Data and Aborted Run — Page 180

Figure A-11 - Output of the Summary of Thermodynamic Data for a Series of Individual Runs — Page 182

Figure A-12 - Time-Sharing Program for Sample Heat Capacity Calculation — Page 184

Figure A-13 - Time-Sharing Program for Sample Heat Capacity Calculation — Page 185

Figure A-14 - Time-Sharing Program for Sample Heat Capacity Calculation — Page 186

Figure A-15 - Permanent and CRT Output and Run Input of Time-Sharing Program — Page 187

Figure A-16 - Individual Run Printout and Summary Storage for Time-Sharing Program — Page 189

Figure A-17 Input, Output and Storage Operations via Time-Sharing — Page 191

Figure A-18 - Program for Filing Computed Output Summary — Page 192

Figure A-19 - Least Squares Orthogonal Polynomial Fitting Program — Page 194

Figure A-20 - Least Squares Orthogonal Polynomial Fitting Program — Page 195

Figure A-21 - Least Squares Orthogonal Polynomial Fitting Program — Page 196

Figure A-22 - Least Squares Orthogonal Polynomial Fitting Program — Page 197

Figure A-23 - Empty Calorimeter Calibration Coefficients Obtained From the Fitting Program — Page 198

Figure A-24 Comparison of Original and Simulated Empty Calorimeter Heat Capacities — Page 202

Figure A-25 - Sample Heat Capacity Punched Output as Input to Fitting Program and Extrapolation Temperatures Input — Page 204

Figure A-26 - Coefficients for These Powers of the Orthogonal Fitting Polynomial — Page 205

Figure A-27 - Simulation of Heat Capacities for Extrapolated Temperatures Using the Computed Coefficients for each Polynomial — Page 206

Figure A-28 - Comparison of Original and Heat Capacities Simulated by a Two Degree Polynomial — Page 207

Figure A-29 - Empty Calorimeter Calibration Program — Page 209

Figure A-30 - Empty Calorimeter Calibration Program — Page 210

Figure A-31 - Empty Calorimeter Calibration Program — Page 211

Figure A-32 - Individual Run Printout for Empty Calorimeter Calibration — Page 212

Figure A-33 - Empty Calorimeter Time-Sharing Program — Page 214

Figure A-34 - Empty Calorimeter Time-Sharing Program — Page 215

Figure A-35 - Empty Time-Sharing Program — Page 216

LIST OF TABLES

Chapter I

Table 1 - Heat Capacity, Temperature Data for Run 1 Page 12

Table 2 - Heat Capacity, Temperature Data for Run 2 Page 13

Table 3 - Heat Capacity, Temperature Data for Run 3 Page 14

Chapter II

Table 1 - Polycyclohexylmethacrylate Heat Capacity at Various Temperatures for the First Run Page 47

Table 2 - Polycyclohexylmethacrylate Heat Capacity at Various Temperatures for the Second Run Page 49

Chapter III

Table 1 - The Cooling, Annealing and Heating Rates for Series A, B and C Measurements Page 71

Table 2 - Heat Capacities Obtained for PDES for Series A Measurements Page 72

Table 3 - Heat Capacities Obtained for PDES for Series B Measurements Page 75

Table 4 - Heat Capacities Obtained for PDES for Series C Measurements Page 76

Chapter IV

Table 1 - Heat Capacities for Series A Measurements Page 91

Table 2 - Heat Capacities for Series B Measurements Page 94

Table 3 - Heat Capacities for Series C Measurements Page 95

Table 4 - Variation in Unit Cell Spacings with the Number and Size of Defects Page 104

Table 5 - Effect of Polymer Composition on Glass and Melting Transitions Page 107

ABSTRACT

CALORIMETRIC STUDIES OF BULK POLYMERS†

C. L. Beatty* and F. E. Karasz
Polymer Science and Engineering
University of Massachusetts
Amherst, Massachusetts 01002

Usė of thermodynamic data has been amongst the most reliable of tests for determining the nature of transitions for all materials. Polymers exhibit several solid-state transitions whose origin is often unknown. Some of these are undetectable with commercially available rapid-scanning calorimeters. These unresolved transitions of interest range from (1) glass transitions whose ΔC_p is significantly reduced by the presence of crystallinity to (2) transitions connected with polymorphism in polymers, (3) sub-glass transitions detectable by other methods, (4) multiple melting and glass transitions. An existing adiabatic calorimeter[1] has been suitably modified to obtain high precision thermodynamic data. In this report we review briefly, with limited discussion, some recent results in this area.

An Unresolved Glass Transition: Linear Polyethylene

The glass transition of polyethylene has been a matter of controversy with values generally reported in three temperature regions; -20 to -30°C, -80 to -90°C and -120 to -130°C. Normally, the crystallinity of linear polyethylene is too high (80-95%) to

*Present Address: Xerox Corporation, Webster, New York 14580
†This abstract of the thesis work was published in Preprints of the 1972 IUPAC International Symposium on Macromolecules and was presented in part by the author on July 4, 1972 in Helsinki, Finland.

permit determination of the glass transition. However, the combined use of ultrahigh molecular weight samples and a quenching technique have reduced crystallinity sufficiently to present the possibility of measuring the glass transition by heat capacity measurements.

Precision adiabatic calorimetry (Fig. 1) indicates a rather broad transition centered around 145 ± 3°K. The lower curve for a higher crystallinity sample in Fig. 1 is essentially linear over this temperature region and was used to construct a ΔC_p plot (Fig. 2). This heat capacity difference plot accentuates the step-change in C_p required for a classical second-order thermodynamic transition. To the best of our knowledge, this is the first definitive precision thermodynamic determination of the glass transition of linear polyethylene.

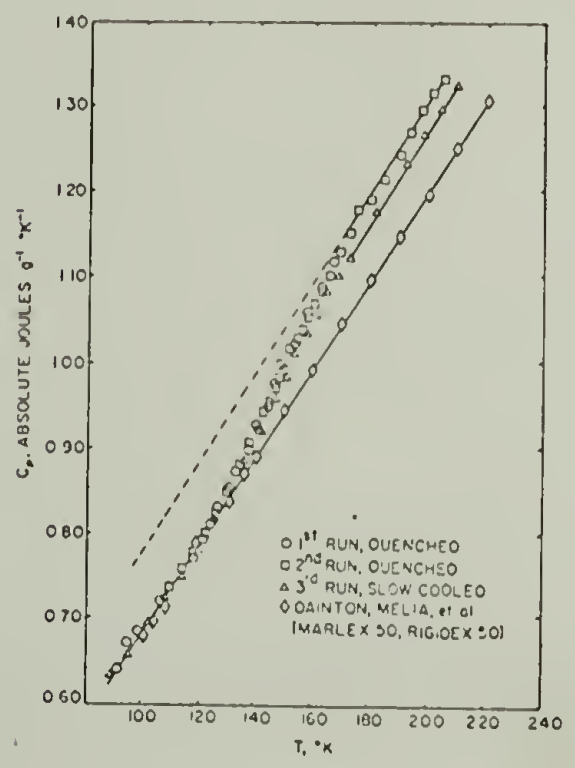

Figure 1
Heat capacity of polyethylenes of various degrees of crystallinity.

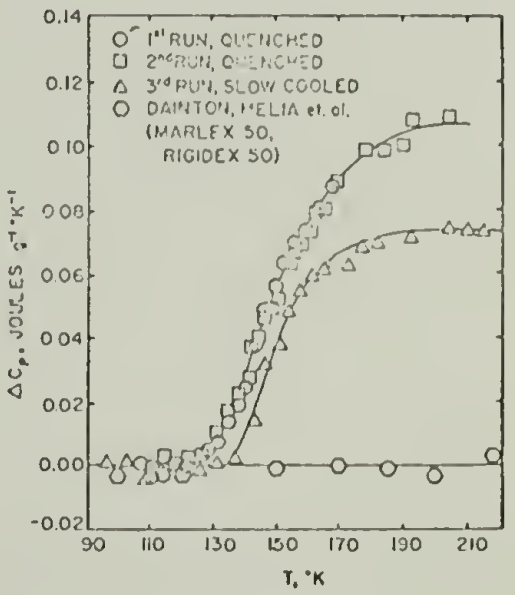

Figure 2
Heat capacity difference plot for the glass transition of polyethylene.

Polymorphism: Smectic Polypropylene

The polymorphic transformation of smectic to monoclinic phase state has been investigated by various techniques[2-6]. However, differential scanning calorimetry data has not been sufficiently precise to adequately analyze the transformation as it proceeds over a very broad (~80°C) temperature range. The transformation process begins immediately after passage through the glass transition and exhibits a double crystallization peak (Fig. 3). This may be indicative of the occurrence of a competitive crystallization transformation. This doublet disappears upon annealing at higher temperatures although crystallization continues to occur with subsequent melting as evidenced by the peak observed due to maintaining constant temperature for 15 hours at 390°K.

Sub T_g Transition: Polycyclohexylmethacrylate

Historically, only the melting and glass transitions, which are highly cooperative transitions requiring the participation of many molecules simultaneously over a narrow temperature range have been observed. However, if the energy difference between conformational states is sufficiently large, the population change may be reflected in the specific heat. As simple cyclohexyl esters have a ΔE of 600-1000 cal/mole for the chair-chair transformation of the cyclohexyl group[7], it was suspected that an anomaly in C_p would be present in the range 120-200°K[8]. As can be seen in Fig. 4, there is an apparent extremely small change in the heat capacity-temperature curve in the direction expected -- the

more stable state having a lower heat capacity. If confirmed, this would be the first calorimetrically detected sub-T_g transition of the polymer solid state.

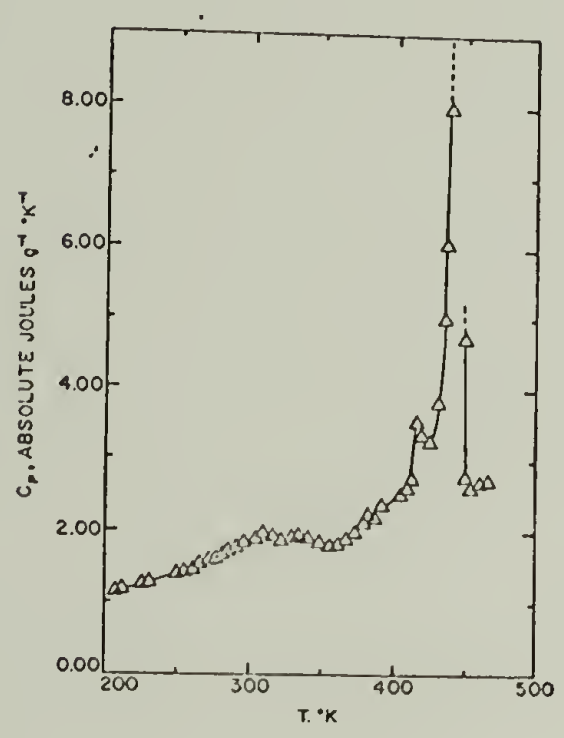

Figure 3
Smectic polypropylene heat capacity as a function of temperature and transformation

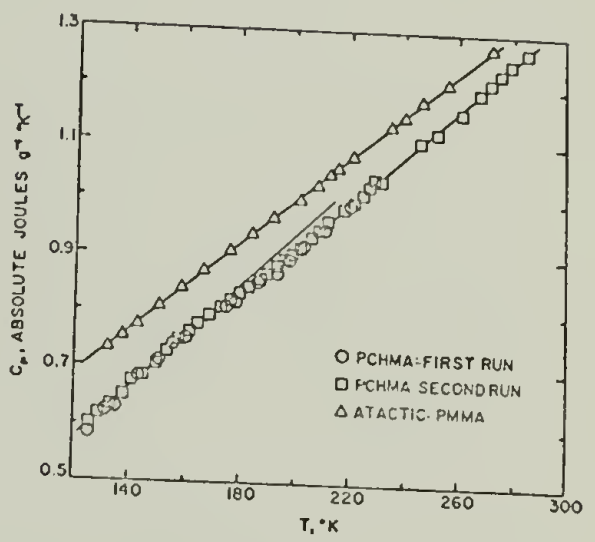

Figure 4
Low temperature C_p anomaly in polycyclohexylmethacrylate

Multiple T_g and T_m: Polydiethylsiloxane

Two glass transitions have been reported for the linear homopolymer of polydiethylsiloxane as well as three and possibly four melting transitions[9]. Our DSC results confirmed the existence of this previously reported complex situation with the exception that only one low temperature peak ascribable to the glass transition could be routinely observed. The heat capacity results (Fig. 5) indicate unambiguously that the glass transition occurs at 130 ± 2°K. This is 20° below the T_g of polydimethylsiloxane -- the

previously lowest T_g for a polymer reported[10]. Thus, the DSC-obtained glass transition of polydiethylsiloxane appears to be a melting transition arising from the presence of (1) oligomer, (2) polymorph, or (3) an impurity.

Characterization of a New Polymer: Poly-ε-caprolactone

Poly-ε-caprolactone has been synthesized recently[11] and the crystal structure[12], hydrodynamic properties[13] and dynamic mechanical properties of the homopolymer and blends[14] have been studied. These and current investigations in our laboratory have prompted our thermal characterization study. The glass and melting transitions (Fig. 6) occur at 209 ± 2°K and 336.5 ± 1°K respectively.

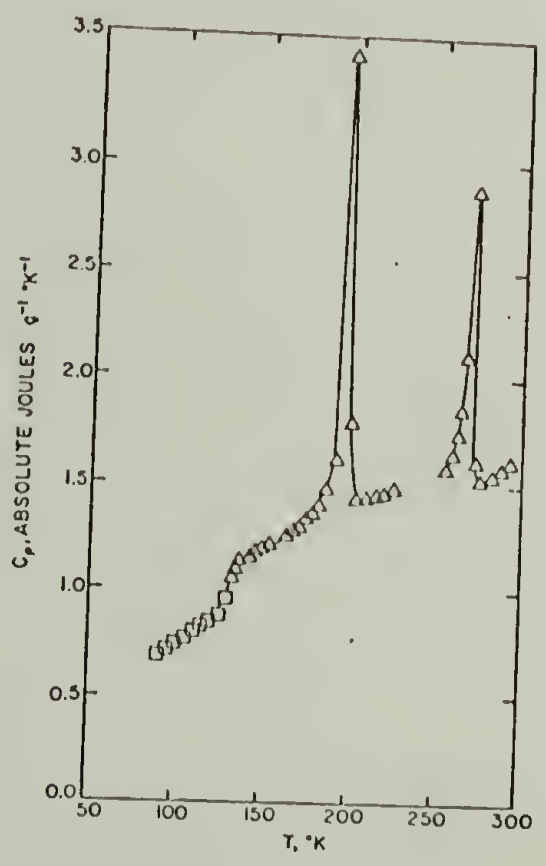

Figure 5
The glass and melting transitions of polydiethylsiloxane.

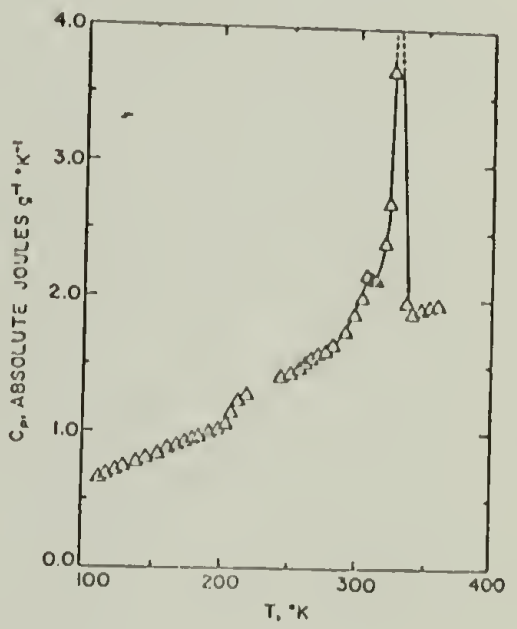

Figure 6
The heat capacity of poly-ε-caprolactone.

REFERENCES

1. Karasz, F. E. and J. M. O'Reilly, Rev. Sci. Instr., 37, No. 3, 255 (1966).
2. Natta, G. and P. Corradini, Nuoro Cimento (Suppl.), 15, 40 (1960).
3. Zannetti, R., Fichera, A., G. Celotti and A. Ferrero Martelli, European Polymer J., 4, 399 (1968).
4. Schael, G. W., J. Appl. Polymer Sci., 10, 901 (1966).
5. Wuerth, W. F., Ph.D. Thesis, MIT, Dec. 1967.
6. Gezovich, D. M. and P. H. Geil, Polymer Sci. and Engr., 8, No. 3, 202 (1968).
7. Eliel, E. C., Angew Chem., 77, 784 (1965).
8. O'Reilly, J. M. and F. E. Karasz, J. Polymer Sci., C, No. 14, 49 (1966).
9. Lee, C. L., O. K. Johannson, O. L. Flaningam and P. Hahn, ACS Polymer Preprints, 10, No. 2, 1319 (1969).
10. Polmanteer, K. E., J. Thorne, and J. D. Helmer, Rubber Chem. and Tech., 39, 1403 (1966).
11. Lundberg, R. D. and J. V. Koleske, J. Polymer Sci., A-1, 7, 2915 (1969).
12. Bittiger, H. and R. H. Marchessault, Acta Cryst., B26, 1923 (1970).
13. Koleske, J. V. and R. D. Lundberg, J. Polymer Sci., A-2, 7, 897, (1969).
14. Koleske, J. V. and R. D. Lundberg, J. Polymer Sci., A-2, 7, 795 (1969).

INTRODUCTION

This thesis consists of a series of four papers concerning the thermodynamics of polymeric solid-state transitions. The topics investigated range from glass transitions and sub-glass transitions to liquid crystalline and melting transformations. The unifying link, aside from thermodynamic and solid-state interests, is the need and use of a highly precise and accurate calorimeter for data acquisition.

These chapters are written for publication and as such are self-contained (i.e. figures, tables, references, etc., are included). The normal publication format of introduction, experimental, results, and discussion of results are used for all of these papers. The thesis abstract and the polyethylene chapter abstract have already been published as noted in the text.

The appendix is the instrument operation manual and will be published internally for future instrument operators.

CHAPTER I

THE GLASS TRANSITION OF POLYETHYLENE*

C. L. Beatty and F. E. Karasz
University of Massachusetts
Amherst, Massachusetts 01002

ABSTRACT

The glass transition temperature of polyethylene has been a matter of controversy with values reported in three temperature regions, -20 to -30°C, -80 to -90°C and -120 to -130°C. Quenching an ultra-high molecular weight sample can reduce crystallinity sufficiently to present the possibility of detection of Tg by heat capacity measurements. Precision adiabatic calorimetry has shown a ΔCp of 0.060 j g^{-1} K^{-1}, equivalent to 6.25% change for an eight million molecular weight quenched polyethylene sample at 145°K. Higher crystallinities, achieved by milder crystallization conditions and/or by using lower molecular weight species, make this discontinuity virtually undetectable - even in large scale plots of the function $(dS/dT)_p$ which is known to improve sensitivity.

This work was supported by AFOSR Grant 68-1434.

* presented in part by the author on December 27, 1971 at Winter Meeting of the American Physical Society in Cambridge, Mass.

CHAPTER I

THE GLASS TRANSITION OF LINEAR POLYETHYLENE

C. L. Beatty* and F. E. Karasz
University of Massachusetts
Amherst, Massachusetts 01002

Although polyethylene is the simplest and most widely investigated polymer, the glass transition temperature, Tg, has continued to be a matter of controversy. This has been primarily due to the small amount of amorphous material normally present -- with the resultant small change in properties at Tg. Consequently, only the more sensitive techniques, such as dynamic mechanical loss, NMR, etc. can be expected to detect Tg.

The claims for Tg have been grouped into three temperature regions -20 to -30°C, -80 to -90°C and -120 to -130°C[1-4]. Dynamic mechanical loss peaks are noted in the -25°C and -125°C temperature regions for branched polyethylene (BPE)[5,6] while the -25°C transition is either absent[7-9] or barely detectible[10-12] in linear polyethylene (LPE). Crist and Peterlin[13], by investigating a series of BPE's by wideline NMR, have shown that the beta process (-25°C) reflects the degree of branching in the material -- not the type of branching nor non-crystallinity. The same effect (i.e. a relaxation peak at -25°C) is noted if acetate or chlorine groups are substituted

* Present address: Xerox Corporation, Webster, New York 14580

for the branch points[14,15] providing additional evidence that this transition is defect related. Ohlberg and Fenstermaker[16] have determined that Tg is -28°C for BPE by observing the change in d-spacing for the amorphous halo as a function of temperature. In addition, thermal expansion measurement of BPE by Simha et al.[17] indicates a transition at -22°C as well as transitions at -125, -60 and 0°C. Consequently, various techniques tend to indicate that a transition occurs in BPE at approximately -25°C whose origin appears to be related to the degree of branching. If true, branched and linear polyethylene are in essence two different polymers and intercomparison is invalid.

The placement of Tg in the -85°C region has been made principally via extrapolation of both LPE and BPE copolymer data[18-22]. Also extrapolation of n-alkane glass transitions to infinite molecular weight yields a value of -73°C for LPE[23]. However, the overall composition of the copolymer probably does not reflect the composition of the non-crystalline regions (as polyethylene is quite crystallizable) thereby rendering such extrapolation doubtful. In support of this, Maurer[24] and Nielsen[25] have shown that crystalline copolymers do not superimpose on the Tg-composition curve defined by completely amorphous copolymers. Some dilatometric data[26] has also indicated a Tg at -63°C. But this may be an artifact due to impurities as addition of a stabilizer to LPE has been shown to result in a dynamic mechanical loss peak at approximately -60°C under proper crystallization conditions[27]. This has been attributed to phase separation of the stabilizer. However, a recent correlation of

ESR spin-probe results with the glass transition of various polymers indicates that the glass transition of both BPE and LPE occurs at 190°K[28]. Hager[29], using a uniquely designed calorimeter, obtained thermal data on BPE indicating that Tg was near 240°K.

The gamma relaxation (-125°C) has been attributed to various origins -- crystalline[9,10,18,30,31] and amorphous[7,20,32,34] or a combination of contributions from both[32]. Regardless of the mechanism, Willbourn[34] has shown that the γ-relaxation occurs in any polymer containing a series of four or more methylene sequences. Recently, Schatski[33] has disavowed his previously proposed crankshaft model as a possible mechanism for this transition while disclaiming that the gamma relaxation is Tg. However, extrapolation of Tg from low (up to 40%) sequential methylene to 100% content for polyesters and polylactones yields values of -165°C and -141°C respectively for Tg[35]. Similarly, an extrapolation of a series of polyethers to 100% ethylene content yields a value of -135°C for LPE[36]. However, brittle point temperatures and qualitative crystallization data also indicate that the -125°C transition is Tg for both BPE and LPE[34]. Additionally, Mandelkern and Stehling has presented evidence for a change in rate of thermal expansion in this temperature region[26,37] and indications of a thermal anomaly from DSC data[37]. Transitions at higher temperatures were observed by Mandelkern and coworkers.

The evidence for two components of the γ-relaxation stems from dynamic mechanical measurements[32,37] and wideline NMR[38]. However, recent contradictory dilatometric data by Davis[39] indicate

that there is a transition which the author relates to Tg at 240°K. MacKnight[3] concluded from copolymer studies that the γ-relaxation consisted of two overlapping peaks at -140°C and -120°C. Since the lower temperature relaxation also occurs in polycrystalline n-paraffins[40], it is, by analogy, attributed to the crystalline component. However, this question is unsettled as Peterlin and coworkers[13,41] have shown that removal of amorphous fractions by fuming nitric acid treatment of LPE single crystals results in the absence of the γ-relaxation via NMR measurements. Subsequently, Shen and Cirlin[42] have embedded similarly treated LPE single crystals in polystyrene and their internal loss transition results indicate that a gamma doublet exists regardless of the presence or absence of amorphous material. Recently the absence of both the γ and α relaxation peaks was demonstrated for a specially prepared essentially defect free n-eicosane, n-$C_{20}H_{42}$, single crystal[35]. Cold-working does not induce a γ peak indicating that the γ-relaxation may not be crystal defect related. However, γ irradiation of a n-eicosane crystal resulted in observation of both α and γ relaxation peaks as well as a small but distinct maximum near 230°K. Measurement of NMR spectra at "magic angle" rotation was recently used to eliminate broadening due to magnetic dipole-dipole interactions[44]. It was concluded that in polyethylenes ranging in density from 0.962 to 0.919 g/cm^3 contain two amorphous phases. Several resonance techniques tend to indicate that γ-relaxation may occur in imperfectly crystallized material although the observed magnitude is enhanced by increasing the degree of non-crystallinity.

This controversy concerning Tg results in part from the nondefinitive nature of the techniques used and absence of sufficient amounts of disordered material to allow utilization of classical and definitive thermodynamic techniques. Additionally, work on samples of variable branch content, distribution, thermal history, etc. add to the confusion. However, both the effect of quenching from the melt and of increasing molecular weight[45,46] upon reducing crystallinity are well known. Measurement of Tg via DSC measurements using these combined techniques has been attempted with some degree of success by Mandelkern and coworkers[7]. These techniques have been utilized in this work to allow preparation of samples of LPE of low crystallinity in an attempt to detect a ΔCp change characteristic of Tg (i.e. a second-order thermodynamic transition).

EXPERIMENTAL

The ultra-high molecular weight linear polyethylene examined in this work was an Allied A-C-8x sample of approximately eight million molecular weight kindly donated by A. F. Margolis. The viscosity average molecular weight is approximately 7.5-8.0 million while the number average molecular weight is judged to be in excess of 350,000[47]. The branching, as determined by infrared measurements, is less than 1 per 10,000 carbon atoms. Due to the intractability of the polymer, further fractionation was not attempted.

Sample films were prepared by compression molding between sheets of teflon-coated aluminum foil at 170°C for 20 minutes

prior to quenching into liquid nitrogen. Preliminary determinations of crystallinity were performed on a Perkin-Elmer DSC-1B. Subsequent crystallinities were determined with a GE XRD-5 wide angle x-ray diffractometer using Ni filtered Cu radiation. Natta's method[48] was used for determination of the percent crystallinity. The crystalline morphology, as determined by small angle laser light scattering, does not appear to be spherulitic as illustrated in Figure 1. Subsequent studies indicate that rod-shaped spherulitic precursors are formed due to incomplete crystallization[49]. Similar structures are obtained during incomplete crystallization from the glass state of polyethylene terephthalate[50]. Silicone oil was used to minimize secondary scattering. Initially a different crystalline phase was suspected, however, the crystalline unit cell dimensions, as obtained from wide angle x-ray diffraction, are equivalent to those for higher crystallinity linear polyethylene. Measurement of Tg was attempted on the DSC-1B by decalibration[51] and utilization of large volume sample pans. Temperatures near -150°C could be achieved by using helium as a purge gas and extended equilibration time. Further preliminary calorimetric measurements were performed on a DuPont 900 thermal analyzer equipped with a DuPont DSC cell - capable of temperatures down to -190°C. For calibration purposes, a semicrystalline sample of polydimethylsiloxane within viscosity 441,000 centipoise of known Tg and Tm[52] was also examined.

A precision adiabatic calorimeter was used to measure the heat capacity of the quenched eight million molecular weight (8MPE-Q)

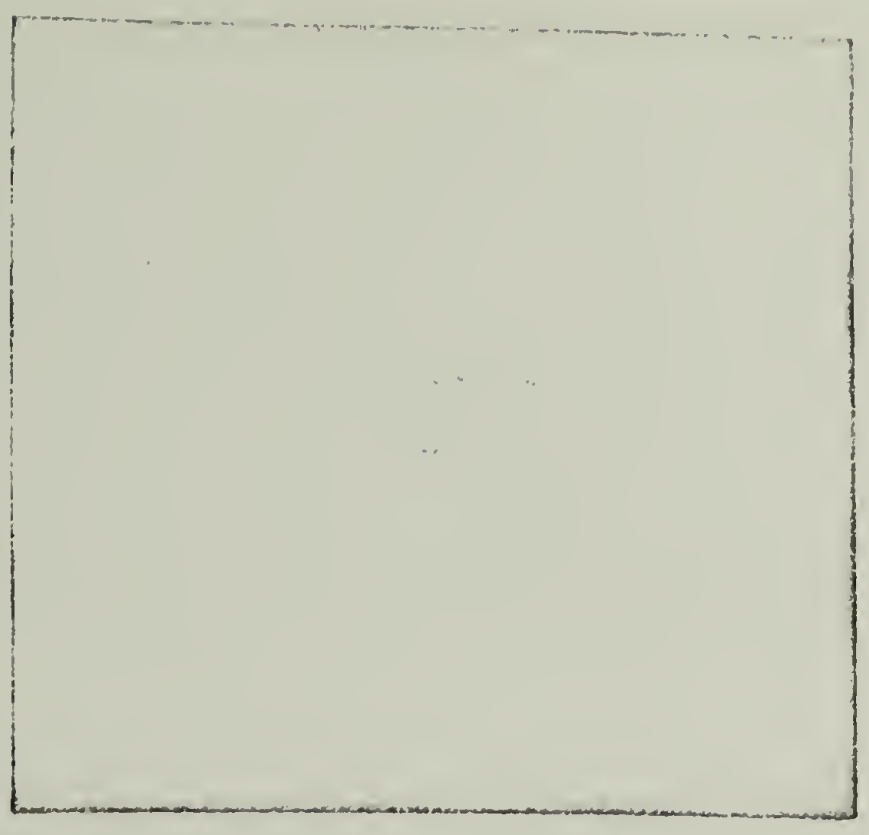

A

B

Figure 1

Small Angle Laser Light Scattering Pattern of Quenched Ultra-High Molecular Weight Linear Polyethylene (A) without and (B) with beam stop. Photo (B) was exposed for a longer period of time in an effort to detect the typical clover-leaf pattern of spherulitic material.

sample from 77° to 273°K. Figure 2 is a block diagram describing the essential features of the system. The details are described elsewhere[53] with minor modifications[54].

The quenched films were cut and packed into the calorimeter, achieving a sample weight of 40.882 grams, prior to evacuation and sealing under a small helium pressure to enhance thermal equilibration. The polymer was typically heated at approximately 15°K hr^{-1} in runs of 2 to 5 deg K. The precision of the measurements has been estimated to be better than ± 0.1 percent over the temperature range reported in this paper.

RESULTS

Considerable effort is required to obtain adiabatic calorimetric data. Therefore, DSC scans of all samples are routinely performed using a Perkin-Elmer DSC-1B in our laboratory. Polydimethylsiloxane Tg and Tm agreed well with the calibration. However, contradictory results for repetitive scans of the polyethylene samples prompted runs at low temperatures with empty pans. To our dismay, similar results could be obtained. J. Illinger, Watertown Arsenal, repeated the measurements on a DuPont DSC with analogous results.

Nevertheless, three series of measurements were made through the gamma relaxation region - two passes from the quenched 8MPE and the third on the same sample crystallized slowly from the melt in the calorimeter under high vacuum conditions. The sample was at room temperature for approximately 120 hours prior to installation

BLOCK DIAGRAM OF SYSTEM

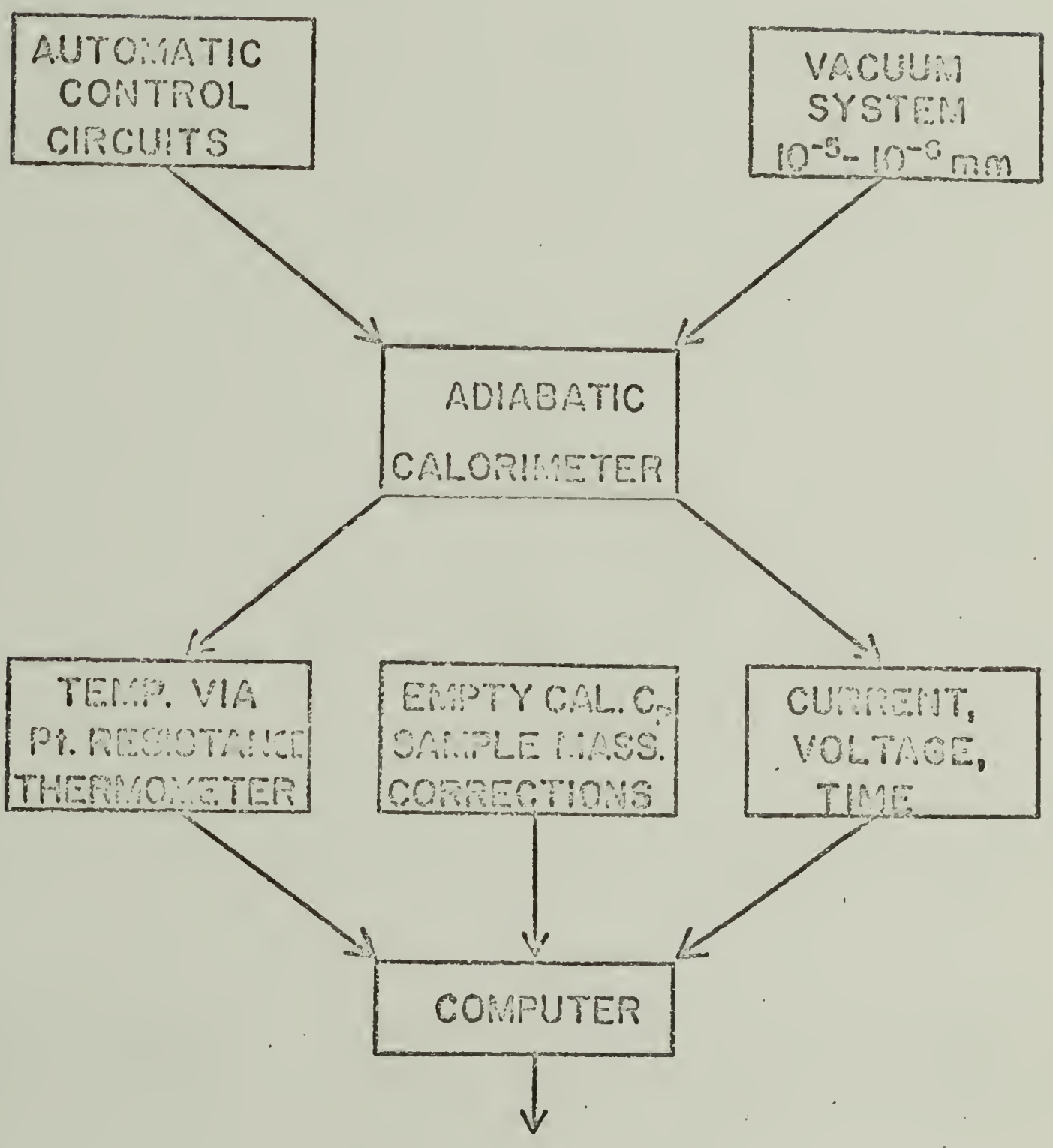

$$C_P = \frac{\int_{t_1}^{t_f} E(t)\, I(t)\, dt}{T}$$

Figure 2

Schematic Diagram of Calorimeter Operation

and cooling. The first series of measurements were made after cooling to 80°K at an average rate of 5°K hr^{-1}. After equilibration at this temperature for ~90 hours, heating runs of 2 to 5°K were made using rates of 6 - 12°K hr^{-1} up to 170°K. The second series of measurements on the quenched sample was performed using similar conditions after cooling to 100°K at an average rate of 3°K hr^{-1}. The sample and calorimeter were equilibrated for 20 hours prior to reheating into the melt to 443°K.

The melted sample was slowly cooled (~2°K hr^{-1}) at the end of the second series of measurements to achieve maximum crystallinity. To further enhance complete crystallization, the sample was annealed in situ for ~30 hrs at 380°K. Prior to the third series of measurements, the calorimeter was cooled approximately 6°K hr^{-1} to 77°K. Heating conditions for the slow-cooled series were essentially identical to those of Run 2 for the liquid nitrogen quenched material.

The experimental data for the three series of measurements are tabulated in Tables 1 - 3 and plotted in Figure 3. The observed step change in Cp (Figure 3) occurs over a broad range of temperature (~40°K) and the magnitude of the change is crystallinity dependent. The lower curve of high crystallinity (~80%) linear polyethylene does not possess a discernable change. In fact it can be satisfactorily represented over the entire temperature range (Figure 3) by a straight line. Note that all the data, irrespective of percent crystallinity, coincides in the lower temperature region below 125°K. In fact, agreement of one part in one thousand is obtained for our data

Temperature °K	Heat Capacity Absolute Joules g^{-1} $°K^{-1}$
91.4373	0.6428
95.4822	0.6714
99.4177	0.6845
103.1722	0.7018
106.8562	0.7200
110.4618	0.7376
113.9956	0.7531
117.4621	0.7743
121.0332	0.7925
124.7691	0.8184
128.2481	0.8353
131.4803	0.8544
134.7290	0.8780
137.9325	0.8999
141.0132	0.9227
143.9843	0.9501
146.9128	0.9774
149.9534	0.9994
153.0791	1.0229
156.1550	1.0443
159.1408	1.0637
163.0550	1.0911
167.4106	1.1182

Table 1

Heat Capacity, Temperature Data for Run 1

Temperature °K	Heat Capacity Absolute Joules g^{-1} $°K^{-1}$
110.2498	0.7366
114.0784	0.7593
118.0838	0.7770
122.0382	0.7995
126.1977	0.8231
130.6136	0.8527
134.6535	0.8819
138.2512	0.9056
141.1255	0.9254
143.1501	0.9457
144.7498	0.9569
146.3411	0.9706
147.9432	0.9828
149.7469	0.9946
151.7050	1.0165
153.9076	1.0272
155.9151	1.0396
158.0257	1.0548
160.2199	1.0694
162.3563	1.0858
165.2955	1.1022
172.1911	1.1541
175.2156	1.1788
179.0372	1.1929
184.1097	1.2186
189.4909	1.2475
193.6214	1.2740
197.3504	1.2995
200.9785	1.3200
204.8824	1.3344
209.3246	1.3556
213.7197	1.3803
221.8528	1.4313
225.7535	1.4541
229.5611	1.4884
233.4472	1.5018
241.0453	1.5788
264.1802	1.7731
269.2679	1.7518
274.1074	1.8037
280.3527	1.8479
285.4167	1.9100
290.4458	1.9454
295.3673	1.9899

Table 2

Heat Capacity, Temperature Data for Run 2

Temperature °K	Heat Capacity Absolute Joules g^{-1} $°K^{-1}$
89.9735	0.6255
95.9507	0.6551
102.6018	0.6964
108.8262	0.7264
114.5457	0.7501
119.8853	0.7792
125.2907	0.8144
131.0167	0.8455
136.7311	0.8796
142.1213	0.9032
146.8113	0.9555
150.3733	0.9754
153.6939	1.0073
157.3042	1.0300
160.9876	1.0544
164.8891	1.0772
168.9179	1.0968
173.0508	1.1200
177.3079	1.1512
181.6979	1.1740
192.4389	1.2334
197.6120	1.2678
204.7495	1.3039
210.2877	1.3319

Table 3
Heat Capacity, Temperature Data for Run 3

Table 3 cont.

214.9551	1.3604
220.8832	1.3891
226.7385	1.4279
237.3117	1.4819
242.2817	1.5233
247.9127	1.5682
252.9670	1.5822
257.0292	1.5974
264.5679	1.6732
269.0897	1.7043
273.2463	1.7393
278.3905	1.7630
284.4287	1.8084
290.6815	1.8620
297.1522	1.9157
302.3951	1.9652

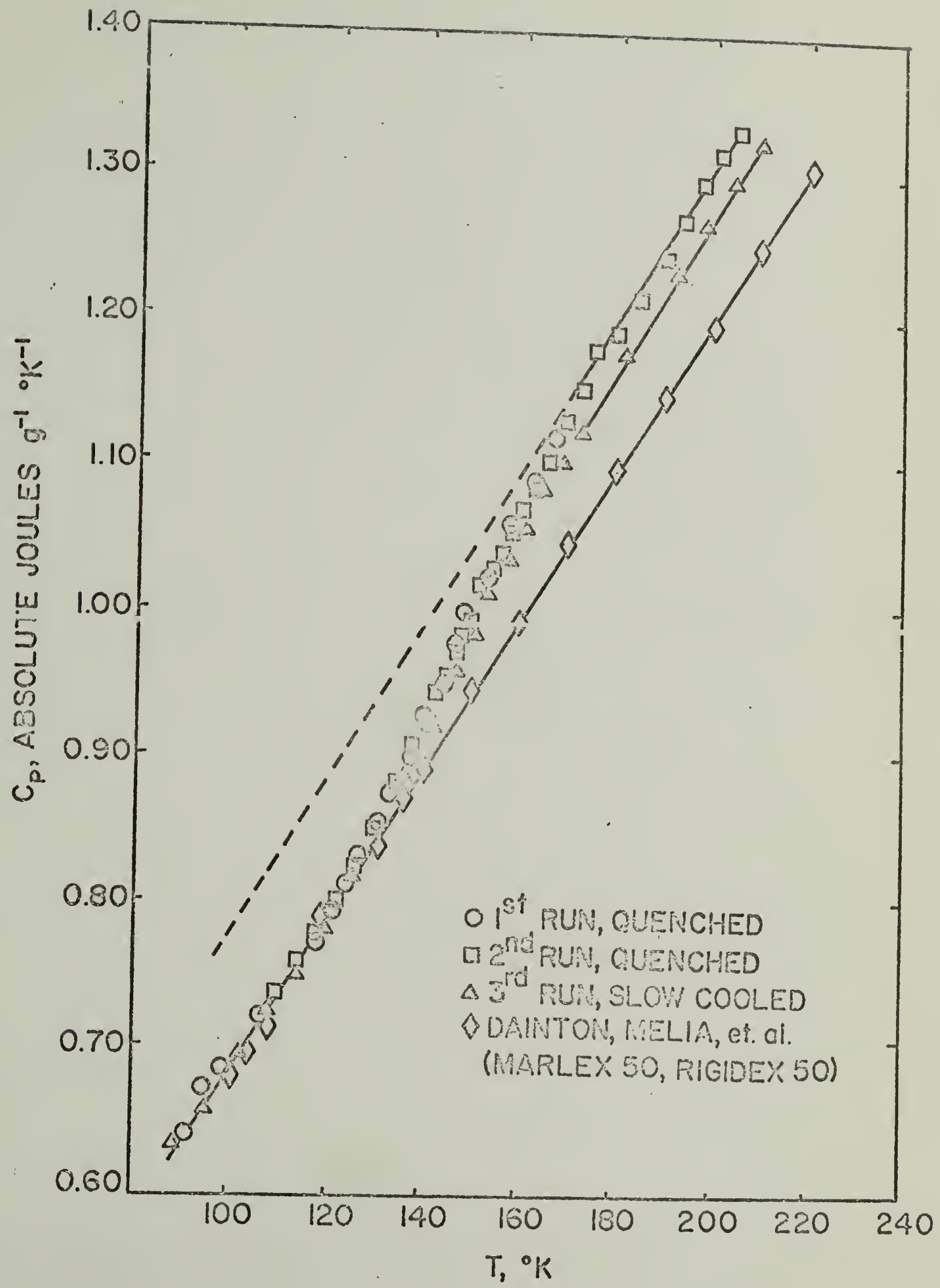

Figure 3

The Low Temperature Heat Capacity
of Linear Polyethylene of Low Crystallinity.

and the adiabatic calorimetric data of Marlex[50] obtained by Dainton, Melia et al.[55] at 100°K. Comparison in the melt was on the order of forty parts in one thousand. Also the data for Runs 1 and 2 slow good reproducibility through the transition region. In addition, the step-change mid-point is not significantly altered by variation of crystallinity. However, the magnitude of the step-change observed ΔCp is definitely dependent upon crystallinity. Crystallinities as low as 30% were measured via DSC for the liquid-nitrogen quenched samples. However, due to variability in sample preparation, the crystallinity for the first and third runs fall in the range of 35 - 45% and 50 - 55% crystallinity respectively.

The characteristic glass-transition step-change in heat capacity can be more readily observed in the heat capacity difference, ΔCp plot (Figure 4). These ΔCp curves were obtained by substracting the linear heat capacity curve for the ~80% crystalline linear polyethylene. This, in effect, removes the crystalline contribution to the heat capacity resulting in clearer exposition of the thermodynamic transformation occurring in the non-crystalline material.

As data reduction requires simulation of the empty calorimeter by a ten term orthogonal polynomial, there was concern that there might be some systematic error in simulation and/or data reduction. However, a subsequent series of measurements on polypropylene[56] (Figure 5) agrees well with published high quality adiabatic calorimetric data[55] over the entire temperature range in question, thereby confirming that the observed polyethylene transition is not an experimental artifact.

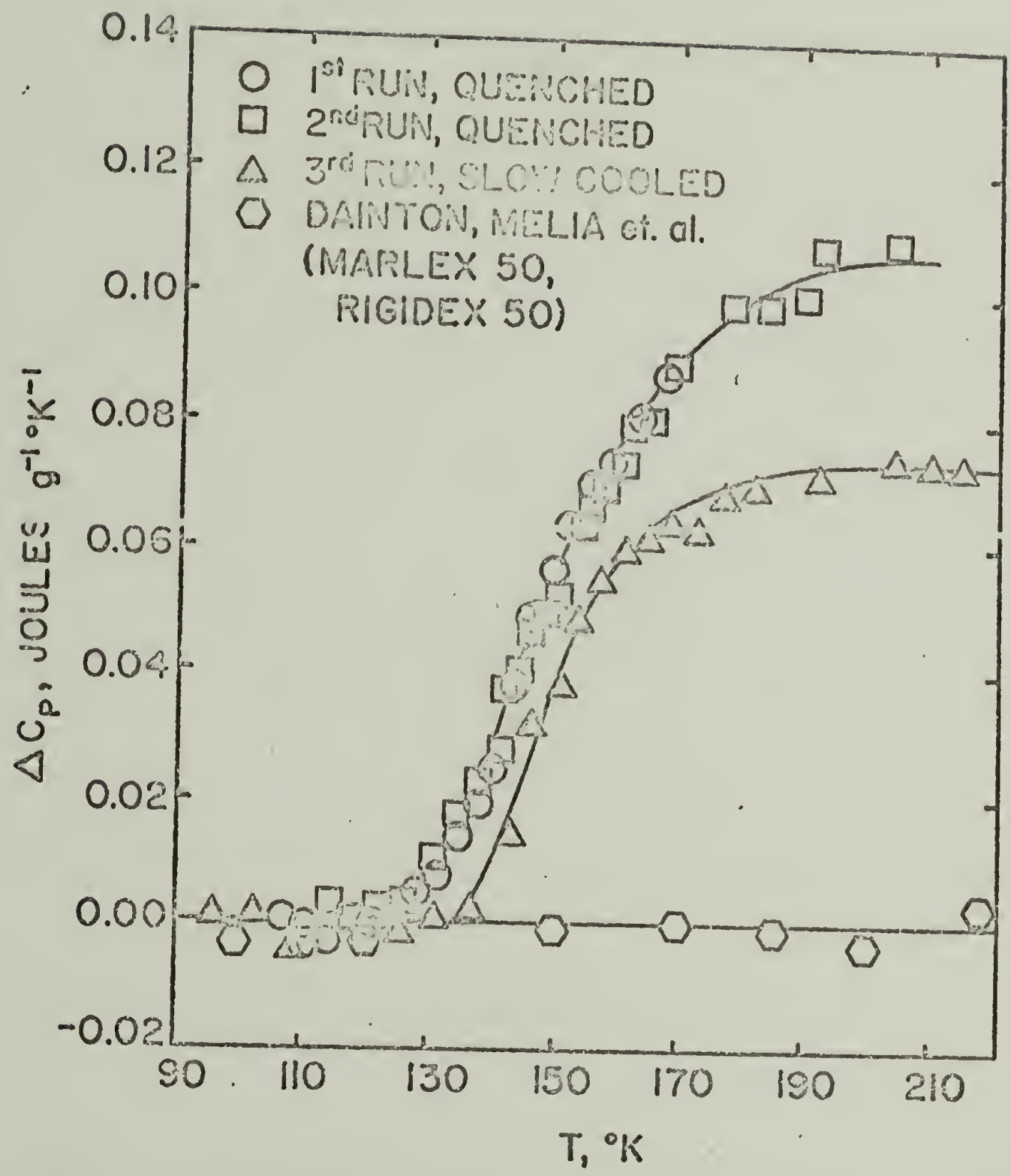

Figure 4

Heat-Capacity Difference Plot
of 35-45% Crystallinity and 50-55% Crystallinity Samples.

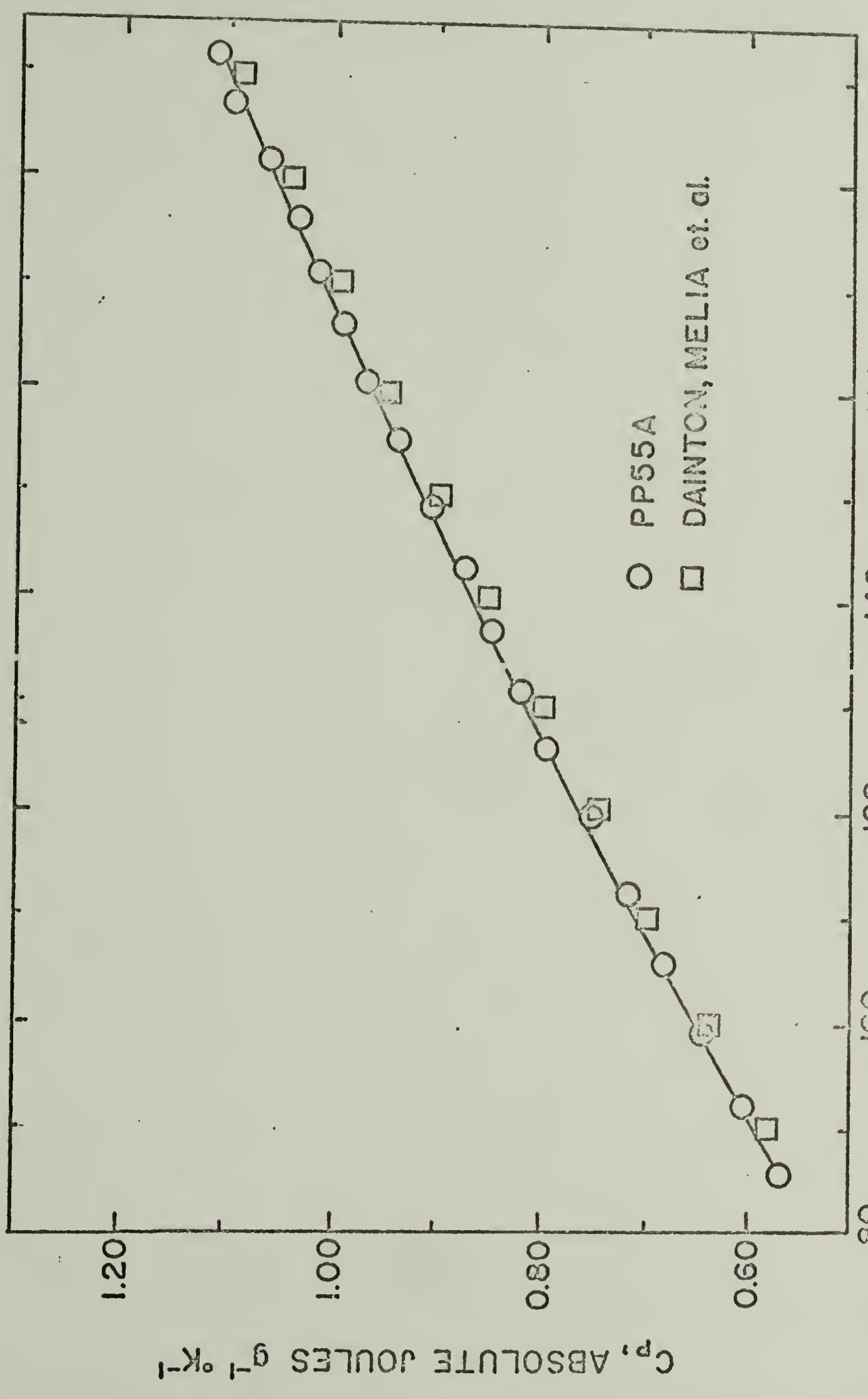

Figure 5 Polypropylene Data Obtained Immediately After the Polyethylene Measurements

The possibility that the observed change in heat capacity is due to a crystalline phase transformation is doubtful as the sample was at room temperature about 120 hours prior to measurement. In addition, wide-angle x-ray diffraction of both quenched and slow-cooled material yields the same unit cell. However, it is known that linear polyethylene prepared at -70°C undergoes an irreversible triclinic to orthorhombic crystal transformation upon warming to room temperature[57].

DISCUSSION

As pointed out in the Result Section, a step-change in heat capacity is illustrated in plots of both heat capacity of the semicrystalline sample (Figure 3) and heat capacity of the amorphous content (Figure 4). Such a change is reminiscent of a second order thermodynamic transition, although the characteristic broadness of polymeric glass transitions prevent classification as such without controversy. Note that the observed increase in heat capacity is a function of crystallinity as required for a glass transition. Also note that at temperatures below the step-change, heat capacity is essentially independent of crystallinity as expected below Tg.

Although thermodynamics is the classical definitive test for determination of transitional classification, inspection of the other temperature regions of controversy is required for completeness. Note in Figure 6 that there is no comparable anomaly in the heat capacity curve near 240°K, the range of controversy. However, extrapolation of calorimetric measurements on samples of various

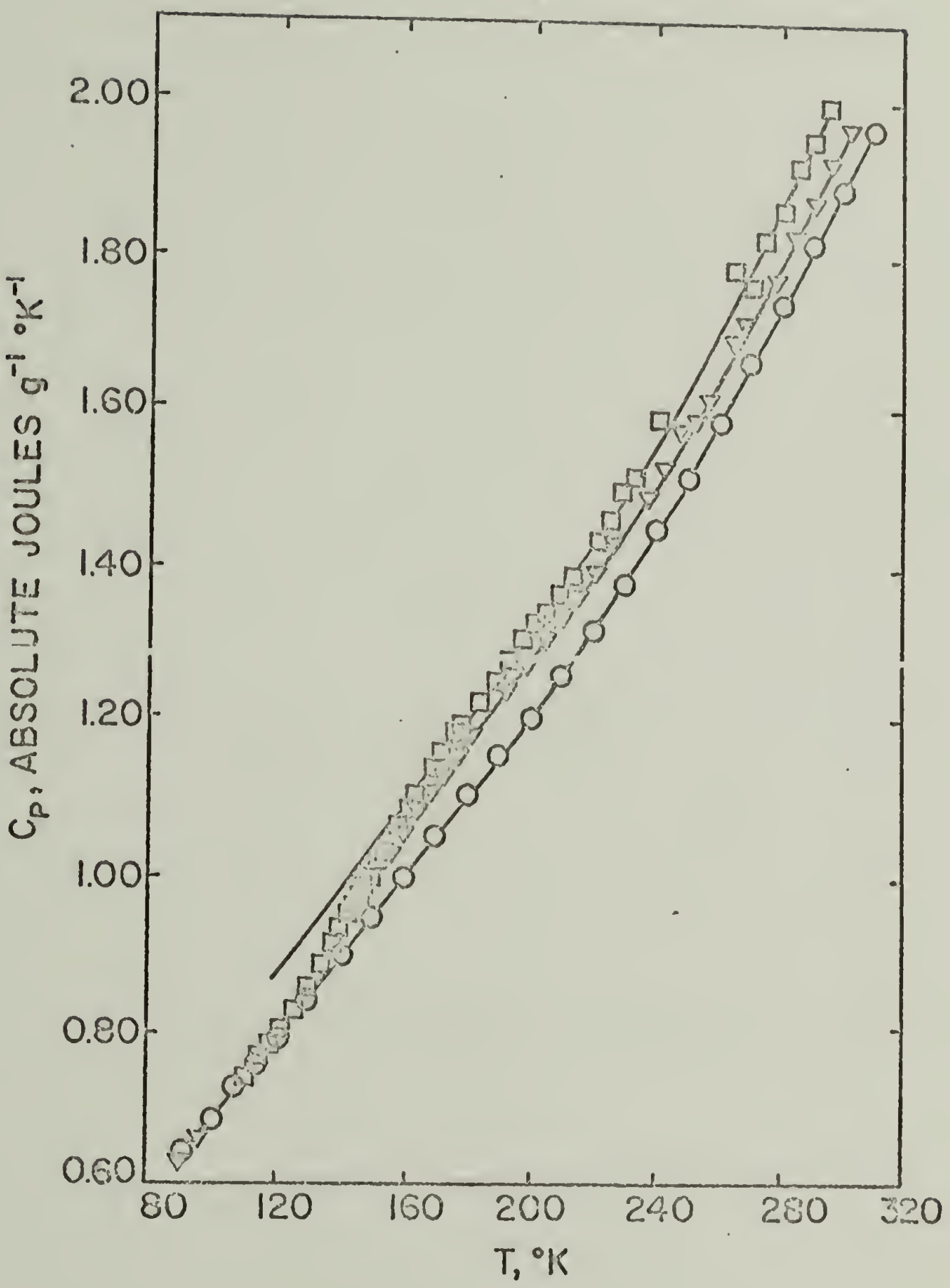

Figure 6

The Heat Capacity of Three Crystallinities
(0-80%, Δ - 50-55%, □ - 35-40%)

high crystallinities (~60%) to zero percent crystallinity by Wunderlich[58] have indicated that the glass transition of linear polyethylene occurs near 240°K. In contrast, deviation of heat capacity curves above 110°K was observed by Reese[59] for 0% and 100% crystallinity. These were curves obtained by linear extrapolation of heat capacity versus crystallinity data. Recently, measurement of drift rate variation in a similar adiabatic calorimeter has been used in an attempt to detect the glass transition using high crystallinity (~71%) samples[60]. An anomaly in drift rate is concluded to be evidence of glass transition. More recently a step-change in heat capacity has similarly been observed at 145°K and at 240°K[61]. Interestingly a recognizable discontinuity in CP at 240°K is observable in this range for branched polyethylene[62]. Branch content of the linear polyethylene exhibiting a transition at 240°K was not disclosed. Although undoubtedly the occurrence of these heat capacity anomalies are real, the higher temperature transition may be, in fact, due to either a branched or a constrained non-crystalline component.

Fischer and Kloos[63] then have developed a technique that utilizes small angle x-ray peak intensities for determining the variation in intercrystalline electron density as a function of temperature. This variation in intercrystalline density was determined for solution grown crystals LPE and BPE with obvious slope changes occurring at -125°C and -26°C respectively. They are currently investigating the effect of branch content upon the glass transition measured by this technique whose results, fortunately, are independent of

crystallinity. Similarly the activation energy for diffusion of $n\text{-}C_4H_{10}$ through LPE at 50°C was correlated with the γ-relaxation activation energy[64]. This evidence supports the hypothesis that the γ-relaxation is a cooperative mechanism involving the correlation of bond rotation and free volume.

Recently a new more sensitive differential scanning calorimeter (the DSC-2 produced by Perkin-Elmer Corporation) was utilized in an effort to confirm our previously obtained results. An identical sample and quenching techniques similar to those reported in this paper were used. The results[65] illustrated in Figure 7 are in excellent agreement considering the differences in instrument design and sample preparation.

Wunderlich[66] has indicated that the excess heat capacity of amorphous polyethylene over and beyond the crystalline polyethylene between 120°K and 230°K can be attributed to the change in gauche-trans ratio. Recent low temperature infrared spectroscopy results on polyethylene indicate that the ratio of gauche (1352 cm^{-1}) to trans (1368 cm^{-1}) bands pass through a maximum at approximately -130°C[67]. This was associated with the glass transition and as additional evidence that the γ-relaxation is not related to the crystalline phase. Also of interest if that Raman spectroscopy of LPE indicates that crystal field splitting of the methylene wagging mode is increased at -160°C compared to that observed at room temperature[68]. Also splitting is observed for the B_{2g} skeletal stretching and the B_{3g} methylene twisting modes at -160°C but not

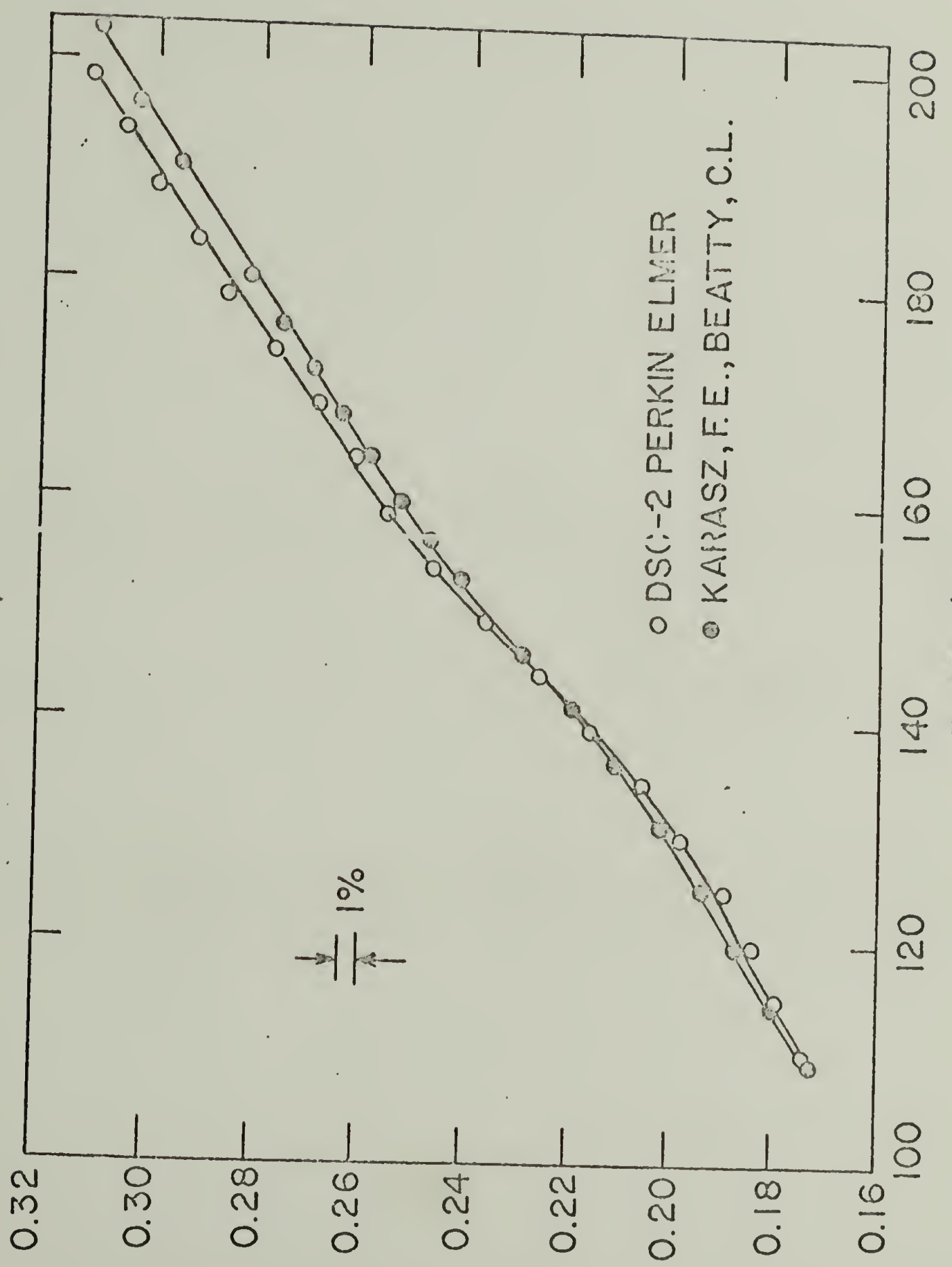

Figure 7 Comparison of DSC and Adiabatic Calorimetrically Obtained Results for the 145°K Region

at room temperature. These results indicate that random molecular motion has been significantly reduced at low temperatures. The minimum temperature for observation of crystal field splitting was not reported.

It is generally accepted that polymeric materials have significantly higher impact strengths above the glass transition than below. Dart impact values for high density polyethylene increase twenty fold between 148°K and 173°K indicating that the low temperature region is the glass transition[69]. Also the storage modulus of LPE decreases sharply by a factor of two at 145°K with no anlaogous change in the 240°K region[37]. The low temperature tensile properties of the essentially alternating copolymer of tetrafluoroethylene and etnylene were recently reported[70]. This copolymer is 50-60% crystalline and exhibits a brittle-tough transition in the range -190 to -110°C. Characterization of recently prepared highly oriented transparent linear polyethylene in our laboratories have indicated that the γ-relaxation is significantly reduced[71]. This is in contrast to the findings on transparent polyethylene prepared in a different manner[72]. Viscoelastic relaxation processes in both BPE and LPE were studied over a wide range of frequencies by Stachurski and Ward[6]. One of their conclusions was that comparison of LPE and BPE is not only a question of comparison of different fractions of phases but also of different kinds of amorphous phases.

Analysis of our data with cognizance of this controversy followed two approaches - the construction of heat capacity difference plots similar to that previously used to elucidate the step change in heat capacity (Figure 4) and the use of encraty diagrams. If

the same linear base line is used for construction of a ΔCp curve as was used for 145°K plot, then Figure 8 results. Note that although there is an obvious change in slope near 240°K, there is not a step-change indicative of the glass transition.

A complicating design feature of our adiabatic calorimeter is that a small amount (~60 mg) of polydimethylsiloxane is used as a heat transfer medium between the calorimeter and a temperature-sensing support ring. This weight is insignificant compared to the overall calorimeter weight (~500 g) and careful control of amounts added allow for data correction over the entire temperature range. The melting of polydimethylsiloxane doubles the error of measurement near -40°C to ~0.2 - 0.3%. The observed change in heat capacity as illustrated in Figure 2 is ~10%. The increase in error due to polydimethylsiloxane at other temperatures is insignificant.

However, inspection of Figure 6 will show that all three heat capacity curves regardless of percent crystallinity change slope near 240°K. Also the curves remain essentially parallel throughout the region from just above the observed step-change in heat capacity to room temperature. Consequently, it appears that the phenomena at 240°K is independent of crystallinity. Note that the curves of lower crystallinity are shifted to higher values of heat capacity as expected due to the greater number of modes of motion available to non-crystalline material.

Since a heat capacity anomaly was not observed in the approximately 80% crystalline curve and the 240°K change of slope is essentially independent of crystallinity, it was used as an approximation to the

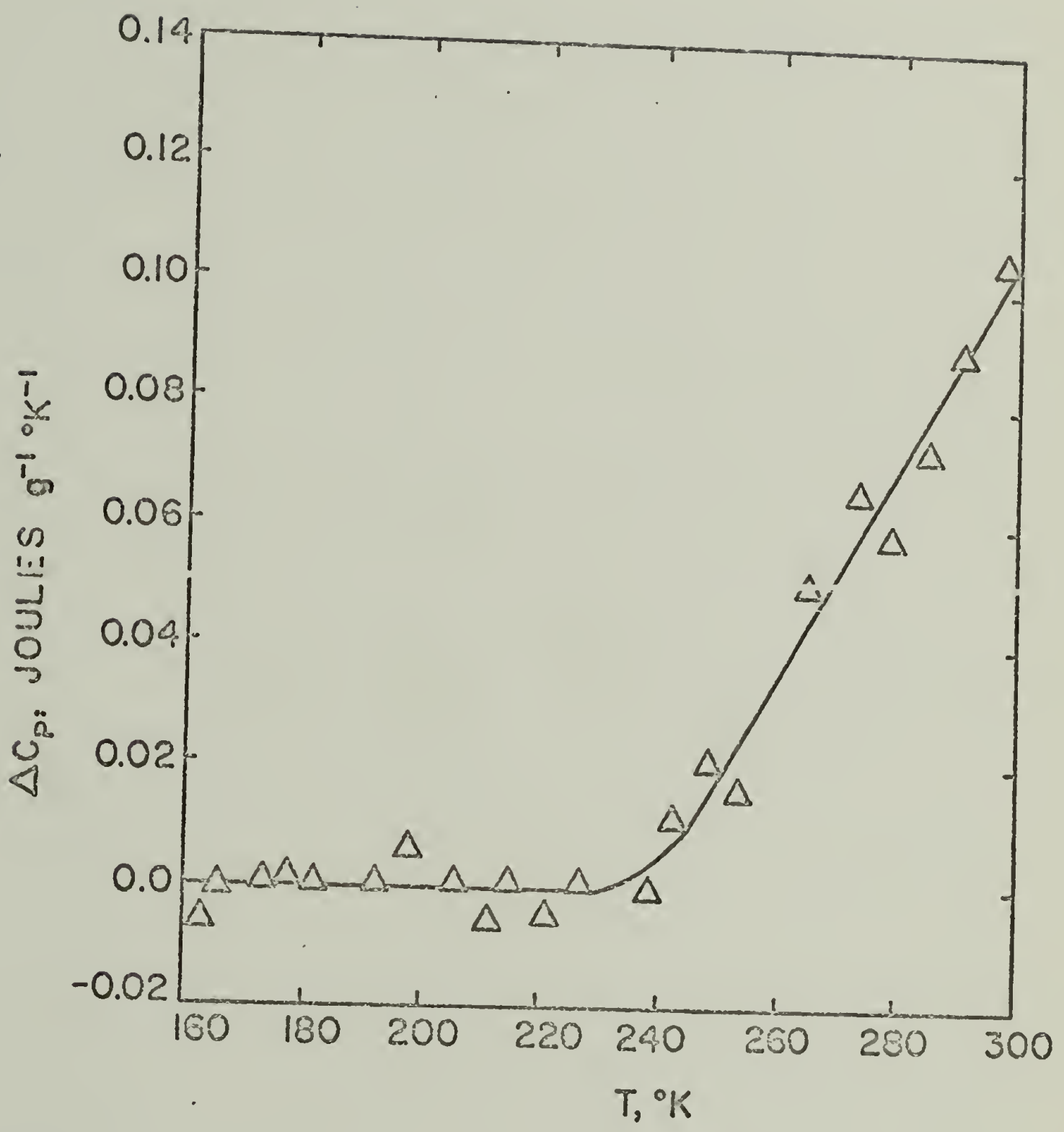

Figure 8

Heat Capacity Difference Plot Constructed by Linear Extrapolation of a Base Line from Below Tg

100% crystallinity heat capacity curve spanning the 240°K region. Subsequent construction of a ΔCp curve using this base line indicates that there is essentially no change in heat capacity of the non-crystalline material in this temperature range (Figure 9). The mechanism resulting in the heat capacity slope change at 240°K is unknown. However, the contribution to heat capacity from low frequency optical vibration between $2 - 5 \times 10^{-3}$ cps, which include the modes of C-C stretching and C-H bending, increases from 2% at 120°K to 40% at 400°K[66] and their activation may be responsible for the increase in heat capacity above 240°K.

The power of heat capacity difference plots for elucidation of small heat capacity changes superimposed upon a monotonically varying background is readily observable by comparison of the magnitude of changes in Figures 4 and 8 with Figure 9.

The use of encraty as a sensitive means of detecting transitions was convincingly illustrated by Dole[73]. Encraty is the calorimetric obtained quantity, Cp/T, transferable thermodynamically to $(dS/dT)_P$[74]. The advantage of using encraty, aside from sensitivity, is that it is obtained directly without possible confusing difference computations. Inspection of Figure 10 reveals that a step-change in heat capacity is observed at 145°K - corresponding to similar observations for other polymer glass transitions. The low temperature maximum in Cp/T near 50°K is commonly observed for hydrocarbons and has been previously observed for polyethylene[75]. However, a plot of the 240°K region (Figure 11) using scale units of the same size does not indicate any anomaly.

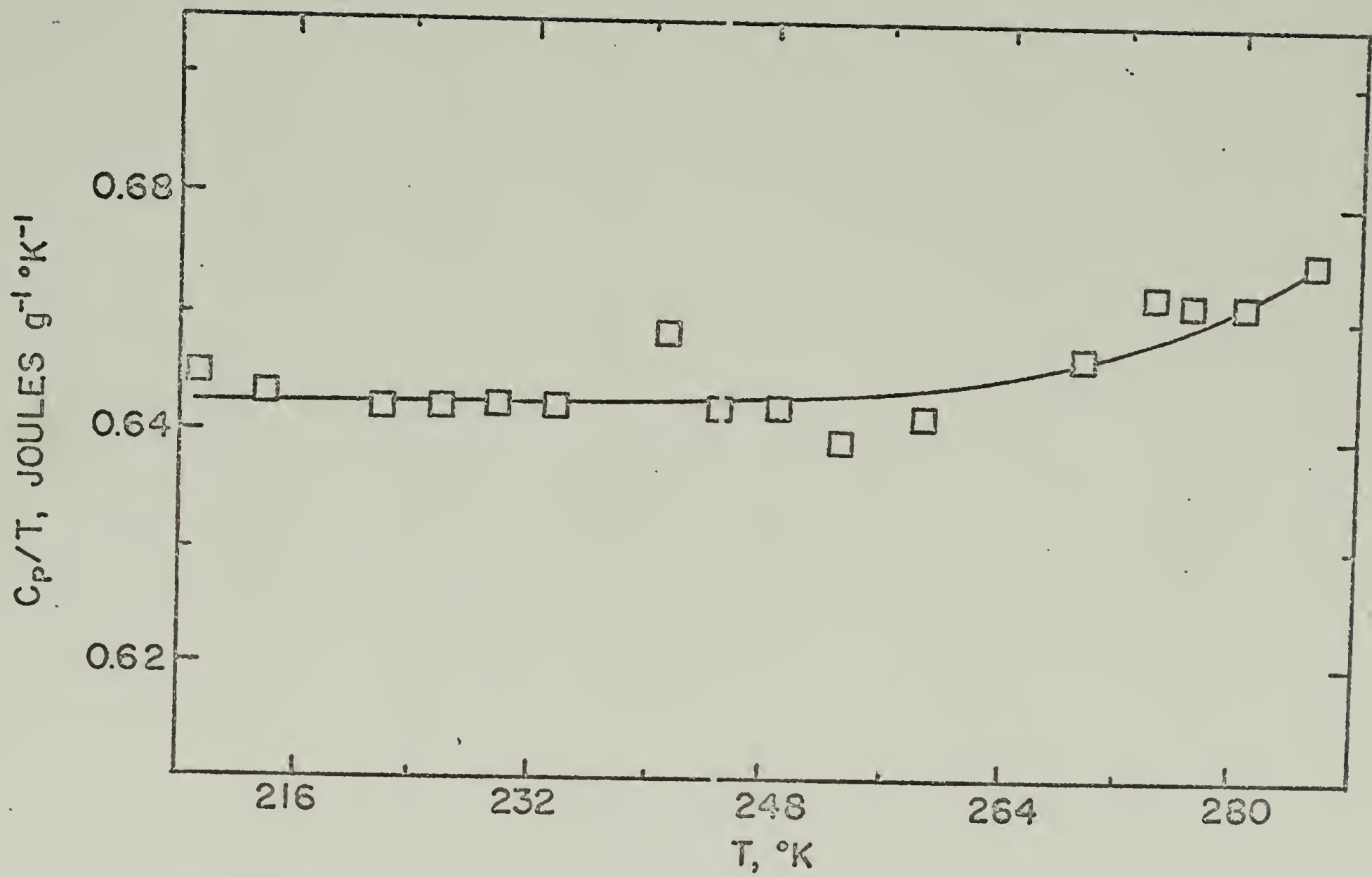

Figure 9

Variation of Encraty in the 240°K Region

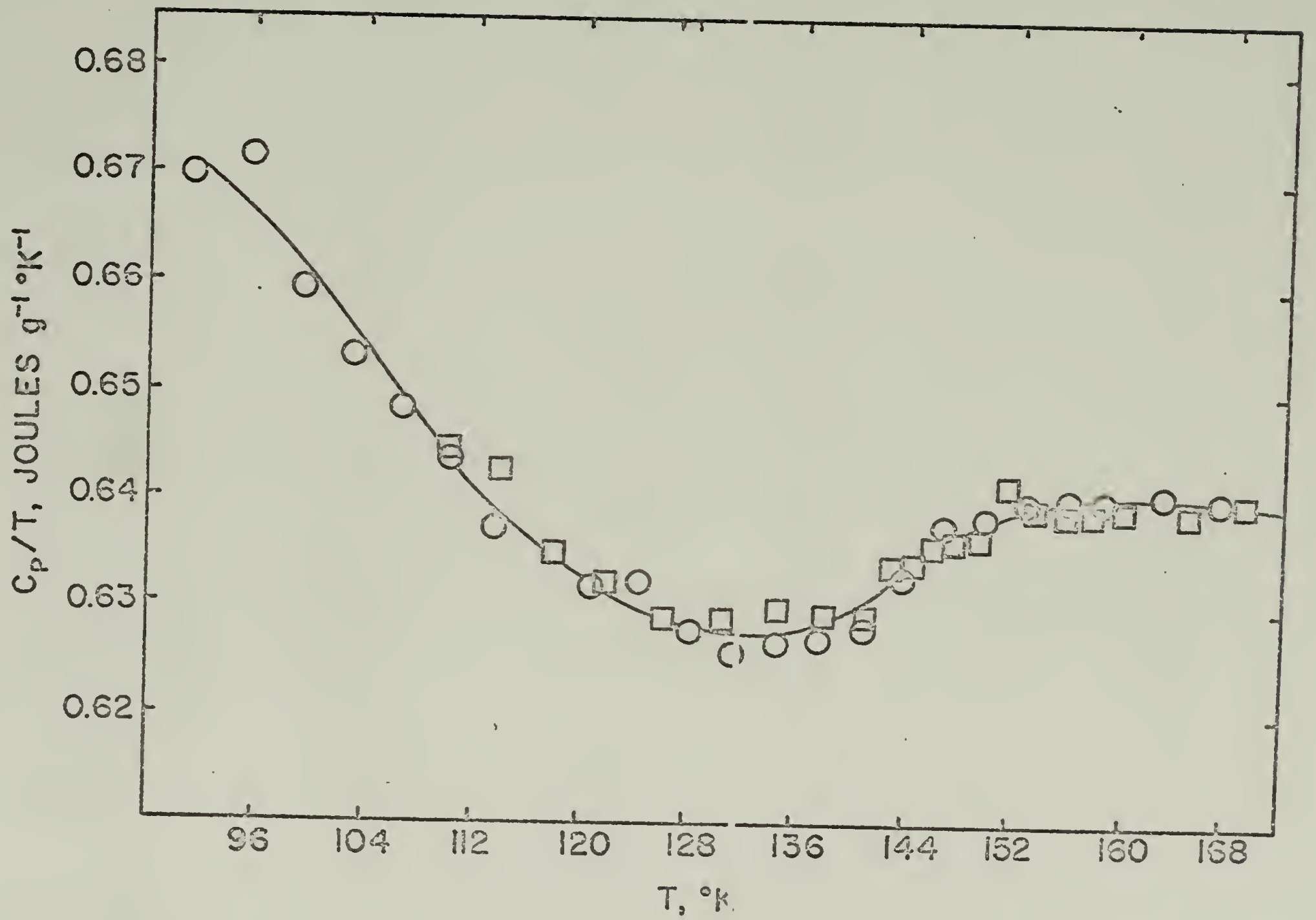

Figure 10

Encraty of Quenched Eight Million Molecular Weight Linear Polyethylene for the 145°K Region

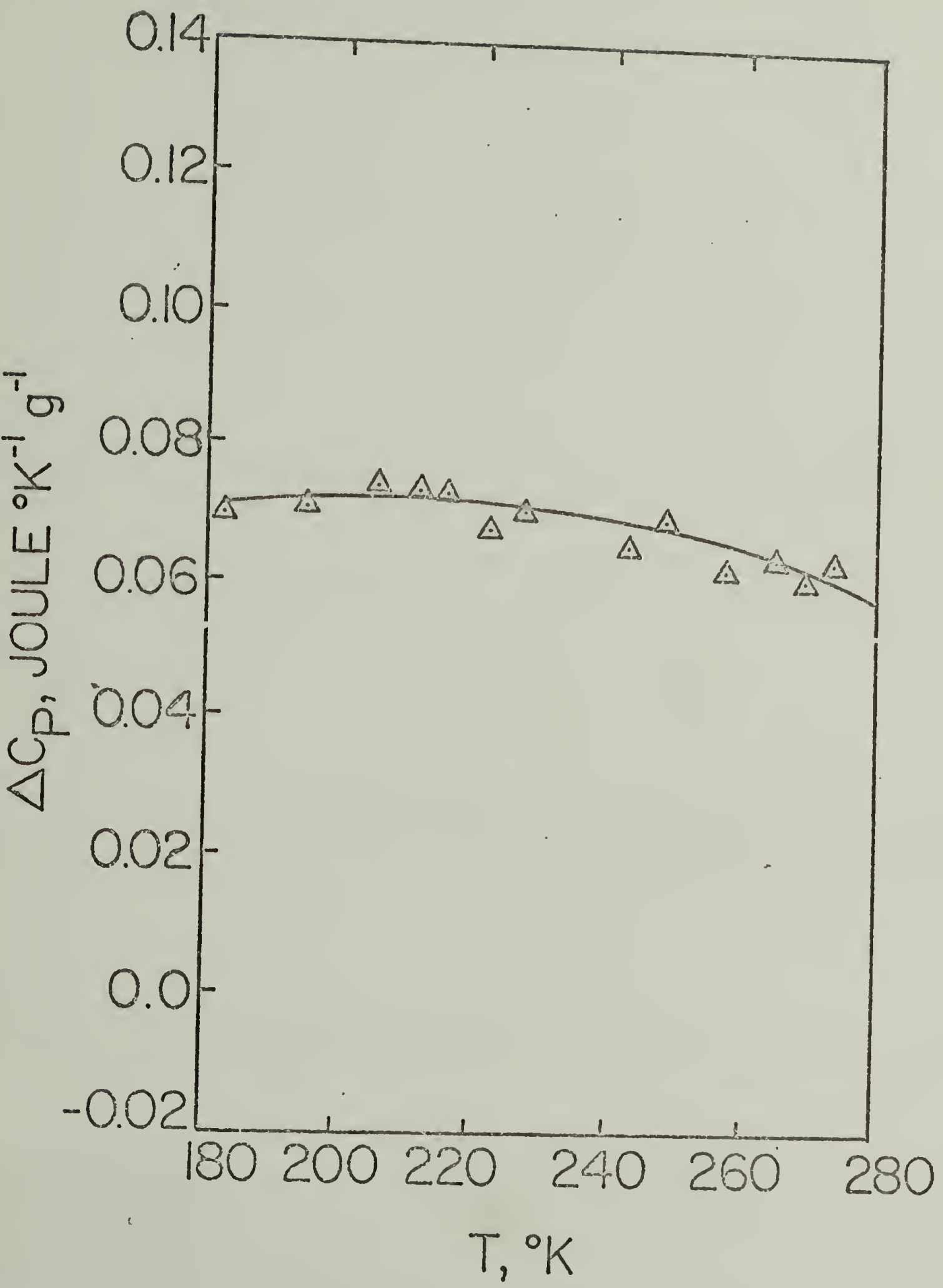

Figure 11

Heat Capacity Difference Plot Using the 80% Crystalline Curve for a Base Line.

The fact that no anomaly is observed at 145°K for the 80% crystallinity sample is initially perturbing. One would expect a linear relationship between the step-change at Tg and the amount of noncrystalline material present. O'Reilly and Karasz[76] indicated that such a linear relationship is often not observed and may be attributable to amorphous-crystalline interactions. Wunderlich[77] has divided polymer chains into "beads" relatable to units of motion in the liquid phase. Use of this method results in a relatively constant ΔCp/bead value for different observed values of ΔCp at Tg. The bead model ΔCp at Tg for polyethylene is 2.5 cal deg^{-1} $mole^{-1}$ or 3.75 joule $deg^{-1}gm^{-1}$ (assuming 28 gm/mole). The experimentally observed heat capacity differences at Tg for several semi-crystalline polymer including polyethylene are uniformly lower as indicated by the abscissa values in Figure 12. Note that heat required for fusion is plotted versus the observed ΔCp at Tg in Figure 12 and definite non-linearity is observed for a variety of semi-crystalline polymers. If true two phase behavior existed, the relationship between heat for fusion and ΔCp at Tg would be linear.

It is obvious from comparison with the other semi-crystalline polymers that polyethylene is not unusual in its behavior. Presently, a sample of approximately 20% crystallinity linear polyethylene is being investigated to further confirm the similarity of LPE behavior with that of other semi-crystalline polymers. The factors that interrelate the non-linear behavior for all these systems will be discussed later[78]. Sharma, Mandelkern and Stehling[79] have recently investigated the relationship of changes in linear and bulk coefficients

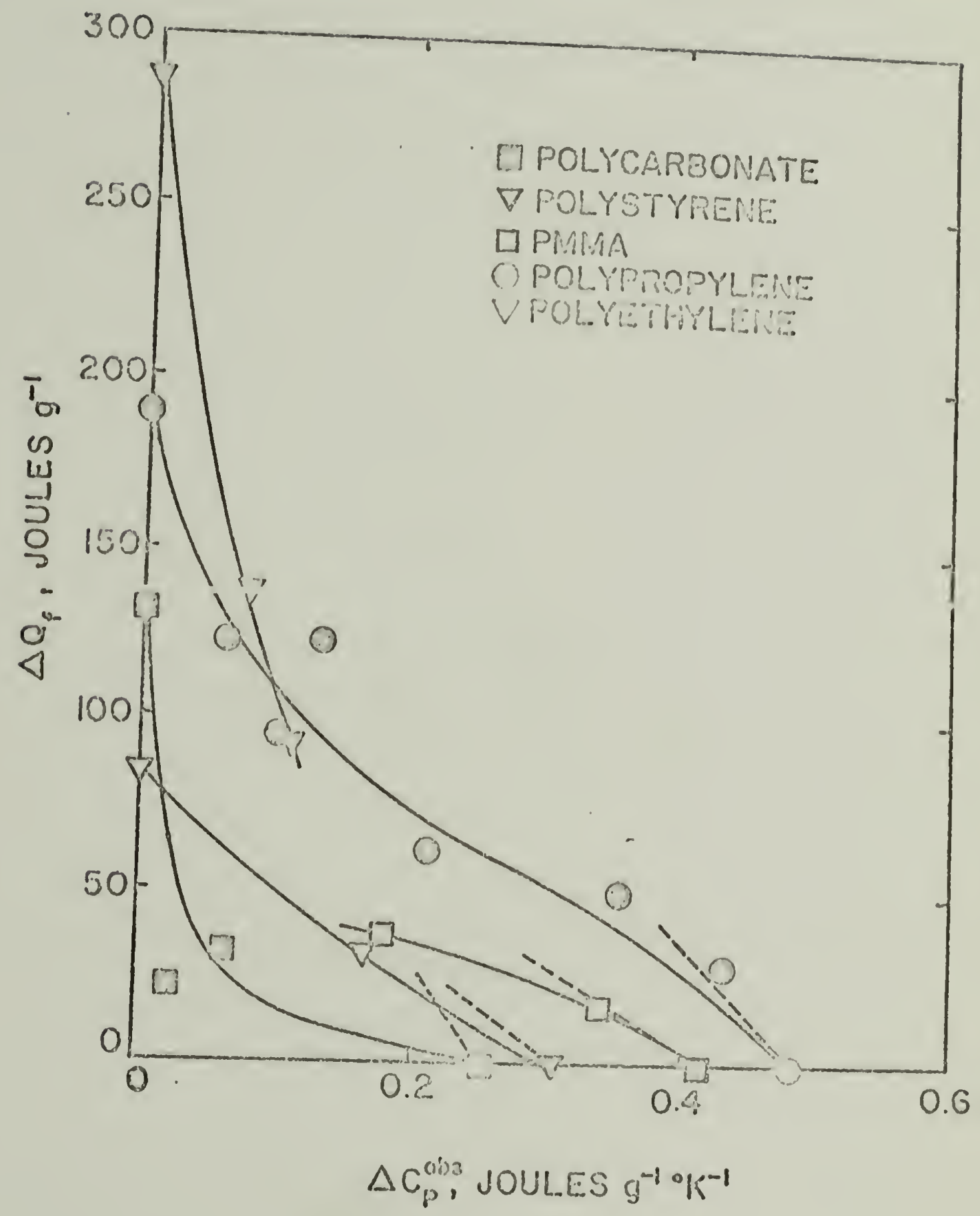

Figure 12

The Variation of Heat Capacity Difference at Tg
With the Energy Required for Fusion

of expansion with respect to Tg. They have shown that Tg and Tg products (i.e. $Tg\Delta\beta$ and $Tg\Delta\alpha$) do not yield a constant value of $\Delta\beta Tg = 0.113$ as proposed by Simha and Boyer[80]. However, trends of these functions seem obvious and we suggest that the observed deviations may be due, in part, to interaction effects as discussed above.

Although considerable confusion exists in the literature probably due primarily to variability in sample composition and preparation, it can be concluded based on the thermodynamic evidence presented here, that the glass transition of a highly linear polyethylene occurs at 145° ± 5°K. Equally clear based on other evidence is the conclusion that the glass transition of branched polyethylene is considerably different. On the basis of known experimental results, it is expected that the glass transition will gradually shift to lower temperatures as a function of the distribution and degree of branching. Also variation of morphological features may well result in different levels of crystalline - non-crystalline interaction. This area is currently being investigated as it may be possible to observe both transitions calorimetrically for appropriate samples. Also it seems reasonable that the γ and β relaxations arise from different molecular mechanisms based upon the molecular composition and environment of linear and branched material respectively.

REFERENCES

1. Boyer, R. F., Rubber Chem. Technol., 36, 1303 (1963).
2. McCrum, N. G., B. E. Read and G. Williams, "Anelastic and Dielectric Effects in Polymeric Solids", John Wiley & Sons, Inc., New York, New York (1965).
3. McKenna, L. W., T. Kajiyama and W. J. MacKnight, Macromolecules, 2, 58 (1969).
4. Stehling, F. C. and Mandelkern, L. Macromolecules, 3, No. 2, 242 (1970).
5. Kline, D. E., J. A. Sauer and A. E. Woodward, J. Polymer Sci., 22, 455 (1956).
6. Stachurski, Z. H. and I. M. Ward, J. Macromol. Sci. Phys., B3 (3), 445 (1969).
7. Bohn, V. L., Kolloid-Z., 194, 10 (1964).
8. Eby, R. K., and J. P. Colson, J. Account. Soc. Amer., 39, 505 (1966).
9. Sinnott, K. M., J. Appl. Phys., 37, 3385 (1966).
10. Pechhold, W., V. Eisele and G. Knauss, Kolloid-Z, 196, 27 (1964).
11. Illers, V. K. H., Rheol. Acta, 3, 202 (1964).
12. Kline, D. E., J. A. Sauer, and A. E. Woodward, J. Polym. Sci., 22, 455 (1956).
13. Crist, B., and A. Peterlin, J. Macromol. Sci. Phys., B4 (2), 791 (1970).
14. Nielsen, L. E., J. Polym. Sci., 42, 357 (1960).
15. Schnieder, K. and K. Wolf, Kolloid-Z, 134, 149 (1953).

16. Ohlberg, S. M. and S, S. Fenstermaker, J. Polym. Sci., 32, 514 (1958).

17. Zakin, J. L., R. Simha and H. C. Hershey, J. Appl. Polymer Sci., 10, 1455 (1966).

18. Illers, K. H., Kolloid-Z., 190, 16 (1963).

19. Tobolsky, A. V., "Properties and Structure of Polymers, "Reinhold Publishing Corp., N. Y., 1962.

20. Kantos, E. G. and W. P. Slichter, J. Polymer Sci., 61, 61 (1962).

21. Manaresi, P. and V. Giannello, J. Appl. Polymer Sci., 4, 251 (1960).

22. Baldi, L. and R. Zannetti, Matere Plastiche Elastomers, 31, 1309 (1965).

23. Miller, A. A., J. Polymer Sci., A-2, 6, 249 (1968).

24. Maurer, J. J., Rubber Chem. Technol., 38, 979 (1965).

25. Nielsen, L. E., J. Polymer Sci., Part C, 16, 2379 (1967).

26. Dannis, M. L., J. Appl. Polymer Sci., 1, 121 (1959).

27. Kawaguchi, T., J, Appl. Polymer Sci., 2, 56 (1959).

28. Boyer, R. F., to be published.

29. Hager, N. E. Jr., Rev. of Sci. Instr., 35, No. 5, 618 (1964).

30. Hoffman, J. D., G. Williams and E. Passaglia, J. Polymer Sci., Part C, 14, 173 (1966).

31. Takayanagi, M., Proc. Intern. Congr. Rheol., 4-5, Kyoto, Japan, 1963, 161 (1965).

32. Gray, R. W. and N. G. McCrum, J. Polymer Sci., A-2, 7, 1329 (1969).

33. Schatski, T. F., Bulletin of Am. Phys. Sci., Series II, 16, No. 3, CK4, 364 (1971).

34. Willbourn, A. H., Trans. Faraday Soc., 5, 4717 (1958).

35. Koleske, J. V. and R. D. Lundberg, J. Polymer Sci., A-2, 10, 323 (1972).

36. Faucher, J. A. and J. V. Koleske, Polymer, 8, 44 (1967).

37. Stehling, F. C. and L. Mandelkern, Macromolecules, 3, No. 2, 242 (1970).

38. Bergmann, V. K. and K. Nawotki, Kolloid-Z., 219, 131 (1967).

39. Davis, G. T., NBS, to be published.

40. Tsuge, K., H. Enjoji, H. Terada, Y. Ohzawa, and Y. Wada, Japan, J. Appl. Phys., 1, 270 (1962).

41. Olf, H. G. and A. Peterlin, Kolloid-Z., 215, 7 (1967).

42. Shen, M. and E. H. Cirlin, J. Macromol. Sci., Phys., B4 (4), 942 (1970).

43. Crissman, J. M. and H. Passaglia, J. Appl. Phys., 42, No. 12, 4636 (1971).

44. Schneider, B., H. Picova and D. Doskocilova, Macromolecules, 5, No. 2, 120 (1972).

45. Tang, L. H. and S. Bucksen, J. Phys. Chem., 62, 1530 (1958).

46. Fatou, J. G. and L. Mandelkern, J. Phys. Chem., 69, 417 (1965).

47. Margolis, A. F., Allied Chemical Corp., private communication.

48. Natta, G., AHi. Accad. Nazi, Lincei, Rend., 8 (8), 11 (1957).

49. Prudhomme, R., Univ. of Mass., private communication.

50. Misra, A., Univ. of Mass., private communication.

52. O'Reilly, J. M. and F. E. Karasz, to be published.

53. Karasz, F. E. and J. M. O'Reilly, Res. Sci, Instr., 37, No. 3, 255 (1966).

54. Beatty, C. L., Ph.D. Thesis, Univ. of Mass., (1972).

55. Dainton, F. S., D. M. Evans, F. E. Hoare and T. P. Melia, Polymer, 3, 286 (1962).

56. Beatty, C. L. and F. E. Karasz, to be published.

57. Magill, J. H., S. S. Pollack, and D. P. Wyman, J. Polymer Sci., 3, 3781 (1965).

58. Wunderlich, B. and H. Baur, Adv. Polymer Sci., 7, 151 (1970).

59. Reese, W., J. Macromol. Sci. Chem., A-3 (7), 1257 (1968).

60. Chang, S. S., ACS Polymer Preprints, 13, No. 1, 322 (1972).

61. Chang, S. S., private communication.

62. Chang, S. S. and A. P. Bestul, to be published.

63. Fischer, E. W. and F. Kloos, J. Polymer Sci., B, 8, 685 (1970).

64. Lowell, P. N. and N. G. McCrum, J. Polymer Sci., 9, 477 (1971).

65. Fyans, R., Perkin-Elmer Corp., private communication.

66. Wunderlich, B., J. Chem. Phys., 37 (10), 1203 (1962).

67. Jackson, J. F. and T. S. Hsu, ACS Polymer Preprints, 12, No. 2, 726 (1971).

68. Boerio, F. J. and J. L. Koenig, J. Chem. Phys., 52, No. 7, 3425 (1970).

69. Turley, S. G. and H. Keskkula, J. Polymer Sci., C, No. 14, 69 (1966).

70. Modena, M., C. Garbuglio and M. Ragazzini, J. Polymer Sci., 10, 153 (1972).

71. Weeks, N., private communication.

72. Kwei, T. K., T. T. Wang, and H. E. Bair, J. Polymer Sci., C, No. 3, 87 (1970).

73. Smith, C. W. and M. Dole, J. Polymer Sci., 20, 37 (1956).

74. Dole, M., Kolloid-Z, 165, 40 (1959).

75. Dole, M. and B. Wunderlich, Makromolekulare Chem., 34, 29 (1959).

76. O'Reilly, J. M. and F. E. Karasz, ACS Polymer Preprints, 5, No. 2, 351 (1964).

77. Wunderlich, B. and L. D. Jones, J. Macromol. Sci. Phys., B3 (1), 67 (1969).

78. Beatty, C. L. and F. E. Karasz, to be published.

79. Sharma, S. C., L. Mandelbern and F. C. Stehling, J. Polymer Sci., 10, 345 (1972).

80. Simha, R. and R. F. Boyer, J. Chem. Phys., 37, 1003 (1962).

CHAPTER II

CALORIMETRIC DETERMINATION OF THE SUB-GLASS TRANSITION OF POLYCYCLOHEXYLMETHACRYLATE

C. L. Beatty* and F. E. Karasz
Polymer Science and Engineering Department
University of Massachusetts
Amherst, Massachusetts 01002

INTRODUCTION

A. CLASSIFICATION OF THERMODYNAMIC TRANSITIONS

Thermodynamic analysis of transitions is the classical definitive test of the nature of transformations of all materials including polymers. However, polymeric systems exhibit maxima via resonance techniques that are not always resolvable in heat capacity measurements. This is particularly true for sub-Tg transitions. The rationalization is that the specific heat includes all modes of motion from very low frequencies to optical frequencies, thereby masking small diffuse transitions. Therefore, there is a reduction in the capability of detection of transformations that are not either (1) cooperative or (2) do not have both a large potential energy barrier and a large energy difference between states.

The observed heat capacity anomalies may be classifiable as a first-order (melting), a second-order (glass transition), a lambda, and a Schottky transformation. First order thermodynamic

* Present Address: Xerox Corporation, Webster, New York 14580

transitions are invariably easily detectible for polymers and are characterized by a discontinuity in Cp via adiabatic calorimetry. Melting is a cooperative transition perturbed by finite crystal size, crystal perfection and molecular weight heterogeneities[1]. The glass transition is readily observable for amorphous polymers but the characteristic step-change in Cp may be significantly reduced by crystallinity[2,3]. Lambda anomalies arise when the disordering phenomena is cooperative and result in different slopes above and below the transition as well as a discontinuity in the second-order derivatives at T_λ. In contrast, Schottky transformations occur when the order-disorder phenomena is non-cooperative[4] and are characterized by a rounded diffuse maximum in Cp as opposed to the sharp discontinuous peak observed for lambda and first-order transitions. Schottky ΔCp anomalies have been observed in gases[5], metals[6], and molecular organic compounds[7] but not in polymeric systems to the best of our knowledge. Although current investigation of the smectic to monoclinic polypropylene transformation of polypropylene indicates that it may also fall into this general glass of thermodynamic transitions. However, if sub-Tg relaxation maxima detected by resonance techniques may be relatable to pendant group motions as reported[8,9,10], then it is reasonable to assume that thermodynamic cooperativity between these groups, being separated by the polymer chain would be weak if not absent. Consequently, a sub-Tg transition due to pendant group motion would be expected to exhibit a Lambda anomaly if cooperativity occurred and a Schottky

anomaly if the motions occurred in an uncooperative manner - providing the detectibility criteria set forth earlier is obeyed.

B. POLYCYCLOHEXYLMETHACRYLATE BACKGROUND

In an effort to test this line of reasoning, the cyclohexyl chair-chair transformation of polycyclohexylmethacrylate, PCHMA, appeared to meet those criteria satisfactorily. Figure 1 illustrates that in the chair conformation of cyclohexane two geometrically distinct types of carbon-hydrogen bonds are present. Six of the C-H bonds (Fig. 1a i) are parallel to the three fold axis of symmetry and are called axial. The other six positions (Fig. 1a ii) are approximately in an equatorial belt around the three-fold axis and hence are called equatorial. As soon as a substituent is introduced into the cyclohexane ring, the molecule may adopt a preferred chair conformation with the substituent, either axial or equatorial. Owing to repulsive nonbounded interaction between axial groups, the equatorial conformation is generally favored[10,11,12]. Hoff, Robinson and Wilbourn[13] initially observed dynamic mechanical loss maxima in PCHMA at about -80°C at 1 Hz that was absent in polyphenylmethacrylate and attributed the transition to the chair-boat conformational change. However, Karpovich[14], Lamb and Sherwood[15] identified that the corresponding ultrasonic dispersion occurred only for cyclohexyl derivatives for which the two chair forms are not identical and concluded that it was a chair-chair and not a chair-boat transformation. Supporting data from low molecular weight compounds indicate that the stability order is chair >

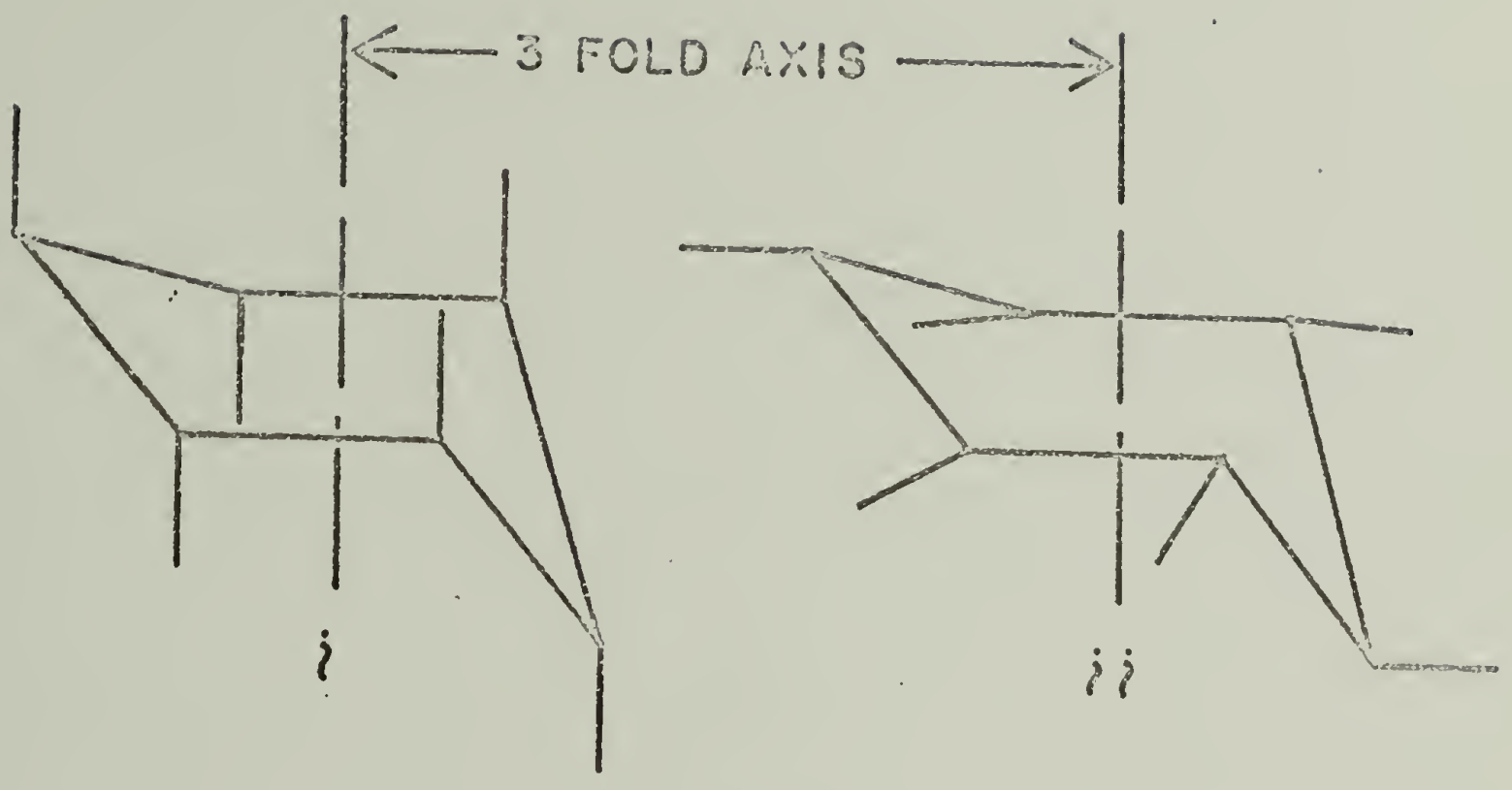

(a)

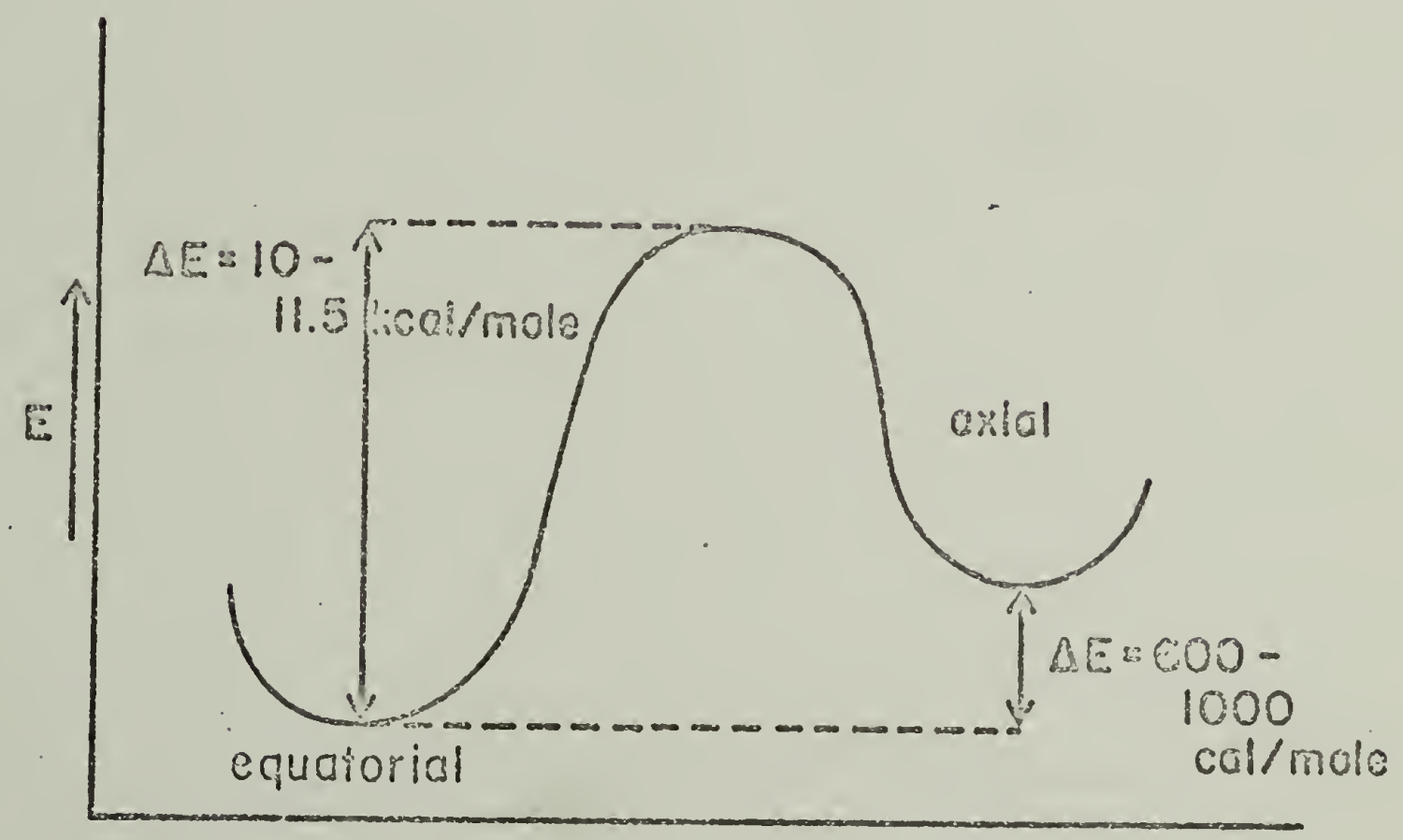

(b)

Figure 1

(a) The Axial and Equatorial Positions of the Chair Conformation.
(b) A Schematic Description of the Energies Involved in the Interconversion of the Conformers.

twist-boat > boat[33]. Subsequent dielectric and mechanical loss measurements by Heijboer[16-18] and Ishida[19] have confirmed the existence of this transition in PCHMA and cyclohexane halogen derivatives and led to the conclusion that the cyclohexyl dispersion was independent of molecular environment (i.e. viscosity and/or free volume). Confirming proton spin lattice relaxation data shows a maximum in relaxation time, τ_1, in PCHMA compared to no maximum for polyphenylmethacrylate[20]. Frosini et al. have examined series of polymers of different chemical construction but having a common cyclohexyl pendant group[21]. All of these polymers, except for polyvinylcyclohexane exhibit the chair-chair transformation. The range of observed activation energies ranges from 10 to 11.5 Kcal/mole providing an appreciable barrier to interconversion of the two forms. Also, measurements on low molecular weight ethers and esters indicate an energy level difference of 600-1000 cal/mole between the two states[22]. Using the two-level model proposed earlier[23] for calculating low temperature specific heat anomalies, an interconversion of the two chair forms might be expected between 120° - 200°K. As previously noted[24], high precision adiabatic calorimetry has particular advantage in that measurements of slow and/or small thermal energy changes are possible.

EXPERIMENTAL

A. SAMPLE

A sample of atactic polycyclohexylmethacrylate was purchased

from Cellomer Associates Inc., Webster, New York. The sample, after crushing to a fine powder, was vacuum dried for 46 hours prior to loading. Elemental analysis confirmed the chemical composition and purity precluding further purification. The molecular weights M_n, M_w, and M_z and distribution, $\frac{M_w}{M_n}$, were determined by GPC using tetrahydrofuran at 34°C. In addition, M_n was determined by membrane osmometry in dioxane at 37°C. A Laue x-ray diffraction photograph was obtained with a General Electric XRD-5 source using filtered radiation from a 5 mil sample cooled at a rate of ~10°C hr. through the glass transition. A 10 hours exposure was made at room temperature using a vacuum Laue camera described elsewhere[25] and V_2O_5 filtered C_n K_α radiation.

B. CALORIMETRIC

The high precision adiabatic calorimeter used is a modified version of the basic design described elsewhere[26]. In the present study, liquid nitrogen was used as the external refrigerant.

The sample and a small quantity of helium, to enhance thermal equilibration, were sealed in the silver calorimeter cell. The calorimetric mass of the sample was 46.332 g. Cooling rates were in the ranges 0.6 to 40 deg hr^{-1} and an intermittant heating technique with intervals of 2 to 10°C was used with a typical heating rate of 4 to 8 deg hr^{-1}. Equilibration times were normally less than 20 minutes.

RESULTS

Two series of measurements were over the temperature range for which the chair-chair interconversion was expected. After cooling at an average rate of ~25 deg hr^{-1} to 77°K, the sample was held at this temperature for ~20 hours prior to heating. The subsequent series of measurements were made after cooling at an average rate of ~20 deg hr^{-1} from 220°K to 115°K. The sample was equilibrated for 12 hours at 115°K prior to reheating. The experimental heat capacities are recorded in Tables 1 and 2 and are plotted in Figure 2. For comparison purposes, the data for atactic, isotactic, and syndiotactic polymethylmethacrylate, PMMA, obtained previously with this apparatus[27] are also plotted in Figure 2. The isotactic and syndiotactic data are shifted up by 0.05 and 0.1 joules g^{-1} $°K^{-1}$ respectively for clarity as the two sets of data essentially superimpose as reported previously[28].

Both upper and lower linear segments of the PCHMA low temperature data can be represented by the equation $Cp = a + bT$. Both curves were fit to the data by a least squares orthogonal polynomial via computer techniques. The equation for the higher temperature region was used to calculate the extrapolated Cp values at the temperatures for the lower temperature data points. These computed Cp values were in turn substracted from the experimental Cp data to obtain the ΔCp plot of Figure 3.

Since the same sample is in equilibrium before and after each run, additional thermodynamic quantities may be calculated.

PCHMA

Temperature °K	Heat Capacity Absolute Joules g^{-1} $°K^{-1}$
91,8863	0.4594
98,0607	0.4815
103,7306	0.5076
109,3979	0.5329
114,9511	0.5563
120,6714	0.5802
126,4818	0.6061
132,0698	0.6305
137,3157	0.6545
148,0648	0.7045
153,1976	0.7248
158,6115	0.7473
164,4281	0.7770
169,9160	0.7914
174,6575	0.8128
178,8425	0.8294
182,9548	0.8466
186,7618	0.8622
190,2792	0.8699
193,6289	0.8833

Table I

Polycyclohexylmethacrylate Heat Capacity at Various Temperatures for the First Run

Table 1 cont.

196,7275	0.8938
199,7659	0.9092
202,8489	0.9221
206,5578	0.9405
210,4622	0.9567
213,9541	0.9730

Temperature °K	Heat Capacity Absolute Joules g^{-1} $°K^{-1}$
117,9708	0.5721
122,0246	0.5875
125,8602	0.6041
129,7168	0.6202
133,3650	0.6353
137,1301	0.6505
141,2776	0.6688
145,4007	0.6886
149,4359	0.7075
153,4119	0.7242
157,4552	0.7420
161,3878	0.7591
165,1312	0.7731
168,9584	0.7905
172,6298	0.8034
176,2038	0.8170
179,7990	0.8349
183,1354	0.8455
186,2548	0.8559
189,5325	0.8728
192,7208	0.8836
195,9578	0.8970

Table 2

Polycyclohexylmethacrylate Heat Capacity at Various Temperatures for the Second Run

Table 2 cont.

199,1810	0.9085
202,3792	0.9226
205,5298	0.9385
208,5048	0.9479
211,5819	0.9667
214,6009	0.9753
217,4920	0.9907
220,5035	1.0014
224,0091	1.0107
228,1287	1.0377
229,6234	1.0351
245,0365	1.1015
251,4396	1.1280
260,1417	1.1630
266,8822	1.1939
270,6953	1.2128
274,7482	1.2297
279,2398	1.2482
284,4440	1.2723
289,3194	1.2960

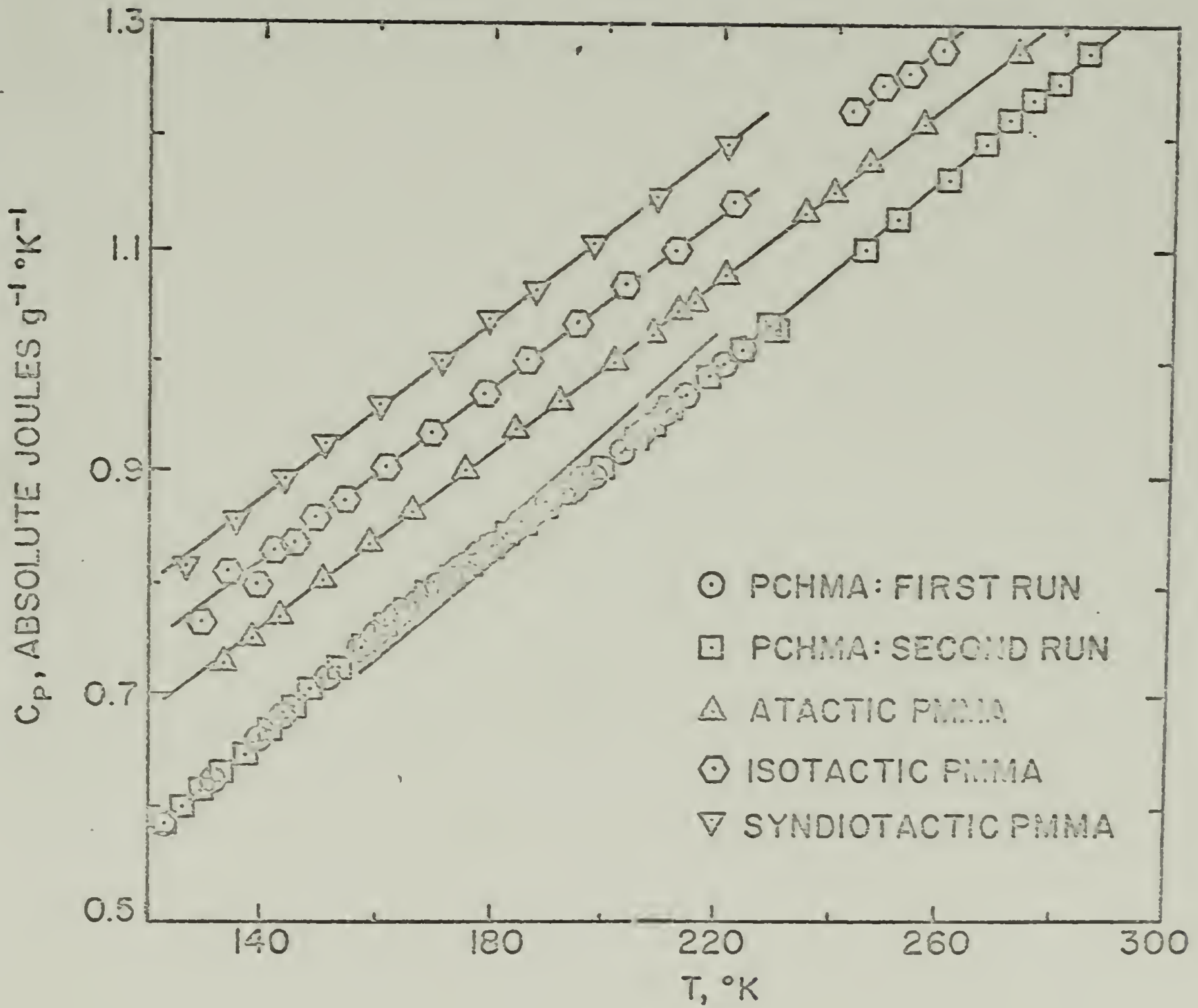

Figure 2

Heat Capacities of PCHMA and PMMA Via Adiabatic Calorimetry. Isotactic and Syndiotactic PMMA are Shifted Upward by 0.05 and 0.1 joule g^{-1} °K^{-1} Respectively for Clarity.

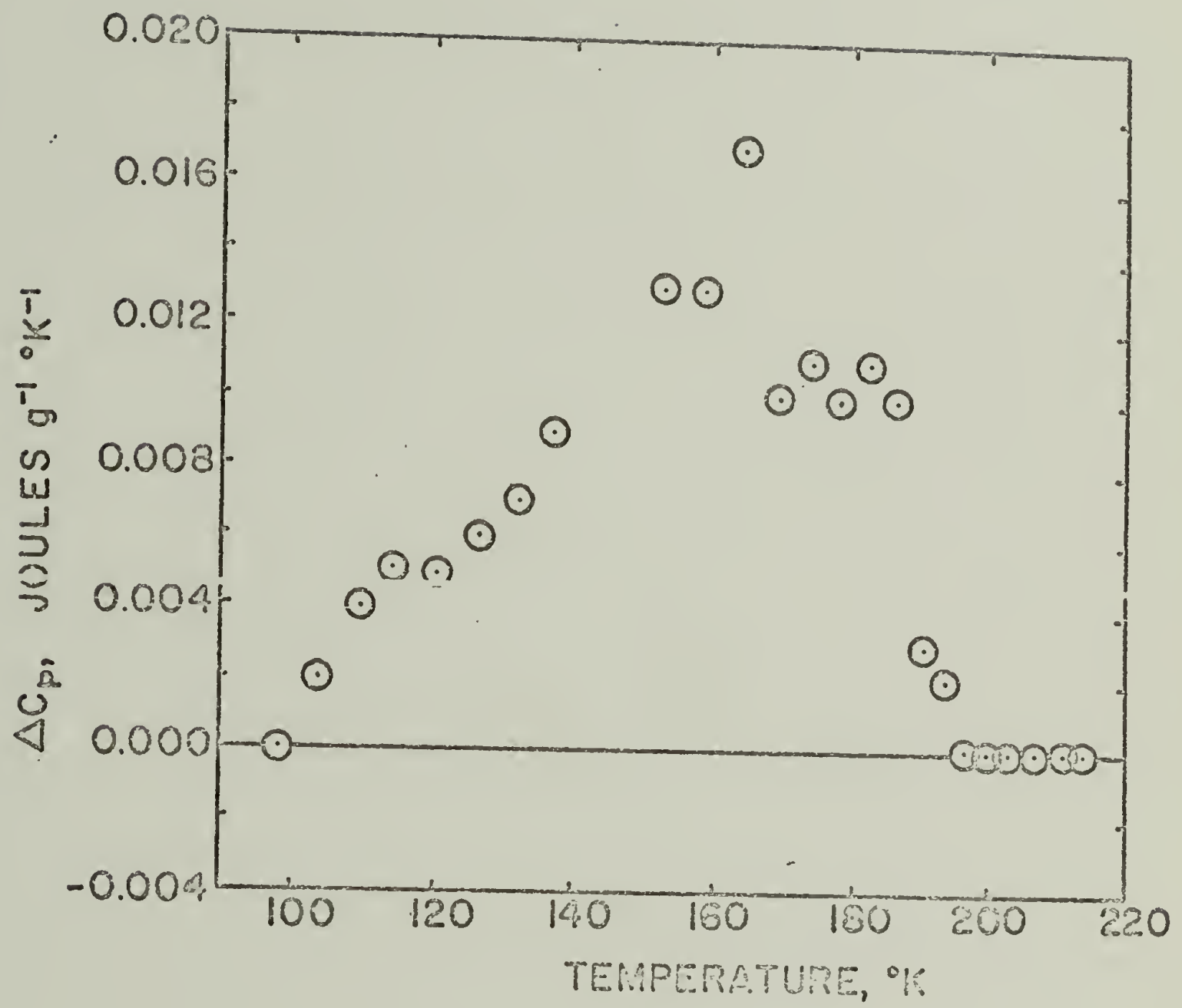

Figure 3

Difference Cp Plot, Obtained as Described in the Text, Illustrating the Transition Breadth.

Figure 4 illustrates the manner in which the encraty quantity CpT^{-1} or (dS)/(dT) changes over the temperature range of interest for PCHMA we well as atactic, isotactic and syndiotactic PMMA[27,28].

The lack of crystallinity at room temperature is illustrated by the Laue x-ray diffraction photograph in Figure 5. It has previously been reported that PCHMA has a bimodal molecular weight distribution[29]. However, our GPC results indicate that this sample has an unimodal molecular weight distribution with a $\overline{M}_n$ of 47,000 compared to a value of 42,100 obtained from membrane osmometry.

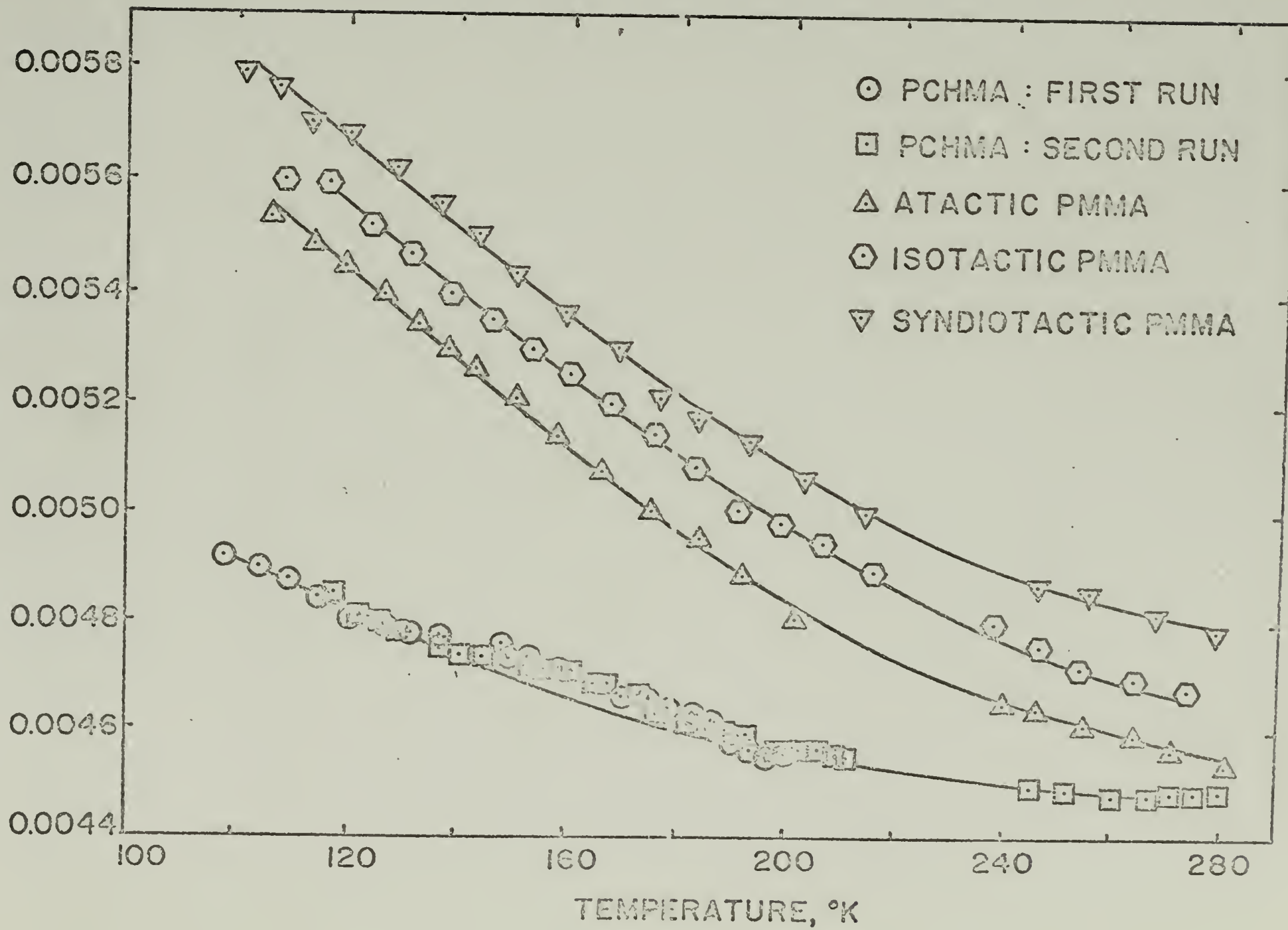

Figure 4

Encraty of PCHMA and Various Tacticity PMMA's.
Isotactic and Syndiotactic PMMA are Shifted to Enhance Clarity.

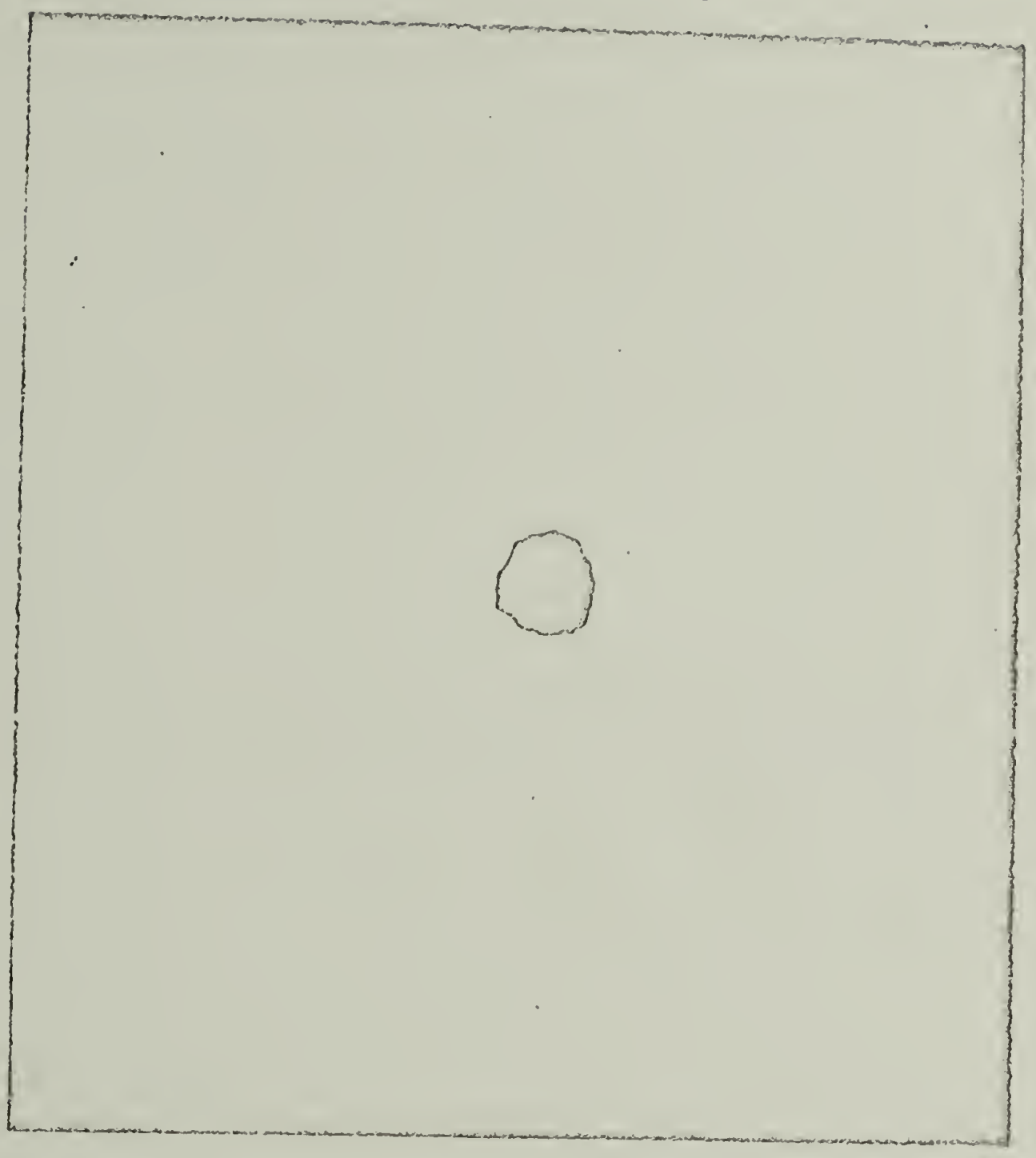

Figure 5

Laue Photograph of PCHMA
Exposed at Room Temperature for 10 Hours.

DISCUSSION

As discussed earlier, sub-Tg relaxations attributable to motions of particular chemical groups, have been observed by various techniques. However, Cp measurements in the past[8,9,10] failed to identify these modes of relaxation presumably because of the general non-cooperativity and small ΔE of these processes. Based on calculations from a two-level model, an anomaly exhibiting a maximum in Cp was expected for the chair-chair transformation of PCHMA. The data obtained in Figure 2 initially was interpreted as a step-change decrease in heat capacity at -193°K. Although the ΔCp is small (~2%), the precision and reproducibility of the data ($\pm$ 0.1%) is sufficient to warrant consideration of such changes. The observed transition could be interpreted as the freezing of the chair conformation in the higher energy axial conformation during cooling which, during subsequent heating, would achieve sufficient energy to overcome the potential barrier between states (Figure 1) resulting in a conversion to the more stable equatorial state from the metastable higher energy axial state.

Note that the data of isotactic, syndiotactic and atactic PMMA (also obtained on this instrument) are included to illustrate that the observed PCHMA anomaly is absent. The only difference in chemical construction of these molecules is that in PCHMA, the cyclohexyl group is substituted for the methyl group on the side chain of PMMA (Figure 6). Consequently, comparisons of these two

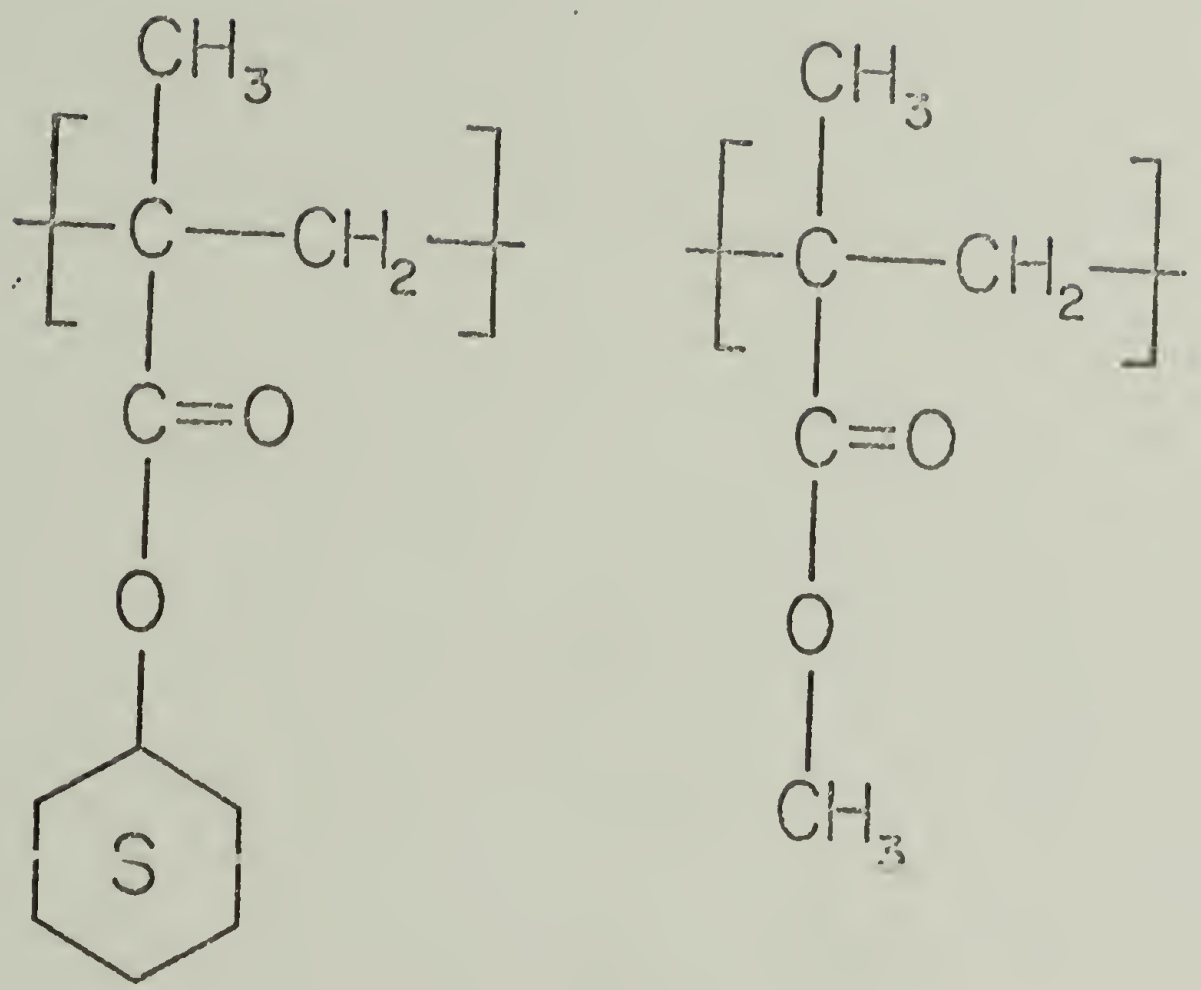

(a) (b)

Figure 6

Repeating Units of: a) Polycyclohexylmethacrylate
and b) Polymethylmethacrylate.

species should reflect that difference - especially for the atactic configurations - being not perturbed by crystallinity.

The encraty, C_p/T, has been demonstrated to be more sensitive to transitions than other thermodynamic quantities[30]. A plot of encraty, Figure 3, indicates that a diffuse maximum is obtained centered at about 165°K for PCHMA whereas this function decreases monotonically over the same temperature range for the PMMA samples of various tacticities. Consequently a ΔCp plot was constructed, as described in the result section, and a diffuse rounded maximum at approximately 165°K was obtained (Figure 4). The x-ray diffraction photograph (Figure 5) confirms that the sample is non-crystalline at room temperature.

The chair-chair transformation, as previously mentioned, may be represented by a two-state system with the two states separated by ΔE. Neglecting the known potential barrier for the present, at $T << \Delta E/_k$, the upper level will be scarcely populated whereas at $T >> \Delta E/_k$ both levels will be nearly equally populated. Only in the range of temperatures where $\Delta E/_k$ is roughly equal to T, will transitions from one level to the other occur in appreciable amounts. This rapid charge in internal energy would correspond to a specific heat maxima with contribution from this transition becoming zero at both high and low temperatures. This maxima would be superimposed on the lattice and other contributions to the specific heat at that particular temperature.

Assuming that the internal energy attributable to the cyclohexyl group may be represented by the following equation:

$$E = N_o e_o + N_1 e_1 \qquad (1)$$

where N and e are the population and energy level of state respectively with the subscripts o and 1 referring to the lower and upper energy levels respectively. Then

$$N_o/N_1 = \exp\ (\Delta E/_{kT}) \qquad (2)$$

$$\text{where } \Delta E = e_1 - e_o \qquad (3)$$

and the specific heat is

$$C_v = \frac{\partial E}{\partial T} = \frac{N k (\Delta E/_{kT})^2 \exp\ (\Delta E/_{kT})}{(1 + \exp\ (\Delta E/_{kT})^2} \qquad (4)$$

The value of ΔE, determined for low molecular weight compounds, is 600 - 1000 cal/mole (Figure 1). The lower value of ΔE, probably high for this solid state low temperature transition, and the experimentally determined peak temperature of 165°K were used to estimate the expected ΔCp from this simple model. A value of 5.3 joule. mole^{-1} degree^{-1} is obtained. The ΔCp observed is 0.014 joule. gram^{-1} degree^{-1} (Figure 4) or 2.4 joule. mole^{-1} degree^{-1} based on the monomer unit of PCHMA illustrated in Figure 5. However, if this latter value is adjusted to represent moles of the cyclohexyl group, then the observed ΔCp is 4.8 joule. mole^{-1} degree^{-1} which is in rather good agreement with the value of 5.3 joule. mole^{-1} degree^{-1} calculated from the very simple two energy level model.

A more exact model which may account for the diffuseness of the transition is now considered by introducing the concept of multiplicity of energy levels or degeneracy. Using Boltzman statistics, since it is a model containing N <u>independent</u> particles of energy levels e_o, e, = $\cdot\cdot$ e_m with degeneracy d_o, d_1 $\cdots\cdot$ d_m, the average internal energy at temperature, T is

$$E = \frac{\sum_{i=o}^{m} e_i d_i \exp(-e_i/kT)}{\sum_{i=o}^{m} d_i \exp(-e_i/kT)} \qquad (5)$$

Again recalling that the specific heat is $\frac{dE}{dT}$ and that for a two-level system

$$E = \frac{N d_i e_i \exp(-e_i/kT)}{d_o + d_i \exp(-e_i/kT} \qquad (6)$$

then the specific heat is

$$C = \frac{Ne_1^2}{kT^2} \frac{d_o}{d_1} \frac{\exp(e_1/kT)}{[1 + \frac{d_o}{d_1} \exp(e_1/kT)]^2} \qquad (7)$$

For $T << \frac{e_1}{k}$ (i.e. below the transition)

$$C = \frac{Ne}{kT^2} \frac{d_o}{d_1} \exp\left(-\frac{e_1}{kT}\right) \qquad (8)$$

For $T >> \frac{e_1}{k}$ (i.e. above the transition)

$$C = \frac{N}{k} d_o d_1 \frac{1}{(d_o+d_1)^2} \left(\frac{e_1}{kT}\right)^2 \qquad (9)$$

The specific heat goes through a maximum when:

$$\frac{dC}{dT} = 0 \quad \text{or} \quad \frac{d_o}{d_1}\left(\exp\left(\frac{e_1}{kT_{max}}\right)\right) = \frac{\frac{e_1}{kT_{max}} + 2}{\frac{e_1}{kT_{max}} - 2} \tag{10}$$

Substituting back into equation 5, the maximum specific heat is

$$\Delta C_{max} = \frac{N}{4K} T_{max}\left[\left(\frac{e_1}{kT_{max}}\right)^2 - 4\right] \tag{11}$$

Using values of T_{max} = 165°K and e_1 = 800 cal/mole, the $\frac{d_o}{d_1}$ ratio is calculated to be approximately 1.5 from equation 6. The ΔC_p at the peak maximum is calculated to be ~5 joule/mole/deg using equation 11. These values are in good agreement with the experimental and the simple model estimates of 5.3 joule/mole/deg and 4.8 joule/mole/deg respectively.

The entropy change is represented by the equation

$$\Delta S = R \ell n \left(1 + \frac{d_1}{d_o}\right)$$

and is ~7.6 joules/mole/deg. The experimental equivalent calculated from the integral of the $\frac{C_p}{T}$ vs T plot (Figure 4) is ~1.6 joules/mole/deg calculated on a basis of pure cyclohexyl groups. Using the ΔS expression for back-calculation, value of e_1 can be calculated by using the peak temperature of 165°K and equation 10. The energy difference between states calculated in this manner is ~980 cal/mole which is in the range 600 - 1000 cal/mole previously determined for low molecular weight compounds.

Consequently, based upon this data and the work of Heijboer[16-18] and others[12-15,19-21] discussed earlier, it appears that at low temperatures (~130°K) essentially only the equatorial conformer exists, whereas above the transition there is a distribution of states influenced by temperature but heavily weighted in the favor of the stable conformer and that at intermediate temperatures, (i.e. the transition), the inter-conversion of conformers is occurring. This type of order-disorder behavior has been observed by Westrum[7] and McCullough[30] for solvents and by other investigators for metals[6] and inorganic materials[31]. In metals, the return to the equilibrium ordered state is characterized by the Curie temperature. Westrum[7] has recently reported similar adiabatic calorimetric results for the transformation from one twisted conformation to another for a macrocyclic hydrocarbon, 2.2-paracyclophane ($C_{16}H_{16}$, di-p-xylene). Analogous behavior was noted in that the slope of Cp vs T before the transition is higher than after the transition and that a rounded diffuse maximum is observed. The conformational change of this molecule has been ascribed to a Schottky-type thermodynamic transformation.

The characteristic features of a Schottky transformation is a rounded diffuse maximum in Cp via adiabatic calorimetry indicating that the transition is, at best, weakly cooperative. The chair-chair transformation of PCHMA is expected to be essentially non-cooperative as only nearest neighbors can influence the behavior of other side groups. Transmission of cooperativity through the main chain is deemed small due to the separation in distance and due to the

flexibility of the intervening side chain. In fact, relatively rigid attachment to the main chain to gain cooperativity could probably result in constraining the cyclohexyl group to the stable equatorial conformer due to steric considerations. This may indeed explain why the chair-chair transformation is not observed by dynamic mechanical measurements for polyvinylcyclohexane.

CONCLUSIONS

1. Polymer thermodynamic transitions are classifiable in a manner similar to all other materials.
2. The well established chair-chair conformation of polycyclohexylmethacrylate has been observed calorimetrically for the first time and can be represented by a simple statistical thermodynamic model.
3. Other sub-Tg relaxation may be observed calorimetrically when higher precision calorimeters evolve and/or the observation criteria outlined herein is satisfied.

REFERENCES

1. Wunderlich, B. and H. Baur, Adv. Polymer Sci., 7, 151 (1970).
2. O'Reilly, J. M. and F. E. Karasz, ACS Polymer Preprints, 5, No. 2, 351 (1964).
3. Beatty, C. L. and F. E. Karasz, to be published.
4. Fowler, R. H., Statistical Mechanics. Cambridge Univ. Press, Cambridge, (1936).
5. Gopol, E. S. R., Specific Heats at Low Temperatures. Heywood Books, London (1966), p. 142.
6. Garland, C. W., Phys. Rev., 135, A 1696 (1964).
7. Andrews, J. T. S. and E. F. Westrum, Jr., J. Phys. Chem., 74, 2170 (1970).
8. Karasz, F. E., J. M. O'Reilly, H. E. Bair and R. A. Kluge, ACS Polymer Preprints, 9, No. 1, 822 (1968).
9. Karasz, F. E., H. E. Bair and J. M. O'Reilly, J. Phys. Chem., 69, No. 8, 2657 (1965).
10. Boyer, R. F., Polymer Engr. and Sci., 8, No. 3, 161 (1968).
11. Beckett, C. W., K. S. Pitzer and R. Spitzer, J. Am. Chem. Soc., 69, 2488 (1947).
12. Blaha, K., O. Cervinka and J. Kovar, Fundamentals of Stereochemistry and Conformational Analysis. Iliffe Books, London (1971)
13. Hoff, E. A. W., D. W. Robinson and A. H. Willbourn, J. Polymer Sci., 18, 161 (1955).
14. Karpovich, J., J. Chem. Phys., 22, 1767 (1954).
15. Lamb, J. and J. Sherwood, Trans. Faraday Soc., 51, 1674 (1955).

16. Heijboer, J., Kolloid-Z., 148, 36 (1956).

17. Heijboer, J., Kolloid-Z., 171, 7 (1960).

18. Heijboer, J., J. Polymer Sci., 8, C, No. 16, 3413 (1968).

19. Ishida, Yoicha and Kaoru Yama Fuji, Kolloid-Z., 177 (2), 97 (1961).

20. Powles, J. G., B. I. Hurt and D. J. H. Sandiford, Polymer, 5, 505 (1964).

21. Frosini, V., P. Magagnini, E. Butta and M. Baccaredda, Kolloid-Z., 213, (1-2), 115 (1966).

22. Eliel, E. L., Angew. Chem., 77, 784 (1965).

23. O'Reilly, J. M. and F. E. Karasz, J. Polymer Sci., C, No. 14, 49 (1966).

24. Karasz, F. E. and D. J. Hamblin, Rept. BPR 15, Natl. Phys. Lab., England, May (1963).

25. Statton, W. O.,J. Polymer Sci, 58, 205 (1962).

26. Karasz, F. E. and J. M. O'Reilly, Rev. Sci. Instr., 37, No. 3, 255 (1966).

27. O'Reilly, J. M. and F. E. Karasz, to be published.

28. O'Reilly, J. M., H. E. Bair and F. E. Karasz, Bull. Am. Phys. Soc., 9, 285 (1964).

29. Merz, E. H., J. Polymer Sci., 3, No. 5, 790 (1948).

30. Wilkinson, R. W. and Malcolm Dole, J. Polymer Sci., 58, 1089 (1962).

31. Westrum, E. F. and J. P. McCullough 'Thermodynamics of Crystals' in "Physics and Chemistry of the Organic Solid State", 1, eds. Fox Labes and Weissberger Interscience, New York (1963).

32. Stout, J. W. and W. B. Hadleg, J. Chem. Phys., 40, 55 (1964).

33. Johnson, W. S., V. J. Bauer, J. L. Musgrave, M. A. Frish, L. H. Dreger and W. N. Hubbard, J. Am. Chem. Soc., 83, 606 (1961).

CHAPTER III

THERMODYNAMIC CLASSIFICATION OF THE MULTIPLE GLASS AND MELTING TRANSITIONS OF POLYDIETHYLSILOXANE

C. L. Beatty* and F. E. Karasz
Polymer Science and Engineering Department
University of Massachusetts
Amherst, Massachusetts 01002

INTRODUCTION

Multiple melting transitions have been reported for a number of polymeric systems. Generally these multiple melting transitions are explained by the presence of different polymorphs[1,2,3], imperfect and/or small crystals[4,5,6] copolymers[7,8] or the presence of incompatible homopolymers. Multiple glass transitions have been reported for blends[10,11] and copolymers[12,13]. In addition, shifting of the glass transition temperature due to the presence of crystallinity[14-18], molecular weight[19,20], crosslinking[21,22] filler[23], pressure[24-28], tacticity[28,29], etc. have been reported. However, until recently there has never been a report of more than one glass transition for a pure homopolymer. Lee and coworkers[30], from DSC measurements, have concluded that two glass transitions exist for the pure homopolymer polydiethylsiloxane. If true, the classical definition of the glass transition would have to be modified - this being simple justification for investigation of this polymer by precision calorimetry. Recently Boyer[31] has reported that all semicrystalline polymers have two glass transitions. The lower temperature transition being the glass

* Present Address: Xerox Corporation, Webster, New York 14580

transition as normally conceived whereas the higher transition occurs as a result of molecular constraints. As discussed previously[32], precision adiabatic calorimetry has definite discriminatory capabilities compared to non-thermodynamic techniques. That is, it would be difficult to confuse a first-order thermodynamic transition with a glass transition.

EXPERIMENTAL

The pure homopolymer $(-Si(CH_2-CH_3)_2-O-)_n$ was kindly donated by Dr. Chi-Long Lee of Dow Corning Corporation. This was a portion of the sample previously studied by Lee and coworkers[30]. Compositional purity was confirmed by elemental analysis.

A portion of the sample was fractionated by addition of methanol to an approximately 1% solution as described elsewhere[33]. The molecular weights of the fractionated and as received sample were determined by gel permeation chromatography (Waters Associates Inc.) using tetrahydrofuran at 100°F. In addition, $\overline{M}_n$ was determined by membrane osmometry at 37°C with toluene as the solvent.

Initial calorimetric investigations were performed on a Perkin-Elmer DSC-1B using the Perkin-Elmer recommended decalibration procedure for achieving temperatures below -100°C. Low-temperature optical microscopy was accomplished by using a simple cooling technique[34] in conjunction with a Zeiss optical microscope. Low temperature x-ray was achieved using Ni filtered Cu radiation from a GE XRD5 diffractometer fitted with a Electronics and Alloys Inc. Refractex I low-temperature cell.

A previously described[35] precision adiabatic calorimeter, since suitably modified[36], was utilized in these investigations. The silver sample cell was filled with 8.795 grams of polydiethylsiloxane, PDES, plus a small quantity of helium, to enhance thermal equilibration. The specimen was cooled at rates varying from 0.1°K hr^{-1} to 10.0°K hr^{-1} as noted in Table I for each series of experiments. Heating rates of 3°K hr^{-1} to 6°K hr^{-1} were normally utilized to achieve temperature increases of 1°K to 6°K per run. Equilibration times were normally less than twenty minutes. The low temperature operating range of the calorimeter was extended to 60°K by pumping on the liquid nitrogen reservoir[37].

RESULTS

Preliminary DSC experiments were made using conditions as close as obtainable to those reported by Lee et al.[30]. Similar results were obtained with the exception that only one low temperature anomaly could be observed. Based on past experience, we would not interpret the obtained DSC results as anything other than a first order transition. However, low temperature DSC data often is not adequately precise or accurate for definitive classification of transitions. Also, the glass transition was expected to occur at a temperature lower than 150°K, the Tg of polydimethylsiloxane[37], analogous to the polyolefin series.

Consequently, three series of measurements designated A, B and C, were made in the adiabatic calorimeter over various temperature

ranges and after cooling at different rates as indicated in Table 1. The latter temperature was reached after cooling through the transitions of interest at a rate of less than 1°K hr^{-1}. The measured heat capacities for all three series are recorded in Tables 2, 3 and 4 and Series A data plotted in Figure 1. The glass transition characterized by the classical step-change increase in Cp is located at 130 ± 5°K both for Series A and C. The observed ΔCp is 0.17 joule g^{-1} $°K^{-1}$ for both Series A and C measurements. Two first-order transitions located at 203 ± 4°K and 270 ± 4°K are also present. The location of the low temperature peak is dependent upon thermal history. The shift of this peak by ~5° as a function of cooling rate and/or annealing time is illustrated in Figure 2. The location of the higher temperature peak is invariant for the ranges of cooling rates, annealing times and heating rates used in these studies.

Weight loss after 48 hours in a vacuum oven at temperatures as high as 80°C was only 8 mg/68.75 g. indicating the absence of solvent and/or volatile low molecular weight species. Molecular weight distribution, as determined by GPC, was unchanged by the thermal cycling in the calorimeter. $\overline{M}_n$, obtained by membrane osmometry, using toluene at 37°C was 112,600 and agreed well the 120,000 value obtained via GPC.

Low-temperature x-ray diffraction traces show that at -20°C diffraction maxima are located at approximately 11.6, 16.0 and 22.0° 2θ, whereas at -100 to -118°C the observed peaks are located at

Series	Average Cooling Rate °K hr^{-1}	Annealing Time Prior to Reheating	Average Heating Rate °K hr^{-1}
A	20	26	5
B	10	6	5
C	1	98	3

Table 1

The Cooling, Annealing and Heating Rates for Series A, B and C Measurements.

First Series

Temperature °K	Heat Capacity Joules $gm^{-1}°K^{-1}$
69.8160	0.6620
75.0410	0.6463
80.7771	0.6510
86.1139	0.6633
91.2665	0.6864
96.1844	0.7122
101.0564	0.7420
105.9446	0.7735
110.7074	0.8016
115.2487	0.8269
119.5728	0.8593
123.7131	0.8863
127.9268	0.9403
132.4996	1.0778
136.3519	1.1190
139.5735	1.1400

Table 2

Heat Capacities Obtained for PDES for Series A Measurements.

Second Series

Temperature °K	Heat Capacity Joules gm^{-1} $°K^{-1}$
120.1484	0.8502
123.9596	0.8769
127.8380	0.9448
131.3877	1.0476
134.6052	1.1146
142.6533	1.1492
146.2226	1.1726
150.0471	1.1829
154.2939	1.2077
158.4923	1.2254
162.7105	1.2479
166.8333	1.2768
170.2371	1.2783
174.0501	1.3424
177.7412	1.3425
181.7397	1.3862
185.4025	1.4691
190.9227	1.6155
195.6479	3.5119
198.7685	1.7639
201.8195	1.4305
205.4934	1.4253
212.6051	1.4379
216.0469	1.4352

Second Series cont.
Page 2

219.0981	1.4619
222.1747	1.4731
225.5977	1.4853
275.1533	1.5085
277.9315	1.6496
280.5716	1.5612
285.7078	1.5914
288.4070	1.6017
293.9613	1.6431

Series B

Temperature °K	Heat Capacity Joules gm^{-1} $°K^{-1}$
179.2122	1.2508
182.8597	1.3545
186.5378	1.4202
190.3164	1.4972
193.8057	6.2665
196.8683	2.0036
199.7365	5.1893
202.8407	1.6433
206.3990	1.4682
209.9094	1.3934
213.8270	1.4712
217.8789	1.4597

Table 3

Heat Capacities Obtained for PDES for Series B Measurements

Series C

Temperature °K	Heat Capacity Joules gm^{-1} $°K^{-1}$
121.5716	0.8525
124.3560	0.8802
127.8991	0.9295
131.5261	1.0244
134.9924	1.0636
138.1615	1.0987
143.8807	1.1334
151.7534	1.1609
154.5735	1.1701
157.3612	1.1717
160.3880	1.2032
163.1803	1.2064
166.0821	1.2336
169.5104	1.2495
172.8196	1.2677
175.8150	1.3067
186.0504	1.3773
189.0068	1.4125
192.1386	1.5423
195.0843	1.7286
197.4273	2.1298

Table 4

Heat Capacities Obtained for PDES for Series C Measurements

Series C cont.
Page 2

199.2977	5.2987
201.2012	3.5705
203.4535	1.5087
206.0037	1.4690
214.2059	1.4661
217.3539	1.4642
221.2081	1.4631
242.8137	1.5280
246.5776	1.5418
250.1860	1.5954
253.7563	1.6444
256.9090	1.7063
259.6030	1.8494
262.4006	1.9736
265.1428	2.1811
267.6789	2.8478
270.1132	3.1570
273.1679	1.9072
276.7414	1.5356
280.0814	1.6132
283.2465	1.5813
286.4458	1.5932
290.2995	1.5702
294.1791	1.5986

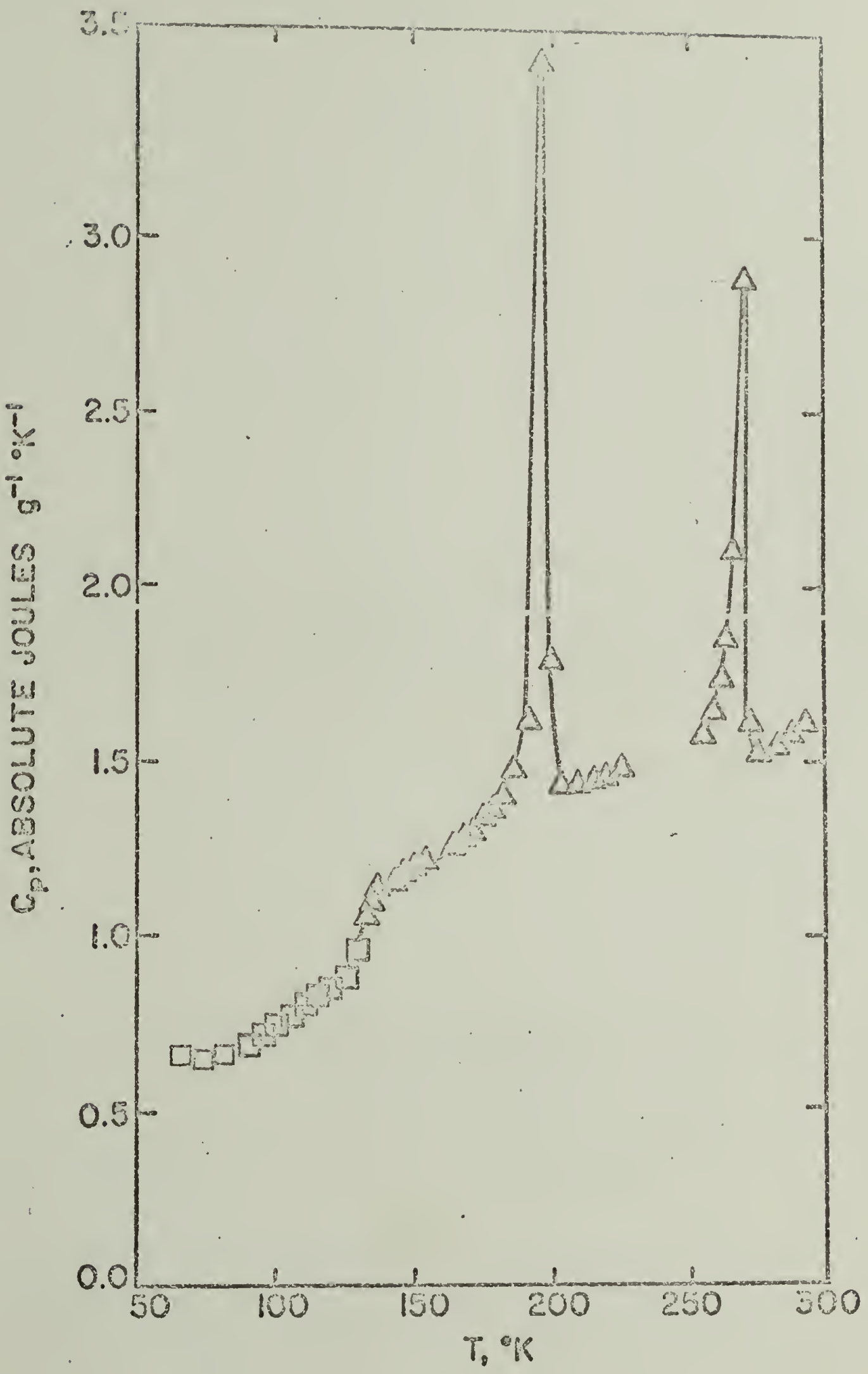

Figure 1

The Heat Capacity of Polydiethylsiloxane;
□ Series A, Δ Series C. Series B Data and overlap of data not shown for clarity.

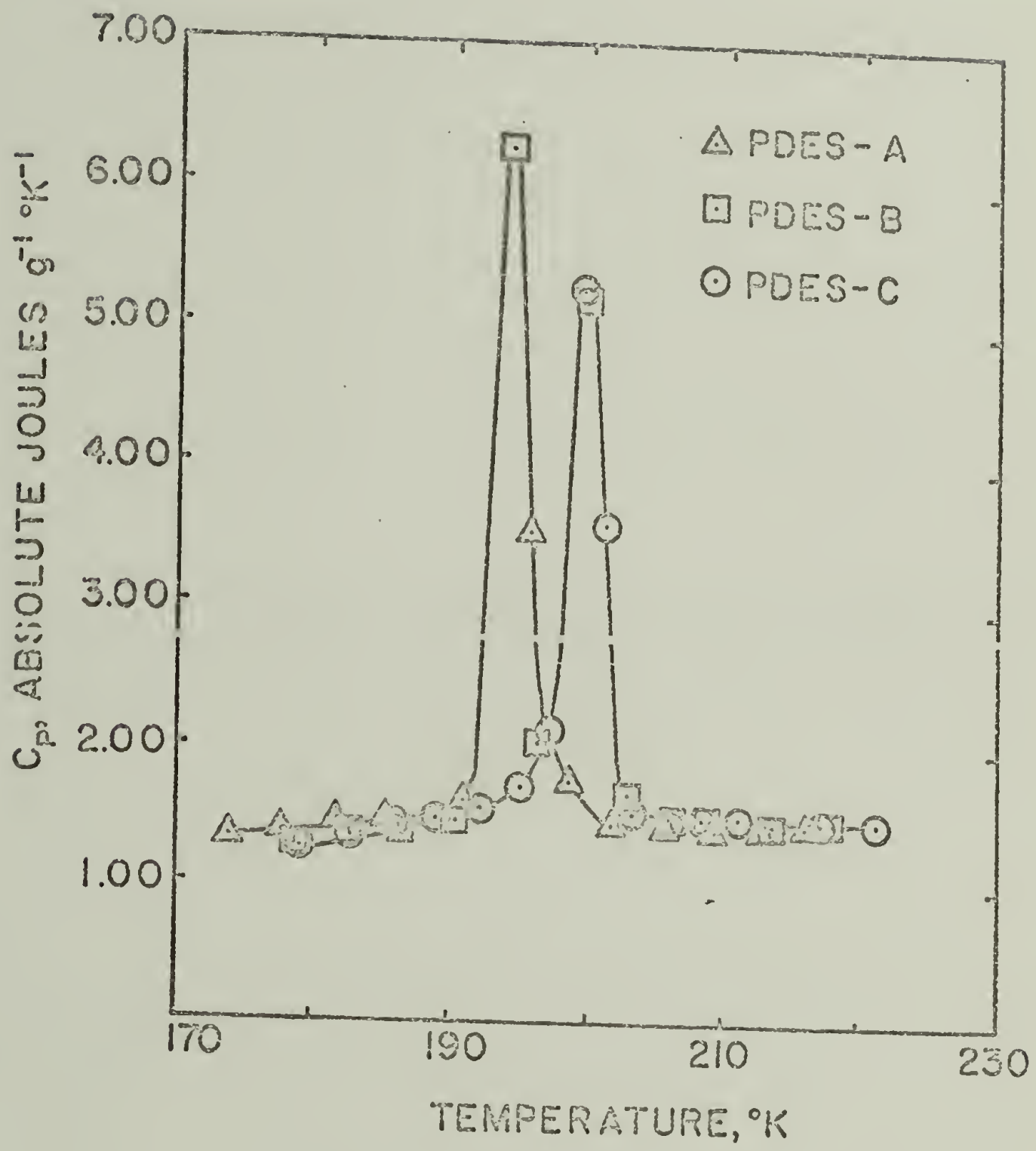

Figure 2

The Variation of Low Temperature Peak
With Crystallization and Annealing Conditions.
See Table 1 for Sample Thermal History

about 13.6, 22.0 and 25.6° 2θ (Figure 3). The wide-angle x-ray diffraction maxima of crystalline polydimethylsiloxane (i.e. < -40°C) occur at 11.67, 19.50 and 23.33° 2θ[38].

DISCUSSION

Polydiethylsiloxane, PDES, has been available prior to 1947[39] when its surface properties were investigated. Despite being in a homologous series with polydimethylsiloxane, PDMS, and the analogy of the complex polymorphism in the polyolefin series, the phase relationship of high molecular weight polydiethylsiloxane has only recently been investigated[30]. The major reason for this lack of interest is probably attributable to the initial crystallization at 270 ± 2°K as this limits the usefulness of PDES as an elastomer. The thermal properties of PDES fluids at high temperatures (20 to 100°C) have been recently investigated[40].

One might expect a decrease in Tg upon lengthening the side chain, based on the decrease from about 260°K to about 250°K for the polyolefin series members, polypropylene and poly-butene-1 respectively. Note the above values are averages as a wide variation of the glass transition have been reported. The previously reported[30] multiple glass transitions of PDES occur at approximately 210°K and 200°K which is significantly above the glass transition of 150°K for PDMS. Cursory preliminary examination via DSC indicated that these peaks were not typical of glass transition behavior but, in fact, appeared to be first order in nature. Subsequent

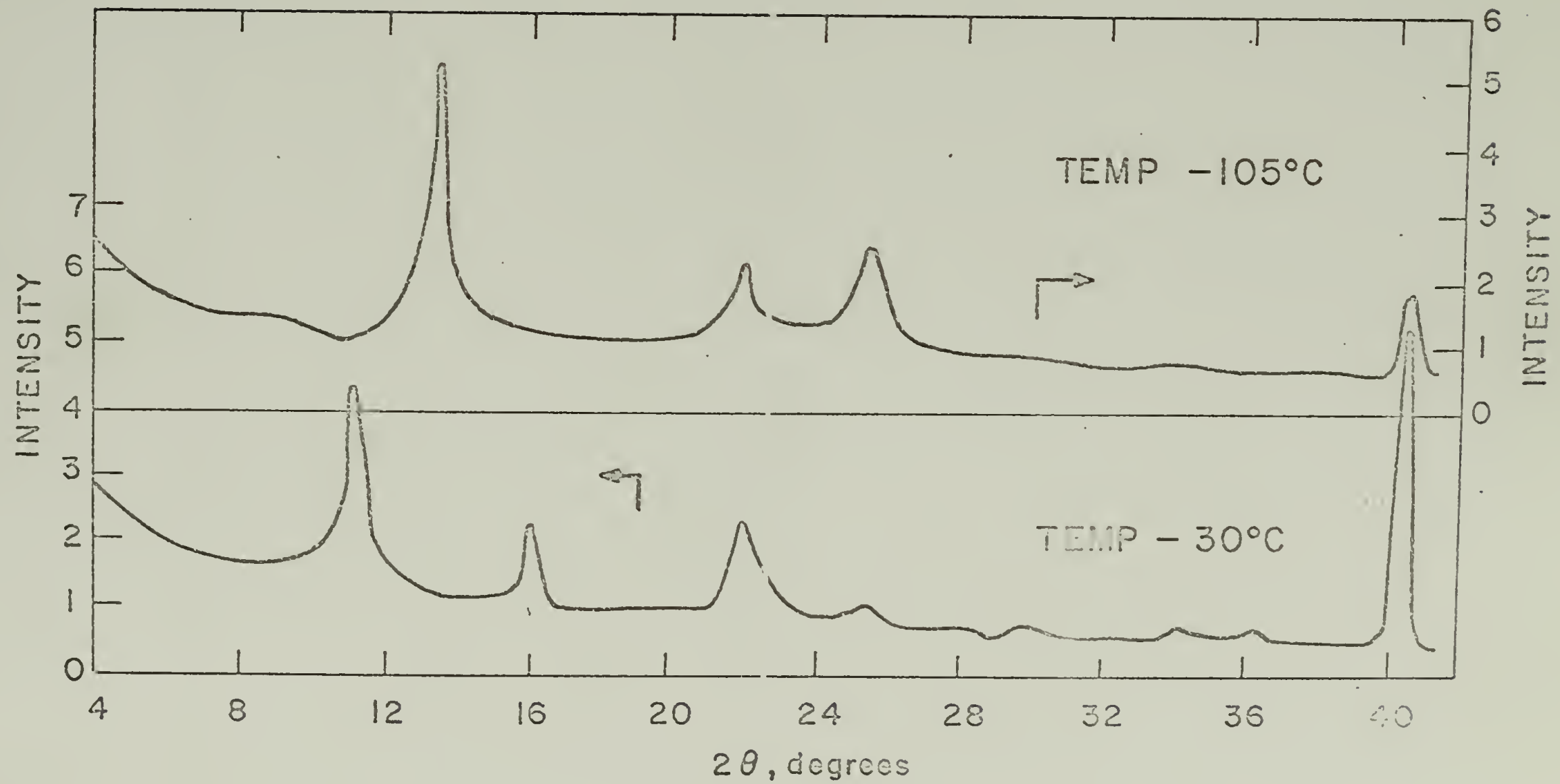

Figure 3

X-ray Diffraction Scans of Polydieth/lsiloxane at Two Temperatures.
The Peak at 40.25 degrees 2θ is Due to the Internal Standard, Tungsten Powder.

adiabatic calorimetric results shown in Figure 1 unambiguously demonstrate that the glass transition occurs at 130 ± 2°K for PDES. This is a decrease of 20° from that of PDMS and illustrates that the free volume concepts used for the polyolefin system are applicable to the polysiloxane series as well. Note that this is the lowest glass transition reported for a high polymer, although several molecular glasses and oligomers have lower glass transitions[41,42]. However, Turdakin and Tarasov[43] measured the glass transition of a PDES oligomers and obtained the same value of 130°K for Tg. The Tm/Tg ratio for PDMS and for PDES (for the 200°K peak) is about 1.5, whereas it is 2.1 for the 270°K PDES peak. Comparable ratios for polypropylene and polybutene-1 are about 1.8 and 1.6 respectively.

Further elucidation of the two observed first order thermodynamic transitions (Figure 1) required modification of existing equipment or use of special attachments to attain temperatures near 170°K. Low temperature optical microscopy, using crossed polars, indicated that upon initial crystallization a mottled green-orange field was obtained. This was followed by a transformation to a solid orange field at temperatures below 170°K. Unfortunately it was impossible to take photographs with this apparatus. However, low temperature x-ray diffraction (Figure 3) does indicate that at intermediate temperatures (200 to 260°K) the observed crystalline diffraction pattern is significantly different from that obtained at 170°K. The crystal structure determination and morphology of these phases is currently being investigated.

Note the rise in heat capacity as temperature is decreased in the 60-65°K region (Figure 1). This was initially discounted as being an experimental artifact of the cooling procedure used. However, confirmation of this upturn has recently been obtained in dielectric relaxation studies at high frequencies[44]. The combined results suggest the existance of a relaxation mechanism operable below the glass transition of PDES.

GPC analysis failed to indicate an oligomeric or cyclic component and elemental analysis has confirmed sample purity. Therefore, the preliminary crystal structure work combined with the observation of two first order thermodynamic transitions are believed to be sufficient grounds to indicate that PDES has at least two crystalline polymorphs. Dielectric studies also indicate that these phases exist.

In conclusion, the glass transition of polydiethylsiloxane has been clearly demonstrated to occur at 130°K. This is lowest recorded polymeric glass transition being 20° below that of the previously lowest reported polymer Tg (150°K for polydimethylsiloxane). In addition, two crystalline phases of PDES have been observed. These observations indicate that polymorphism, as a function of pendant group size, may be similar in the polyolefin and polysiloxane series.

REFERENCES

1. Zannetti, R., P. Manaresi and G. C. Buzzoni, Chim. e Ind., 43, 735 (1961).
2. Flory, P. J., H. D. Bendon and E. H. Keefer, J. Polymer Sci., 28, 151 (1958).
3. Bell, J. P. and Takayuki Murayama, J. Polymer Sci., 7 (A-2), 1059-1073 (1969).
4. Bell, J. P. and Takayuki Murayama, J. Polymer Sci., 7 (A-2), 1033-1057 (1969).
5. Roberts, R. C., Polymer Letters, 8, 381-384 (1970)
6. Booth, C., C. J. Devoy, D. V. Dodgson and I. H. Hillier, J. Polymer Sci., 8, 519-528 (1970).
7. Griskey, R. G. and G. N. Foster, J. Polymer Sci., 8, 1623-1636 (1970).
8. Theil, M. H. and L. Mandelkern, J. Polymer Sci., 8 (A-2), 957-967 (1970).
9. Iwakura, Y. and K. Hayashi, Makromol. Chem., 36, 178 (1960).
10. Bair, H. E., Polymer Eng. and Sci., 10 No. 4, 247-250 (1970).
11. Hughes, L. J. and G. L. Brown, J. Appl. Polymer Sci., 5 (17), 580 (1961).
12. Geiszler, W. A., J. A. Koutsky and A. T. Dibenedetto, J. Polymer Sci., 14, 89-102 (1970).
13. Ikeda, R. M., M. L. Wallach and R. J. Angelo, "Block Polymers" Aggmand, Aggarwal, S. L. Ed., Plenum Press, N. Y. (1970).

14. Koleske, J. V. and R. D. Lundberg, J. Polymer Sci., 7, A-2, 795 (1969).

15. Woods, D. W., Nature, 174, 753 (1959).

16. Newman, S. and W. P. Cox, J. Polymer Sci., 46, 29 (1960).

17. Connor, T. M., B. F. Read and G. Williams, J. Appl. Chem., 14, 74 (1964).

18. Faucher, J. A., J. V. Koleske, E. R. Santee and C. W. Wilson, J. Appl. Phys., 37, 3962 (1966).

19. Beevers, R. B. and E. F. T. White, Trans. Faraday Soc., 56, 744 (1960).

20. Fox, T. G. and P. J. Flory, J. Polymer Sci., 14, 315 (1954).

21. Ueberreiter, K. G. Kanig, J. Colloid Sci., 7, 569 (1952); J. Chem. Phys., 18, 399 (1950).

22. Mason, P., J. PolymerSci., 35, 1523 (1961).

23. Joseph, J. R., J. L. Kardos and L. E. Nielsen, J. Appl. Polymer Sci., 12 (PP), 1151-1165 (1968).

24. O'Reilly, J. M., in Modern Aspects of the Vitreous State, Vol. 3, J. D. MacKenzie Ed., Butterwartis, Washington (1965) Ch.3.

25. Hellwege, K. H., W. Knappe and P. Lehmann, Kolloid-Z., 183, 110 (1962).

26. Gee, G., Polymer, 7, 777 (1966).

27. Rehage, G. and H. Breuer, J. Polymer Sci., C No. 16, 2299 (1967).

28. Cowie, J. M. G. and P. M. Toporowski, J. Macromol. Sci.-Phys., B3 (1), 81-89 (1969).

29. Karasz, F. E. and W. J. MacKnight, Macromolecules, 1, 537 (1968).

30. Lee, C. L., O. K. Johannson, O. C. Flaningam and P. Hahn, ACS Polymer Preprints, 10, No. 2, 1319 (1969).

31. Boyez, R. F., presented at 1972 IUPAC Polymer Symposium, Helsinki, Finland.

32. O'Reilly, J. M. and F. E. Karasz, J. Polymer Sci., C, No. 14, 49 (1966).

33. Lee, C. L. and F. A. Emerson, J. Polymer Sci., 5, A-2, 829 (1967).

34. Beatty, C. L. and F. E. Karasz, to be published.

35. Karasz, F. E. and J. M. O'Reilly, Rev. Sci. Instr., 37, No. 3, 255 (1966).

36. Beatty, C. L., Ph.D. Thesis, Univ. of Mass., 1972.

37. Karasz, F. E. and J. M. O'Reilly, to be published.

38. Adrianov, K. A., G. L. Slonimskii, A. A. Zhdanov, V. Yu. Levin, Yu. K. Godovskii and V. A. Moskalenko, J. Polymer Sci., 10, A-1, 1 (1972).

39. Fox, H. W., P. W. Taylor and W. A. Zisman, Ind. and Engr. Chem., 39, No. 11, 1401 (1947).

40. Nemzer, V. G., Yu. L. Rastorgurev, Plast. Mass., 1, 14 (1970).

41. Masayasu Sugisaki, Hiroshi Suga and Syuzo Seki, Bul. Chem. Soc. Jap., 41, 2586-2591 (1968).

42. Keiichiro Adachi, Hiroshi Suga, and Syuzo Seki, Bull. Chem. Soc. Jap., 44, No. 1, 78-89 (1971).

43. Turdakin, V. A. and V. V. Tarasov, Tr. Mosk., Kheim-Tekhnol. Inst. No. 49, 8 (1965).

44. Pochan, J. M., C. L. Beatty and F. E. Karasz, to be published.

CHAPTER IV

THERMODYNAMIC PROPERTIES OF POLY-ε-CAPROLACTONE

C. L. Beatty* and F. E. Karasz
Polymer Science and Engineering Department
University of Massachusetts
Amherst, Massachusetts 01002

INTRODUCTION

Poly-ε-caprolactone (PCL), $[-(CH_2)_5-\overset{O}{\overset{\|}{C}}-O-]_n$, although first polymerized by Carothers[1], has only recently been polymerized to high molecular weights as the result of new polymerization catalysts[2]. These polyesters, prepared by a ring-opening mechanism, are intrinsically different from dibasic polyesters $(-O-\overset{O}{\overset{\|}{C}}-R-\overset{O}{\overset{\|}{C}}-O-)_n$ in that the chain has a sense of direction due to the uniform orientation of the ester groups within the chains[3,4]. The resultant variation in intra- and inter-molecular forces may result in different behavior, e.g. polypropiolactone can exist in both an extended and a helical conformation. Natural polymers of this type (e.g. poly-β-hydroxybuterate) are optically active[5].

The recent advance in PCL polymerization techniques has resulted in the study of PCL crystal structure[6,7], hydrodynamic properties[8], infrared absorption[9], and physical properties[10]. In turn, the report of compatible PCL-PVC blends over the entire composition range[10] has instigated extensive studies of this system

* Present Address: Xerox Corporation, Webster, New York 14580

by means of optical microscopy[11], dielectric and mechanical relaxation[12], small-angle laser and x-ray scattering[13], etc. in our laboratories. Consequently, thermal characterization of poly-ε-caprolactone is warranted to further elucidate its behavior as a homopolymer and as a component of a compatible polymer blend.

EXPERIMENTAL

The sample, designated PCL-700, was obtained from Union Carbide Corporation in the form of pellets. A Laue x-ray diffraction photograph was obtained at room temperature with a GE x-ray source using a previously described vacuum camera[13] and V_2O_3 filtered Cu radiation. Crystallinities were determined from x-ray diffraction scans obtained from Phillips Type 12045 diffractometer using Ni filtered Cu radiation at room temperature. Natta's method was used to evaluate crystallinities of samples closely approximating the calorimeter samples in molding conditions, and annealing time prior to cooling below Tg. The molecular weights and distribution was obtained via GPC (Waters Associates) in tetrahydrofuran at 34.0°C. A confirming $\overline{M}_n < 30,000$ was obtained by membrane osmometry in dioxane. Elemental analysis was used to confirm purity.

A previously described calorimeter[15], suitably modified[16], was used to measure the heat capacity from 77° to 360°K. Thin films (~5 mil) were prepared by compression molding at ~370°C for ~10 minutes prior to quenching into a liquid nitrogen bath.

The sample (29.658 g) was stored in liquid nitrogen prior to

loading into the calorimeter. The quenched films plus a small quantity of helium, added to enhance thermal equilibration, were not cooled immediately as planned due to experimental difficulties. After 61 hours at room temperature, the assembled calorimeter was cooled to 80°K at an average rate of ~19°K hr^{-1} and was heated during the first series of measurements through the temperature region 80°K to 361°K using heating rates varying from 4 to 10°K hr^{-1}. Prior to the second series of runs, the calorimeter was cooled from 361°K at a rate of 5°K hr^{-1}. Prior to the second series of runs, the calorimeter was cooled from 361°K at a rate of 5°K hr^{-1} over the temperature region to 170°K. Subsequent heating runs of 2 to 4°K were made to 269°K. The sample was then cooled at an average rate of 18°K hr^{-1} to 220°K prior to reheating. Series C measurements from 223°K to 346°K were made using essentially the same heating rates used for Series A. The precision of the data is estimated to be better than ± 0.1% up to 250°K and approach ± 0.3% at higher temperatures.

RESULTS

Three series of measurements (A, B and C) were made. In the first, the heat capacity of quenched film was determined from about 170°K to 361°K. The sample was then cooled slowly through the melt (~2°K hr^{-1}) and annealed for 20 hours to achieve maximum crystallinity for Series B and C runs. The heat capacities of these three series are recorded in Tables 1 - 3 and the overall results are shown in Figure 1. Specific features are discussed below.

Series A

Temperature °K	Heat Capacity Joules gm^{-1} $°K^{-1}$
88.9646	0.5613
95.2426	0.5917
103.2144	0.6243
111.0993	0.6646
117.4512	0.6873
123.2552	0.7101
128.8261	0.7328
134.2447	0.7541
139.0247	0.7819
143.6737	0.7988
148.6311	0.8185
154.0000	0.8427
159.2601	0.8672
164.2300	0.8909
169.1768	0.9090
175.0637	0.9317
180.2343	0.9505
185.5406	0.9716
191.0858	1.0060
196.2140	1.0322

Table I

Heat Capacities for Series A Measurements

Series A
Page 2

200.8571	1.0538
205.2322	1.0915
210.1342	1.1758
214.4402	1.2264
218.8443	1.2637
223.0439	1.2952
239.6989	1.3978
244.5190	1.4031
250.8388	1.4365
257.3900	1.4840
262.4721	1.5155
266.8709	1.5466
271.6757	1.5937
276.5253	1.6137
281.0590	1.6364
285.6494	1.6778
290.1368	1.7410
298.4849	1.8754
302.3860	2.0024
306.3329	2.1742
310.2706	2.1693
313.8554	2.1413
317.0456	2.1122

Series A
Page 3

320.3108	2.4193
323.2478	2.7140
325.7749	3.7052
328.1686	5.0790
330.3692	7.3255
332.1307	10.8118
333.5508	15.1879
334.5901	14.6138
335.4509	10.4763
337.2103	1.9718
339.5519	1.8843
341.7655	1.9006
344.2448	1.8929
347.5573	1.9199
351.5434	1.9190
356.2533	1.9254
360.9943	1.9501

Series B

Temperature °K	Heat Capacity Joules $gm^{-1}°K^{-1}$
176.1499	0.9410
180.6424	0.9515
185.0763	0.9708
189.5949	0.9871
194.1758	1.0079
198.6528	1.0305
203.9178	1.0784
209.2196	1.1508
213.3007	1.1929
217.2192	1.2166
221.2729	1.2436
224.9743	1.2724
240.9848	1.3791
245.0832	1.4402
249.2535	1.4596
256.8923	1.4792
260.4144	1.4969
264.5405	1.5429
268.5755	1.5617

Table 2

Heat Capacities for Series B Measurements

Series C

Temperature °K	Heat Capacity Joules gm^{-1} $°K^{-1}$
223.0965	1.2651
227.9359	1.3027
236.1059	1.3792
246.5875	1.4067
250.1318	1.4286
253.4271	1.4654
256.8636	1.4756
263.5622	1.5459
267.0302	1.5652
270.3927	1.6139
273.7511	1.6693
277.9095	1.7019
282.6882	1.7176
287.4188	1.7821
292.3769	1.8576
299.3845	2.0741
304.2930	2.2135
308.7913	2.1949
312.9755	2.2524

Table 3

Heat Capacities for Series C Measurements

Series C
Page 2

317.3005	2.3201
321.4125	2.3712
325.5139	2.6481
329.1059	4.1804
331.5876	9.6645
333.1098	25.4824
334.1625	21.2660
336.4254	3.0637
341.1405	1.8944
346.3179	1.9218

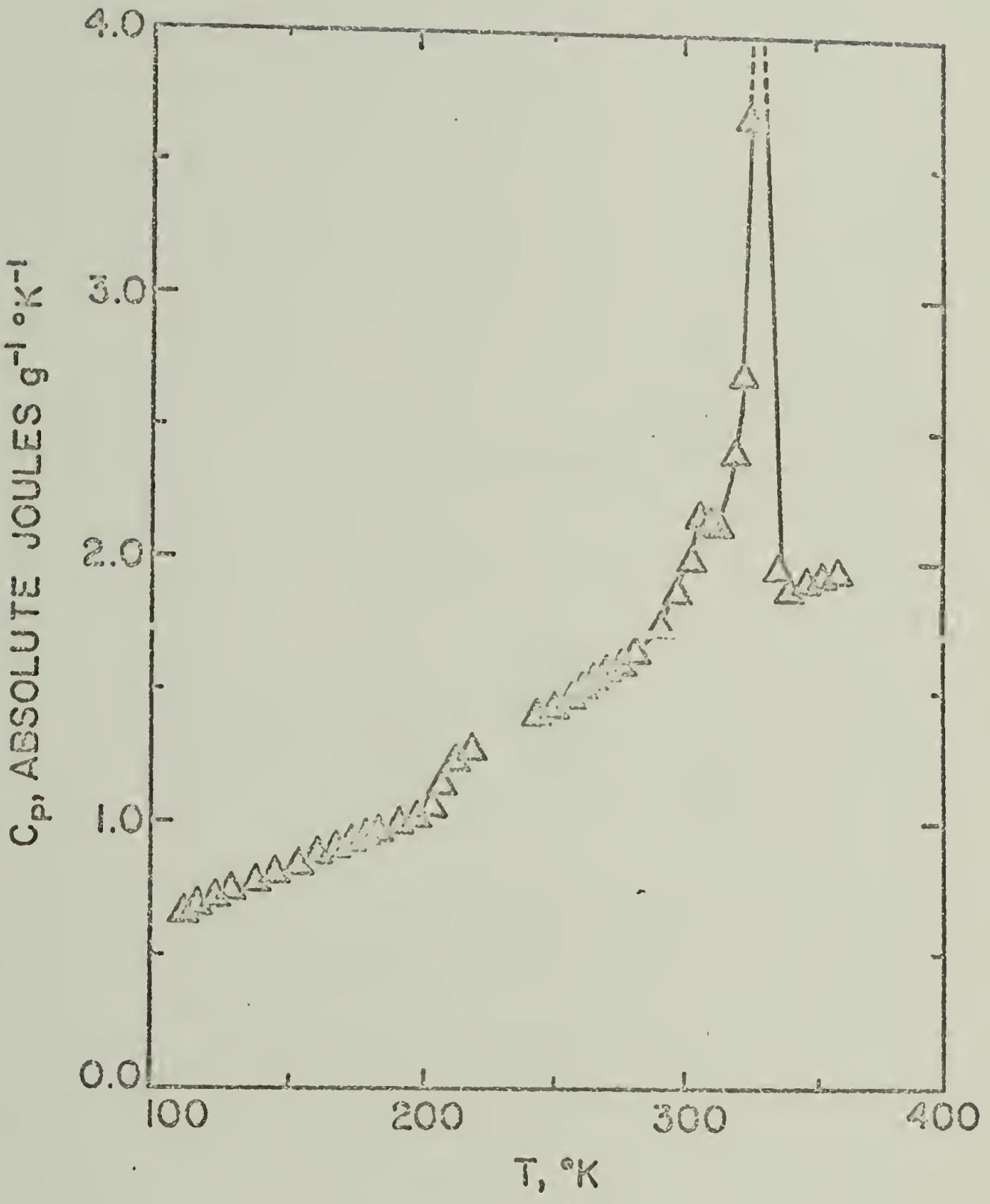

Figure 1

Overall Heat Capacity versus Temperature Results
For Poly-ε-caprolactone.

The measurements of Series A and B extended through the glass transition region. The expected large difference in crystallinity of these two samples was not achieved due to calorimeter operational difficulties. Consequently, crystallization of the quenched material partially occurred with the resultant small difference in ΔC_p at Tg for the two levels of crystallinity as illustrated in Figure 2. The crystallinity for the Series A and B or C, as determined by wide angle x-ray diffraction, are approximately 50% and 33% respectively. The glass transition occurs at 209 ± 2°K and is not shifted within experimental error as a function crystallinity.

Poly-ε-caprolactone melts for both samples at 336.5 ± 1°K (Figure 1). The same melting point for samples of differing levels of crystallinity and crystalline size and perfection is obtained due to the slow heating rates used with the inevitable concomitant annealing. The enthalpy and entropy data are determined point-by-point for each run and are plotted in Figure 3 and 4 respectively. The observed enthalpy and entropy of melting is 85 ± 5 joules g^{-1} $°K^{-1}$ (20.3 cal g^{-1}) and 0.335 ± 0.005 joule g^{-1} $°K^{-1}$ respectively. The Laue x-ray diffraction photograph (Figure 5) confirms the orthorhombic crystal structure previously determined for polycaprolactone[6,7].

Adiabatic calorimetry has been used to investigate many types of polymers but, until this study, not for polylactones. This has been primarily due to the unavailability of high molecular weight polylactones until recently. The observed glass transition (209 ± 2°K) and melting point (336.5 ± 1°K) agree well with previous

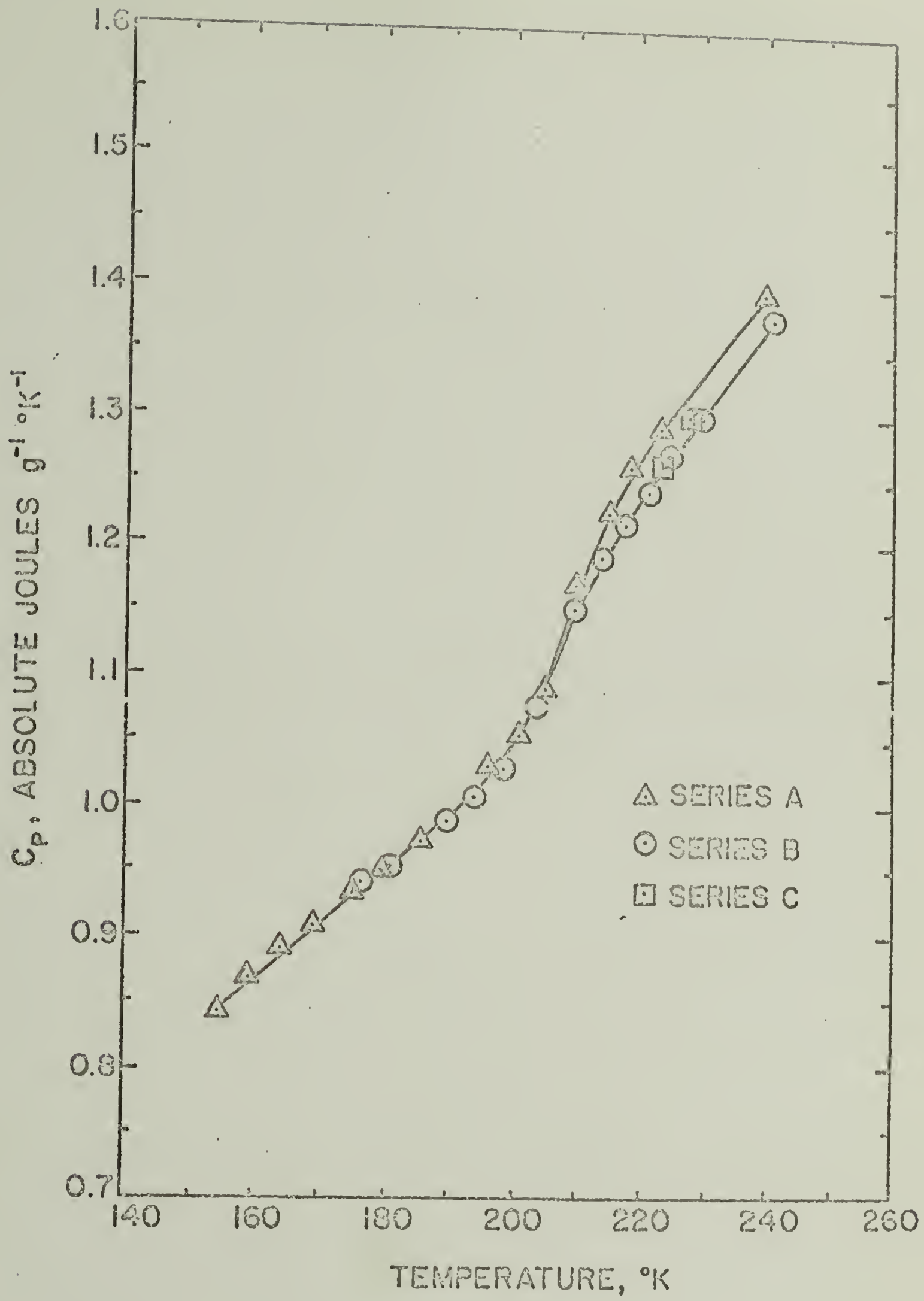

Figure 2

Heat Capacity Differences at Tg Due To Crystallinity
(Δ ±33% and O , □ ± 50% Crystallinity Respectively).

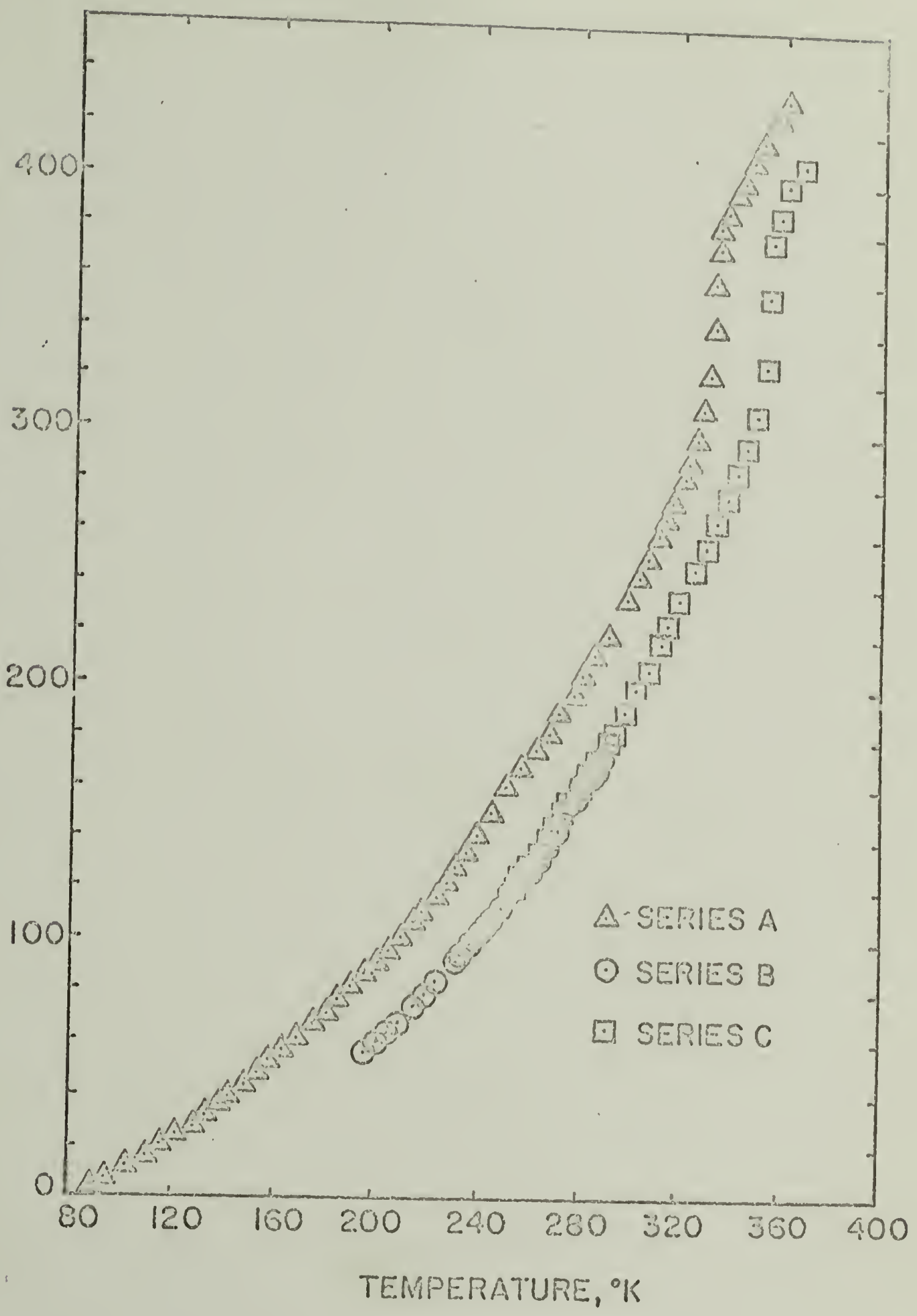

Figure 3

Enthalpy versus Temperature Curve Using Initial Run For Each Crystallinity as Reference Temperature.

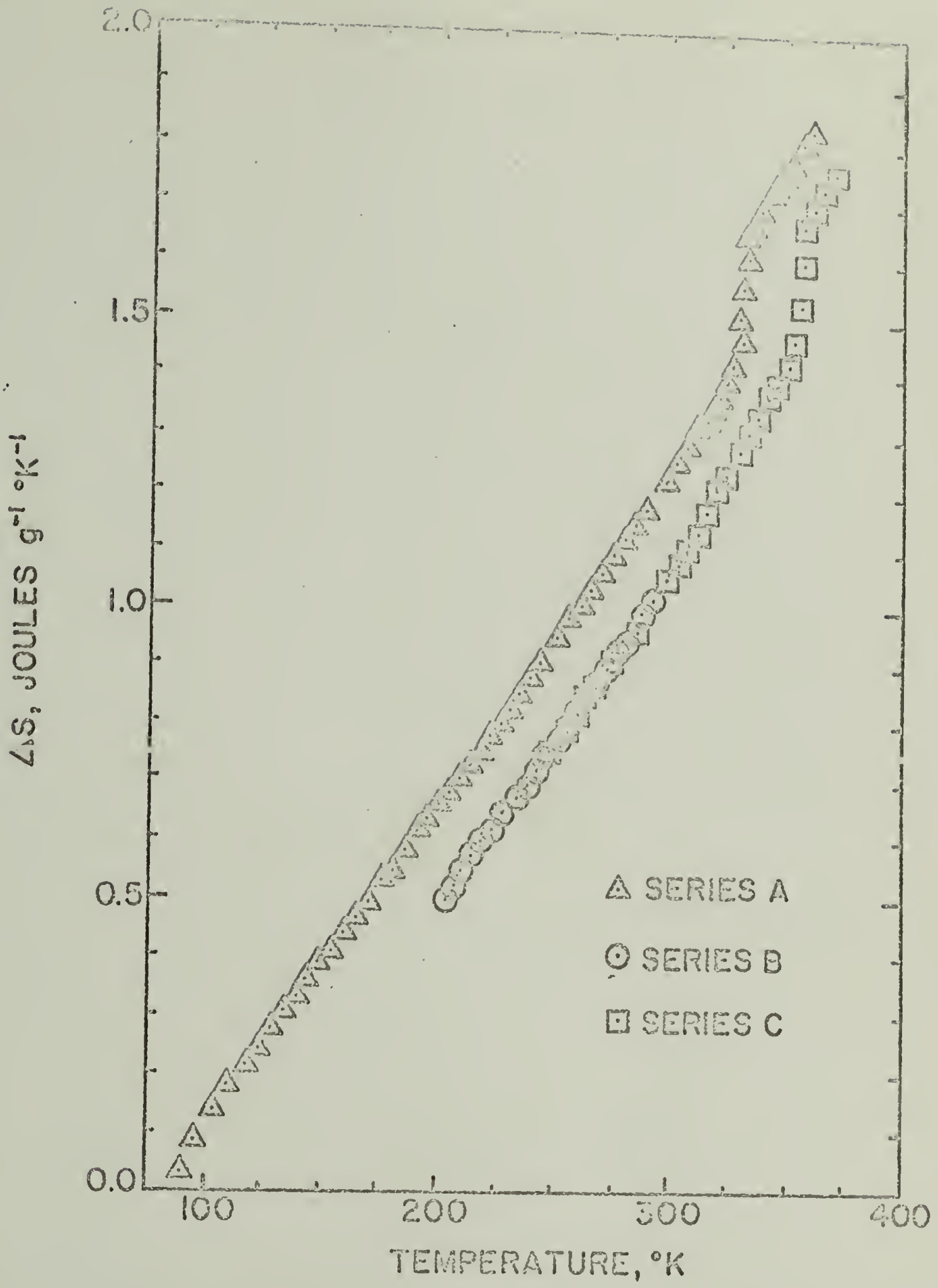

Figure 4

Entropy versus Temperature Using Initial Measurement
For Each Crystallinity Specimen as Reference Temperature.

Figure 5

Wide-Angle X-ray Photograph of Poly-ε-caprolactone

published values of 210°K[10] and 336[6,16] respectively for poly-ε-caprolactone.

The observed enthalpy and entropy of fusion, corrected to 100% crystallinity using the average observed enthalpy and crystallinity yields a heat of fusion of 40 ± 4 cal g^{-1} and 0.083 ± 0.010 cal g^{-1} $°K^{-1}$ respectively. The uncertainty in crystallinity is an appreciable error compared to the calorimetrically observed results. These results do not agree with previous unpublished results[11] of ΔH_f = 20 cal g^{-1}. However, agreement is obtained within experimental error with the value of ΔH_f = 36.3 cal g^{-1} [13] obtained by using a previously reported polymer-diluent melting-point depression technique[17]. The heat of fusion of several diacidic polyesters are normally found at 35 ± 5 cal g^{-1} [18]. The normal separation of ΔS into configurational and volume terms has not been done, as this technique has been demonstrated to be invalid[19].

DISCUSSION

Poly-ε-caprolactone possesses one of the larger repeating units so far studied in polyesters. The rather long sequence of methylenes suggest a possible similarity to branched polyethylene with the carbonyl replacing the branches in low density polyethylene. Therefore, it is not surprising that the unit cell dimensions of PCL and branched polyethylene are quite similar as illustrated in Table 4. Surprisingly, epitaxial crystallization of PCL occurs

Polymer	Unit Cell Dimensions a	b	c	Chain Conformation	Crystallographic Type	Reference
Linear Polyethylene	7.42	4.95	2.55	PZZ*	orthorhombic	26
Branched Polyethylene						
3.6 mole % C_2H_5	7.52	4.96		PZZ	orthorhombic	26
3.1 mole % C_3H_1	7.47	4.97		PZZ	orthorhombic	26
3.4 mole % C_4H_9	7.47	4.97		PZZ	orthorhombic	26
1.4 mole % C_5H_{11}	7.47	4.96		PZZ	orthorhombic	26
Poly-ε-caprolactone	7.50	4.97	1.73	PZZ	orthorhombic	6
Ethylene-CO Copolymers						
0% CO	7.40	4.93	2.55	PZZ	orthorhombic	31
44% CO	——	——	2.54	PZZ	orthorhombic	31
50% CO	7.97	4.76	7.57	PZZ	orthorhombic	31
Poly(ethylene sebacate)	7.40	5.00	16.83	PZZ	monoclinic	27
Poly(ethylene azelate)	7.45	4.97	31.5		orthorhombic	27
Polyglycolide	6.19	5.23	7.02	PZZ	orthorhombic	28
Poly-β-prioplactone	7.73	4.48	4.76	PZZ	orthorhombic	30

Table 4

Variation in Unit Cell Spacings with the Number and Size of Defects

* Planar zig-zag conformation

on LPE but not on BPE[20]. This is contrary to the expected requirement that lattice matching is necessary for epitaxial crystallization.

From initial comparison of unit cell dimensions, it seems that the polyethylene lattice can accommodate the ester groups as a periodic defect without significantly disturbing the polyethylene basal plane. The dramatic melting point depression of poly-ε-caprolactone, compared to polyethylene (50°-60°), can be rationalized on the basis of an expanded lattice due to an increase in the number of lattice defects. However, Stein and coworkers[22] have shown via dielectric, relaxation, mechanical loss measurements, etc., that the carbonyl in carbon monoxide copolymers can reside within the crystal lattice. The polarity of the carbonyl would be expected to partially offset the disruptive defect effect by increased hydrogen bonding with less of a decrease in Tm However, the lowered melting point of PCL and other aliphatic polyesters compared to PE indicate that hydrogen bonding has a relatively minor effect as Tm is not a strong function of the number of carbonyls per unit length of chain for methylene linkages of 4 or greater. Based on dielectric relaxation data[7], it is suspected that the drastic decrease in Tm is primarily due to enhanced chain flexibility and chain rotation. This greater freedom of rotation leads to a significantly higher entropy of fusion compared to polyethylene.

However, the effect of polarity is apparent for shorter methylene sequences. The melting point for polyglycolide, $[-CH_2-COO]_n$, is

220°C, nearly one hundred degrees greater than branched polyethylene. The effects of lattice expansion and polarity are nearly balanced for two methylene sequences between ester linkages as poly-β-propiolactone, $[-(CH_2)_2-COO-]_n$, has a melting point (130°C) similar to that of polyethylene. Inspection of Table 5 illustrates that introduction of an ether linkage into the PE chain in any sequence other than the alternating mode of PMO likewise results in a drastic reduction in Tm. The increase in PMO and PA Tm, compared to LPE, is probably due to hydrogen bonding effects. Neglecting perturbations of crystallinity, crystallite size, etc., the methyl branch in PPO results in a reduction in Tm by 8° compared to PEO while Tg is increased by 9°. However, the introduction of a carbonyl raises the Tm from 38°C for PTHO (the polyether in Table 5 most similar to PCL) to 63°C for PCL possibly reflecting the effect of hydrogen bonding overriding the disruptive defect and rotation effects. Polyhexamethylene adipate, PHA, which was first investigated by Carothers[23] has the same average methylene structure as PCL (Table 4), although the ester linkages are alternately reversed. The unexpected disruptive effect of alternation of 4 and 6 methylene groups between reversed ester linkages, compared to the regular 5 methylene groups in PCL, is reflected in decrease in Tm of 6° and an increase in Tg by 6°. Unfortunately, the unit cell of PHA is not available for comparison.

Recent data on other polylactones[21] indicate that a minimum in Tg occurs when there is a sequence of 5 methylene groups between ester linkages (i.e. PCL). The interaction of ester groups to

Polymer Structure	Name	Tg °C	Tm °C
Polylactones			
$-CH_2COO-$	Polyglycolide		220[28]
$-(CH_2)_2COO-$	Poly-β-propiolactone	-28[21]	130[30]
$-(CH_2)_4COO-$	Poly-δ-valerolactone	-57[21]	53[9]
$-(CH_2)_5COO-$	Poly-ε-caprolactone, PCL	-62	63
Polyesters			
$-C(CH_2)_8COO(CH_2)_2O-$	Poly(ethylene sebacate)(PES)		79[23]
$-C(CH_2)_4COO(CH_2)_6O-$	Poly(hexamethylene adipate)(PHA)	-68	57[23]
Polyethers			
$-CH_2O-$	Poly(methylene oxide)(PMO)	-82[32]	183[32]
$-(CH_2)_2O-$	Poly(ethylene oxide)(PEO)	-66[32]	70[32]
$-(CH_2)_4O-$	Poly(tetramethylene oxide)(PTMO)	-84[32]	38[32]
$-CH_2CHCH_3O-$	Poly(propylene oxide)(PPO)	-75[32]	62[32]
$-CHCH_3O-$	Poly(acetaldehyde)(PA)	-30[33]	165[34]

Table 5

Effect of Polymer Composition on Glass and Melting Transitions

form a pseudobranch point due to polarity in the amorphous phase is a possibility. The crystallinity of PHA is not reported, although a shift in Tg with crystallinity would not be expected based on the dilotomeric work on polyethers and our results on PCL. Previously Koleske and Lundberg have reported a shift in Tg by as much as 18° for PCL as a function of crystallinity[10]. However, in general, resonance techniques such as the torsion pendulum technique used by Koleske and Lundberg result in observation of shifts in Tg not observed by equilibrium techniques. Figure 2 illustrates the difference in ΔCp at Tg for the two different crystalline samples of PCL. Encraty $(dS/dT)p$ or Cp/T is a more sensitive function to transitional change and demonstrates clearly the effect of crystallinity. However, note that the shift in Tg as a function of crystallinity is well within the experimental error (i.e. $\leq 2°K$) for both ΔCp and Cp/T versus plots. The effect of crystallinity upon the ΔCp (i.e. the step-change in Cp) observed at Tg is affected by non-crystalline interactions as previously demonstrated for semicrystalline polymers[25,26].

In conclusion, the glass transition, melting point, and related thermodynamic quantities have been measured for poly-ε-caprolactone. These results appear to be in agreement with available literature values. The interesting relationship of change in Tm and Tg of several polymers of similar crystalline structure have been discussed with respect to the perturbing effect of changes in their chemical composition.

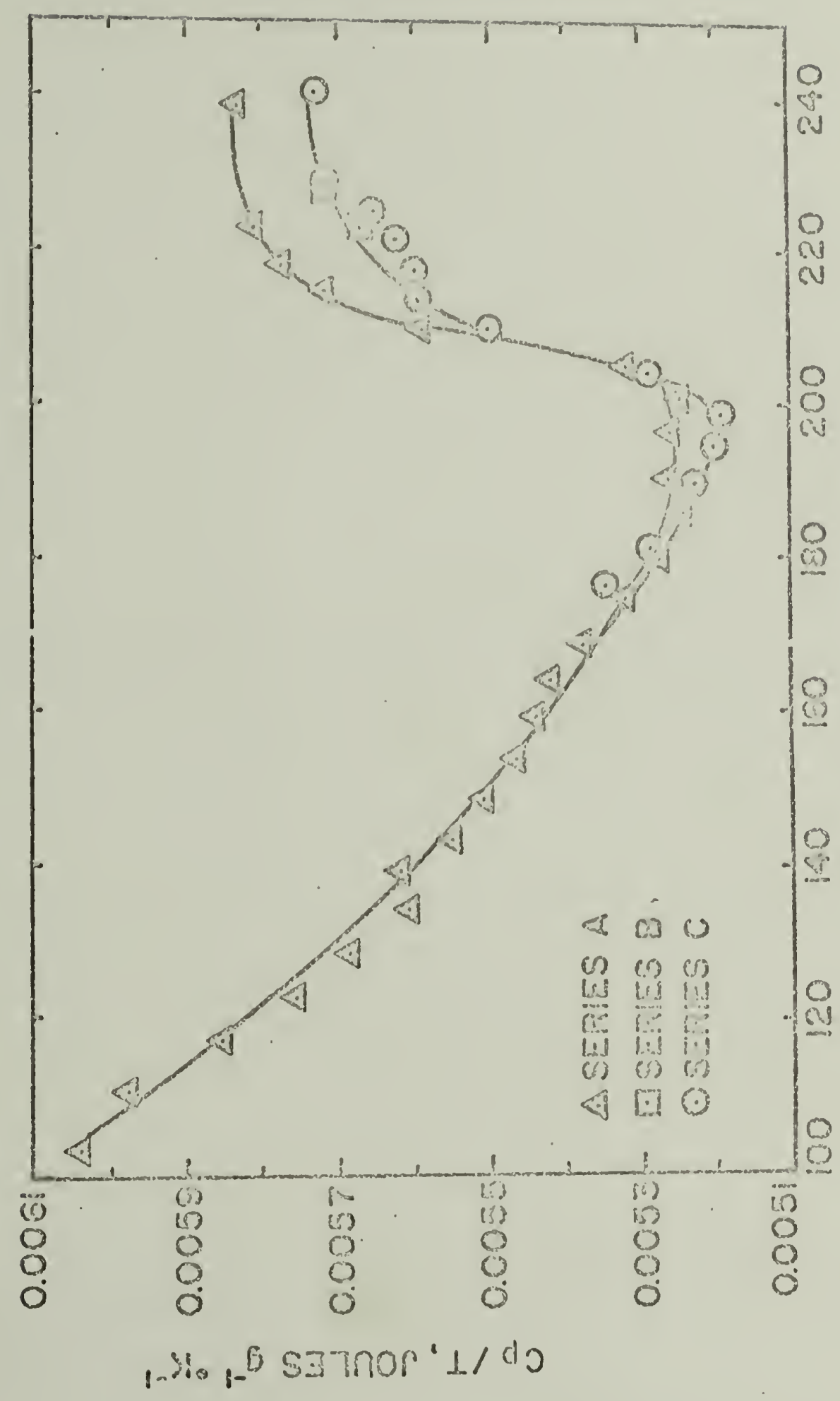

Figure 6

Encraty Differences at Tg Due to Different Crystallinities
(Δ ± 33% and O , □ ± 50% Crystallinity Respectively).

REFERENCES

1. Carothers, W. H., U. S. Pat. 2,071,250 (1937).
2. Lundberg, R. D., J. V. Koleske and K. B. Wischmann, J. Polymer Sci., 7 (A-1), 2915-2930 (1969).
3. Fuller, C. S. and C. L. Erikson, J. Amer. Chem. Soc. 59, 344 (1957).
4. Fuller, C. S. and C. J. Frosch, J. Amer, Chem. Soc., 61, 2575 (1959).
5. Wasai, G., T. Saegusa and J. Furakawa, J. Chem. Soc. Japan, Ind. Chem. Sect. 67, 601 (1964).
6. Bittiger, H. and R. H. Marchessault, Acta Cryst. B26, 1923-1927 (1970).
7. Chatani, Y., Y. Okita, H. Tadokoro and Y. Yamashita, Polymer J., 1, 555 (1970).
8. Koleske, J. V. and R. D. Lundberg, J. Polymer Sci., 7 (A-2), 897-907 (1969).
9. Tadokoro, H.,M. Kobayashi, H. Yoshidome, Kazuo Tai, and D. Makino, J. Chem. Phys., 49, No. 8, 3359-3373 (1968).
10. Koleske, J. V. and R. D. Lundberg, J. Polymer Sci., 7 (A-2), 795-807 (1969).
11. Price, Fraser P., private communication.
12. Wilusz, G. B., unpublished results.
13. Stein, R. S., private communication.
14. Beatty, C. L., Ph.D. Thesis, Univ. of Mass. (1972).
15. Karasz, F. E. and J. M. O'Reilly, Rev. Sci. Instr., 37, No. 3, 255 (1966).

16. Crescenzi, V., G. Manzini, G. Calzolari, and G. Borri, European Polymer J., 8, 449 (1972).

17. Karasz, F. E. and L. D. Jones, J. Phys. Chem., 71, 2234 (1967).

18. O'Malley, J. J., private communication.

19. Klempner, D. and F. E. Karasz, to be published.

20. Takahashi, T., M. Inamura and I. Tsujimoto, Polymer Letters, 8, PP, 651-657 (1970).

21. Koleske, J. V. and R. D. Lundberg, J. Polymer Sci., 10 (A-2), 323-337 (1972).

22. Wilkes, G. L. and R. S. Stein, ONR Technical Report No. 118, Project NR 056-378, Univ. of Mass. (1969).

23. Phillips, P. T. and R. S. Stein. ONR Technical Report No. 119. Project No. 056-378, Univ. of Mass. (1969).

24. Carothers, W. H., J. Am. Chem. Soc., 51, 2560 (1929).

25. O'Reilly, J. M. and F. E. Karasz, ACS Polymer Preprints, 5, No. 2, 351 (1964).

26. Beatty, C. L. and F. E. Karasz, Preprints IUPAC Macromolecules Symposium, 4, 149 (1972).

27. Swan, P. R., J. Polymer Sci., 56, 409 (1962).

28. Fuller, C. S. and C. S. Frosch, J. Phys. Chem., 43, 323 (1939).

29. Holmes, D. R., C. W. Bunn and D. J. Smith, 17, 159 (1955).

30. Shuehino, K., Y. Chatini, H. T. Adokoro, R. Kato and A. Tanaka, Amm. Meeting Soc. Polymer Sci (Japan), May 1966.

31. Chatini, Y., T. Tukizawa and S. Murahaski, J. Polymer Sci., 62, S 27 (1962).

32. Wetton, R. E. and G. Allen, Polymer, 7, [illegible] (1966).

33. Williams, G., Trans. Faraday Soc., 59, 1397 (1963).

34. Vogl, O., J. Polymer Sci., A-2, 2219 (1964).

RECOMMENDATIONS

A. EQUIPMENT

1. Rewiring

Several changes in experimental equipment and/or design are warranted due to the time consumed by maintenance and data collection. The maintenance problems can be rectified by relatively few changes. The major change being rewiring of the calorimeter, (i.e. calorimeter shield, furnace, heaters, all thermocouples and platinum resistance leads), to reduce the number of breaks during handling. The present wiring is very brittle due to repeated thermal cycling. During replacement, choice of a stable high temperature insulating material (e.g. ceramic, polyamide, etc.) would, in effect, allow operation at higher temperatures than allowed by the present insulation - polydimethylsiloxane. The present upper temperature achievable is determined by the quality of vacuum which is in turn limited by the rate of polydimethylsiloxane degradation.

In addition, the leads during rewiring should be subdivided into groups related to the particular functions and parts of the apparatus. That is, thermocouple leads to the shield should be separated from furnace thermocouple leads, from shield heater leads, etc. Identification is best accomplished by physical separation as painted codes tend to fade due to aging and thermal cycling. It would be helpful to twist each segment of wires together prior to gathering into the main umbilical. This would reduce noise by minimizing inductive effects and would also allow separation of individual bundles. Separation of leads into bundles would

also facilitate the changing of groups of leads when failure rate becomes excessive. Also, heater lead bundles need not be continuous and may be joined at junction strips or by plugs located at several points (e.g. shield top, furnace top, radiation platform, etc.). Thermocouple and platinum resistance thermometer leads should remain continuous but several spares should be run during rewiring. Note that sealing the wires in the tulip, although tedious, is not difficult. Application of a thin layer of insulation prior to heater winding is recommended to ensure an adequate dielectric for prevention of possible future grounding. Winding the lid heaters is facilitated by use of a cross with pins that fit the center holes in the lids. The cross is positioned against the lid to allow only one layer of wire to be wound. After winding, keep the cross in place and apply the insulating resin, dry and rotate to finish the insulating and bonding process.

2. Equipment Replacement

Lack of reliable operation by the electronic timer and vacuum meter indicates that they should be replaced. When this is done, it would be advisable to replace with a timer having a digital output. This would be desirable as latter installation of an automatic AC bridge for the Mueller Bridge, digital voltmeters for the calorimeter current and voltage output would allow automatic data acquisition capable of being directly inputted to the computer. This stage of development would still require manual control of top, bottom, and side temperatures and starting and stopping the run. However, further automization might utilize a minicomputer for automatic

control of top, bottom side temperatures, on-off cycle, Δf, etc., as well as data acquisition.

B. CALORIMETRIC

1. Crosslinked Systems

Determine the effect of crosslinking at various temperatures above and below Tg and/or Tm on the thermodynamic properties of glassy and semi-crystalline polymers as a function of temperature. The physical property variations of these systems would also be of interest. Crosslinked ultrahigh molecular weight polyethylene has been studied, although not included in this thesis.

2. Blends

Use precise and accurate adiabatic calorimetry to determine the degree of thermodynamic compatibility achieved for various blend compositions as a function of temperature. An ideal system for study is the poly(phenylene oxide) - polystyrene system as quality heat capacity curves of the homopolymers have already been obtained with this instrument. Also dielectric relaxation, dynamic mechanical loss, differential, scanning calorimetry, etc. studies have already been completed confirming the compatibility of this system as a function of composition.

3. Siloxane Series

Continue polymorphic phase studies of the polysiloxane series using calorimetric and other techniques. Based on the polydiethylsiloxane

work, it is suspected that the other members of this series may be polymorphic analogous to higher members of the polyolefin series.

4. Sub-glass Transition in Polystyrene

Several pieces of data indicate that polystyrene may have a sub-Tg relaxation involving phenyl movement near 50°C. Rogers, C. E. and Dale, W. (J. Polymer Sci., 16, No. 1, 21 (1972)) found that molding at pressures near 3000 atmospheres resulted in enhanced visibility of this transition (when compared to conventional low pressure molded samples) using differential scanning calorimetry. Utilization of such samples for adiabatic calorimetry might result in definitive thermodynamic evidence for this proposed sub-glass transition. If this transition is observed, comparison with respect to the polycyclohexylmethylacrylate chair-chair transition would help determine the generality of sub-glass transition classification and analysis.

5. Plasticizer and Antiplasticizers

The shifting of Tg, modulus, etc. by these modifying materials is well known. However, the thermodynamic interaction of modifier and polymer as a function of temperature is little understood and warrants further examination.

6. Branching

The effect of branching length and distribution on viscosity of polymer solutions and melts has been investigated. However, thermodynamic determination of branching effects above and below

Tg should be relatable to free volume and excluded volume effects. However, such analysis would require very accurate and precise data and have not been made to date.

7. Biopolymers

The solid and solution thermal transitions of biopolymeric materials should reflect upon their chemical and conformational environment. The Karasz-Gajnos theory concerning solvent effects on the helix-coil transition is ample justification for continuing solution studies. To date little, if any, quality calorimetric data exists for biopolymer solid-state transitions, although such transitions are intimately related to life processes.

8. Block Copolymers

The degree of microphase separation and the diffuseness of the interface could hopefully be elucidated by calorimetric analysis of specimens of well controlled morphology. The techniques and variables for control of morphology and degree of phase separation are sufficiently well known to make calorimetric studies feasible.

Appendix A

Operating Manual for the

High Precision Adiabatic Calorimeter

Operating Instructions for the High Precision Adiabatic Calorimeter

I. Introduction

A. Principles of Construction and Operation

II. Procedures Preparatory to Operation

A. Instrument Preparation

1. Battery Care
2. Lead O-ring Fabrication
3. Diffusion Pump Cleaning
4. Mueller Bridge Contact, Switch Contact and Recorder Slidewire Cleaning
5. Instrument Ground
6. Techniques for Cooling to Sub-Liquid Nitrogen Temperatures

B. Calorimeter Loading Procedures

1. Removal of Calorimeter from Support Ring
2. Disassembly of Calorimeter
3. Calorimeter Cleaning
4. Sample Loading
5. Reassembly of Calorimeter
6. Evacuation and Helium Addition
7. Leak Testing
8. Installation of Heaters and Platinum Resistance Thermometer
9. Installation of Calorimeter into the Ring

III. Operating and Trouble-Shooting Procedures

A. Maintaining Adiabatic Conditions

1. Furnace Control
2. Shield Control
3. Vacuum Control

B. Measurement of Heat Input, Q

1. Measurement of Current, I, and Voltage, E
2. Measurement of Run Time, t
3. Constant Temperature Bath for Standard Resistors and Cells
4. Temperature Determination
5. Sequence of Measurements and Raw Data Record

IV. Computation Procedures

A. Rough Estimate of Heat Capacity

B. Drift and Non-Adiabacity Corrections

1. Drift Correction
2. Factor Measurement
3. Non-Adiabatic Correction

C. Computer Data Reduction

1. Sample Computation, Batch
2. Sample Computation, Time-Sharing
3. Fitting Program
4. Empty Calorimeter, Batch Program
5. Empty Calorimeter, Time-Sharing Program

I. INTRODUCTION

A. PRINCIPLES OF CONSTRUCTION AND OPERATION

Thermodynamic studies of materials is related to the change in energy content of the system when it is subjected to a physical or chemical process. Experimental determination of such changes between equilibrium states must necessarily be very precise and accurate as measured heat capacity includes all modes of motion. Consequently, often the desired observable small change is superimposed on a sizable background. High precision and accuracy is also required because the difference between sample and calorimeter is relatively small - due to design and material property considerations. Consequently, the attainment of 0.05% precision is the best achievable with the present design. Although higher precision measurements can be made of other forms of measurement (e.g. ~ 0.01% for electrical energy), commercially available calorimeters are 20 - 200 times less precise than data obtained with this instrument. An additional feature of this instrument is the wide temperature range of operation. Measurements can be made from essentially absolute zero (triple point of helium) to 600°K which encompasses most of the range of interest for polymers. Also the use of automatic control and measuring circuits allow for more efficient and precise acquisition of data. One person can easily operate this instrument compared to two or more operators for manual instruments.

In principle, operation of an adiabatic calorimeter involves the addition of a known quantity of thermal energy, Q, to a sample

of known mass, m_s, in the calorimeter of mass, m_c, with measurement of the subsequent rise in temperature of the sample, ΔT, which is affected by the loss (or gain) in energy, q, from the environment. The interrelationship of these quantities can be easily observed in the following energy balance equation.

$$Q = (m_s S - m_c C)\Delta T + q \qquad (A\text{-}1)$$

Note that all quantities are measured in each measurement except S, which is the unknown sample heat capacity and q, which has to be determined in an ancillary experiment (factor and non-adiabatic corrections). This heat loss, q, is due to both corrective or radiation losses and at constant surface temperature difference, ΔT, can be represented by the equation,

$$q = kA\Delta T + k'p\Delta T \qquad (A\text{-}2)$$

where k and k' are the radiation and conduction heat transfer coefficients respectively, A is the surface area and p is the pressure. At low temperatures (below 200°K) the first term of equation A-2 predominates, whereas at higher temperatures the vacuum deteriorates and the second term becomes more important. The temperature difference between surfaces should remain constant (zero for the calorimeter-shield and < 0.25° for the shield-furnace) due to automatic controls. The entire assembly is enclosed in a vacuum chamber (Figure A-1) to minimize conduction and/or convective losses. Note also that radiation losses are minimized by gold plating the interior surfaces of the heating cans and by

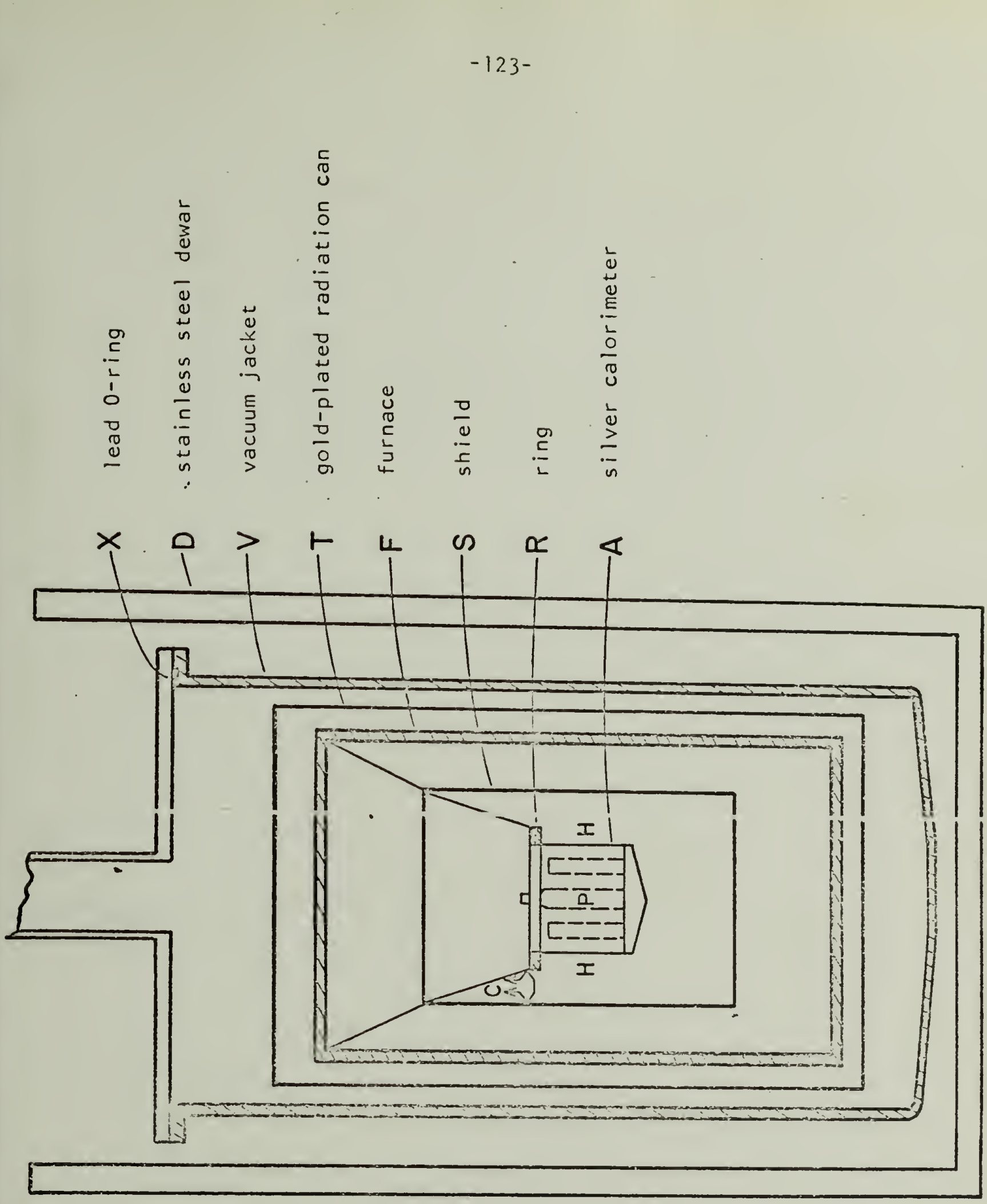

lead O-ring
stainless steel dewar
vacuum jacket
gold-plated radiation can
furnace
shield
ring
silver calorimeter

Figure A-1
Schematic of Calorimeter and Heater Arrangement

a gold plated radiation can between the furnace and the vacuum jacket.

The quantity of thermal energy required, Q, to transfer to successive equilibrium states can be represented by the integral,

$$Q = \int_{t_i}^{t_f} E(t)\,I(t)\,dt \qquad \text{(A-3)}$$

where t_i and t_f are the times of the beginning and end of the run respectively, $E(t)$ and $I(t)$ are the time dependent voltage and current of the calorimeter heaters (H in Figure A-1) respectively.

The temperature rise, ΔT, of the sample and the silver calorimeter is measured by a platinum resistance thermometer (P in Figure A-1). This difference is measured accurately ($\pm$ 0.0001°K). Corrections for drift of calorimeter temperature and non-adiabacity (i.e. heat loss when the temperature difference between ring and shield is non-zero) are used to adjust the temperature rise observed.

The empty calorimeter mass heat capacity produced is determined by experiment and is simulated by a ten term orthogonal polynomial. Calorimeter weight changes are carefully monitored and determine the need for empty calorimeter recalibrations.

During assembly, the sample mass, m_s, is accurately weighed so that the sample heat capacity (S in Equation A-1) can be calculated for each jump in temperature (normally 1 to 10°K). The derived thermodynamic quantities, enthalpy, entropy, encraty, etc., are likewise obtained point by point via the same computer program.

For details of construction and operation, in addition to

this manual, read the reference, Karasz, F. E. and J. M. O'Reilly, Rev. Sci. Instr., 37, No. 3, 255 (1966), and the log books and drawings in the laboratory.

II. PROCEDURES PREPARATORY TO OPERATION

A. INSTRUMENT PREPARATION

1. Battery Care

Preparatory to running the adiabatic calorimeter, batteries need to be fully changed. These batteries are located in Rm 24 (same key as Rm 30) and consist of ten 500 amp. hr. lead acid batteries, (Willard DH-5-1), five 171 amp. hr. lead acid batteries, (Exide Type KX-19A) with straps cut to obtain a 2v and 6v battery from each case and two 90v dry cell B batteries (RCA VSO 90). Eight of the Willard batteries are connected in series to power the calorimeter heaters while the remaining two are used to balance the current and voltage potentiometers (Cryoden and K-3 respectively). Two of the 6v batteries, derived from the Exide batteries, are used to balance the potentiometers and heat (when not operated on AC) the Mueller Bridge. The two 90v dry cells are connected in series and operate the main on - off relay regulating the current supply to shield and furnace heaters. The remaining five 2v and three 6v batteries serve as spares.

A 10 kilowatt charging unit is located in Rm 48 (key #470-839). Connection of the batteries to determine the proper sense of voltage deflection is recommended prior to turning on the charger to prevent accidental discharge due to improper hook-up. Charging rates of 2 - 3 amperes are normally used, although rates of 5 - 6 amperes can be used with adequate monitoring of the degree of charging.

Distilled water is normally added to replace evaporation

losses. However, complete filling prior to charging is recommended to prevent overflow due to expansion during charging. The batteries are located on wooden platforms to reduce the possibility of conduction paths between batteries due to acid overflow and/or flooding of the floor. Also, the battery surfaces require periodic cleaning to reduce surface conduction due to contamination. After cleaning, terminals should be protected from corrosion by coating with vaseline or some other protective film.

2. Lead O-ring Fabrication

Nominal 1/16 inch or 0.060 inch lead wire is shaped in the aluminum O-ring mold. Cut both ends diagonally to obtain a large surface area for joining and butt them together in the groove. Since the lead O-ring will stretch slightly upon handling later, it is advisable to make the diameter approximately 1/16 to 1/4 inch less than desired prior to fusing. After adding flux to the splice, place the aluminum mold and lead wire on an asbestos board with the lead joint region projecting approximately one inch. Use the #5 tip on the gas-oxygen torch and heat the mold from below until the top surface of the lead joint just starts to melt (it will become shiny). Immediately remove the torch. The lead should flow sufficiently to join without a significant reduction in diameter of the wire. Initial attempts may result in imperfect joints so practice with scrap wire is advisable.

3. Diffusion Pump Cleaning

Removal and reinstallation of the diffusion pump (for oil changing) from the glass-metal-glass-metal system requires caution. This is necessary as unrelieved stress on the glass components may result in fracture at the most unappropriate location and/or time. Note and mark the position of the diffusion pump clamps and clamp all unsupported glass lines attached to the diffusion pump prior to loosening the flange bolts. After removal from the system, note the color and odor of the diffusion pump oil. Compare with new oil to determine if changing is required. After cleaning to the base metal with solvents and cleansing powder, dry and add 70 ml of diffusion pump fluid. Note that the stages disassemble for ease of cleaning. Vac-Oil, a siloxane copolymer, is recommended as degradation occurs slowly compared to paraffinic oil, thereby requiring fewer changes of the pump fluid. Reassemble with care to avoid straining the glass. Detection of stress fields in the glass by placing between polarized light source and analyzer is recommended to determine if stress-relief annealing is required.

4. Mueller Bridge Contact, Switch Contact and Recorder Slidewire Cleaning

Vaseline may be used to prevent wear of the resistance commutator contacts. Note that this is a non-bleached vaseline and is slightly tan in color. Bleached vaseline is white in color and is corrosive to the electrical contacts.

On the Mueller Bridge, mercury commutators are used for decade changes in resistance and for normal, reverse platinum resistance

thermometer leads switching. These require periodic cleaning for good electrical contact and prevention of abnormal wear. Normally this can be achieved by simply flushing the contacts with triply distilled mercury. Complete removal and storage of the contaminated mercury from the retaining ring around each commuter is essential for safety.

Occasionally, cleaning is required for the contacts of the various switches and the relay controlling the on - off shield and furnace heater current levels. The switch housings and relay are protected from dust by plastic film and should be carefully resealed after cleaning with a non-lubricant containing aerosol contact cleaner. Lubricant tends to enhance dirt accumulation which can be a major problem.

To obtain optimum response from the recorders, the slide wires, pen carriages and electrical adjustments must be cared for. The gain, dead band, etc. adjustments are adequately described in the respective manuals and do not require routine maintenance. However, due to the dusty conditions of the room it is advisable to periodically (weekly) clean the slide wires (both control and recording in the L & N recorder) with methylene chloride and a lint-free cloth. The pen carriages can also be cleaned with methylene chloride and should be lubricated with a fine machine oil. Contamination of the pen carriage and plugging of the L & N recorder pen often occurs due to overflow and drying of ink. This ink is water soluble and plugged pens can be readily cleaned in warm Alconox-water solution

followed by drying with acetone. Air pressure directed through an eye-dropper aids cleaning and drying of the pen tubing.

5. Instrument Ground

The main instrument ground is achieved through a 3/8" copper stake driven into the earth through a hole drilled into the floor behind the Mueller Bridge table. Periodically a poor ground may result from the relatively short length (~3 feet) of the copper rod and the drying effect of the building on the soil beneath the floor. An improved ground can be obtained by dripping water (via a tee connection to the diffusion pump coolant return line) into the hole for the ground rod. The flow rate of water is controlled by varying the backpressure on the coolant return line by screwclamp adjustment and adjustment of a screwclamp near the entrance to the ground stake. Rock salt may be added occasionally to improve the conductivity.

6. Techniques for Cooling Calorimeter to Sub-Liquid Nitrogen Temperatures

Often it is desirable to obtain calorimetric data at temperatures below the atmospheric boiling point of liquid nitrogen (-196°C) without the expense and trouble of using liquid helium, potentially explosive liquid hydrogen, or other liquified gases. Utilization of reduced pressure is a technique used routinely with liquid helium in attempts to approach absolute zero. To the best of our knowledge, this technique has not been used to extend the cooling range of liquid nitrogen for instrumental data acquisition.

The feasibility of this concept was checked by evacuating the liquid nitrogen filled Union Carbide metal dewar with a mechanical pump. A calibrated thermocouple, inserted prior to evacuation, was used to determine the speed and degree of sub-atmospheric cooling that could be achieved. The observed decrease in temperature was approximately 20 degrees with concomitant solidification of the nitrogen. Nitrogen freezing and temperature stability once cooled was evidenced by being unable to remove the frozen-in thermocouple for about twenty minutes after exposure to atmospheric pressure. Based on the above preliminary experiment, two techniques were devised to extend the lower operating range of the calorimeter.

The initial method utilized a flange-silicone sleeve device to achieve a vacuum chamber above the liquid nitrogen filled in-place dewar. This assembly was previously used to exhaust hydrogen vapors when liquid hydrogen was employed as a coolant. This system was attached to the calorimeter after prior cooling to liquid nitrogen temperature. Note that the helium previously added to the calorimeter to enhance heat transfer should be evacuated prior to removing the dewar for vacuum jacket installation. Also note that the brass dewar protective can and insulation must be removed to permit mating with the sleeve assembly. An O-ring should be used to obtain a vacuum tight seal between the flange portion of the vacuum jacket and the calorimeter frame plate. However, a 1/8" OD rubber hose coated liberally with high vacuum silicone grease, although makeshift, performed adequately. Clearance

between the dewar and vacuum jacket requires that the following procedure be followed to prevent binding. Loosely fasten the jacket assembly to the calorimeter frame plate. Prior to tightening, raise the filled liquid nitrogen dewar to maximum height possible - measure from the lower edge of the relief valve (~29 in.). After raising the dewar gradually into place, tighten the flange screws and then seal the silicone rubber sleeve with large hose clamps. The procedure is reversed for disassembly. Leaks in the silicone rubber sleeve can temporarily be sealed with Apiezon soft wax. Permanent repairs can be made with room temperature curing silicone rubber. Achievement of 60°K normally required more than eight hours with occasional addition of liquid nitrogen. Attainment of vacuum better than 20 inches of water normally required less than 20 minutes. The major disadvantage of this system is that the level of liquid and/or solid nitrogen cannot be determined readily and addition of liquid nitrogen is time-consuming and wasteful. In addition, precooled liquid nitrogen cannot be ádded without difficult disassembly and reassembly.

The second technique has the advantage of being able to visually observe the liquid nitrogen level as well as affording capability for rapid addition of pre-cooled liquid nitrogen. Also this method does not require removal of the dewar with the resultant evacuation and helium addition procedures before and after coolant addition. This results in significant saving in time and more efficient use of coolant.

The assembly consists of a 13" diameter, 3/8" thick plexiglass circle with appropriate pipe and support rod holes symmetrically situated in the radial cuts to form pie shaped pieces. A vacuum port, vacuum gauge and purge valve pass through this plate. A thermocouple can either be passed through a gap in the pieces or through a separate port. The pieces are supported in the center by sheet metal ears (attached to the central vacuum pipe by a hose clamp) with the outer edge and resting on the dewar. Temporary sealing can be achieved by either silicone rubber or with the soft Apeizon wax used for the silicone rubber sleeve repairs as mentioned earlier. It is advisable to achieve more permanent sealing of all parts except the removable section by use of epoxy resin or other rigid adhesive. Note that use of flexible sealants requires that the dewar remained at a fixed height.

When the liquid and/or solid nitrogen level decreases sufficiently, precooled nitrogen can be prepared as described earlier in the metal dewar. Maintenance of coolant temperature by use of a thermocouple is required to prevent nitrogen freezing. After cooled, purge both the preparatory dewar and the calorimeter dewar to minimize freezing and accumulation of water vapor and quickly add the pre-cooled nitrogen after removing the plexiglass pie section. Evacuate after resealing the plexiglass top section.

B. CALORIMETER LOADING PROCEDURES

Several steps are normally required during the cycle of

unloading and loading the Calorimeter. (Note that Calorimeter refers to the silver sample cyclinder whereas calorimeter refers to the entire apparatus.) Although some of these manipulations may not be required for all samples, the following order of procedures recommended is:

1. removal of Calorimeter from support ring
2. disassembly of Calorimeter
3. Calorimeter cleaning
4. sample loading
5. reassembly of Calorimeter
6. evacuation and helium addition
7. leak testing
8. installation of heaters and platinum resistance thermometer
9. installation of Calorimeter into the ring

1. Removal of Calorimeter from Supporting Ring

Prior to removal of the Calorimeter, the three ring screws must be removed and the platunum resistance thermometer and Calorimeter heater leads must be unplugged from the receptacles in the top of the shield side.

Threading the leads into the shield can outside of the ring eases their removal once the Calorimeter is lifted. Normally, the strength of adhesion between the ring and Calorimeter is sufficient to require the application of a force perpendicular to the plane of the ring on its exposed rim. A dissection needle works well. Care must be taken to prevent loss of silicone grease from either

the lower lip of the Calorimeter (via gripping fingers) or from the ring (via lead removal). This is necessary as the silicone grease removed from the calorimeter lower lip is determined later by weighing and this amount is later added during reassembly. Loss of silicone grease from the ring cannot be monitored. The shield lid should be replaced to prevent contamination of the silicone grease remaining on the ring during calorimeter cleaning and reloading. The continuity of the Calorimeter heaters and platinum resistance thermometer should be checked at this time with a VTVM or VOM. Also, all the circuits of the calorimeter should be rechecked for circuit continuity and grounding after Calorimeter removal. Repairs, if necessary, should be made during sample extraction to minimize down time.

2. Disassembly of Calorimeter

Use of the Mikrova Balance:

Initial use of the balance in any series of weighings requires a calibration check using the standard weights stored in the weighing chamber. In addition, the transformer should be turned on approximately 30 minutes prior to weight measurement to prevent abnormal drifting due to thermal non-equilibrium. Duplicate measurements are recommended during weighing as erroneous values are occasionally obtained possibly due to sticking or post equilibration of the balance assembly. Experience indicates that often the first weighing is a few milligrams in error. Obviously, incorrect weights are obtained if the movement of the damping assembly below the

weighing pan is hindered by weighing tissue, etc. Also calorimeter leads must not touch any part of the balance other than the weighing pan assembly.

Reproducibility of measurement also requires that the mass weighed be located in the center of the pan. A check of the zero reading after each weighing is recommended as silicone grease or dirt, etc. may be deposited on the pan by the Calorimeter assembly. Note that dimming of the room lights enhances the brightness of the scale reading. A protective hood, constructed to allow weighing without changing room illumination, was found to be more inconvenient than room darkening.

The as-removed Calorimeter assembly is weighed after the preliminary balance warm-up and calibration has been made. The Calorimeter is now disassembled in the following order with careful weighing after each step:

1. Weigh the as-removed Calorimeter assembly. Comparison of this weight with the installation weight will determine the quantity of silicone grease removed or deposited on the ring. This estimate is, of course, subjected to change as leakage of the helium out of and air into the Calorimeter may have occurred during the completed run.
2. Carefully remove with cotton swabs (Q-tips) all the high vacuum silicone grease from the Calorimeter lower lip - the part that rests on the support ring in the calorimeter. The weight of silicone grease removed will be added to the lower lip upon reassembly.

3. Remove the bottom protective cone.
4. Carefully unwind the platinum resistance thermometer and Calorimeter heater leads by gently prying up the silver clips located around the diameter of the Calorimeter outer surface. After unwinding and untangling the leads very carefully, remove the heater units and the platinum resistance thermometer from the re-entrant wells of the Calorimeter base. Initially, gentle upward prying of the heater units with tweezers may be required. This can be achieved easily by inserting the tip of the pin of curved-tip tweezers into the small hole through the projecting end of the heater unit just below the solder connections. Remove all silicone grease, weigh and store on clean tissue under a glass beaker, etc. in a safe location. Weight of silicone grease removed can be obtained from the difference in weight of the cleaned and as-removed heaters and platinum resistance thermometer. The difference in weights of the Calorimeter assembly before and after removal yields the weight of the as-removed heaters and platinum resistance thermometer.
5. Weigh the Calorimeter assembly before and after removal of silicone grease from the re-entrant wells. The sum of this weight and that obtained in Step 4 determines the amount of silicone grease that will need to be added to the re-entrant wells during re-assembly.
6. Open the vent screw and note if there is an audible hiss.

Reweigh and note quality of sealing. Make change in estimate of silicone grease deposited or removed from the ring. Also there should be agreement in weights obtained during assembly in air before and after the complete run.

7. Remove the lid assembly noting the weight of the lid screws as a group and the lid assembly. Compare weight with those obtained during assembly and note if any sample is retained on the inner lid surface.
8. Disassemble the lid assembly recording all component weights. The small lid O-ring can be readily removed by prying gently with the small spatula stored in the balance weighing chamber.
9. Remove the large teflon-coated stainless steel O-ring by a gentle prying motion with the 1/2" wide spatula likewise stored in the balance weighing chamber. Weigh and store with the small lid teflon-coated O-ring in a run codified envelope.
10. Weigh the Calorimeter base and sample to confirm the value obtained during assembly. The sample is now ready for extraction.

If the Calorimeter can be cleaned without soxhlet extraction of the sample or immersion of the Calorimeter in solvent, then steps two and three can be eliminated. Obviously the same steps during reassembly will also be omitted.

3. Calorimeter Cleaning

The Calorimeter is cleaned by extracting with a good solvent

in a large soxhlet described in Figure A2. As in all soxhlet operations, cooling rate and heat input must be properly adjusted for the solvent-polymer system used. Similarly addition of boiling chips is required to prevent bumping during solvent boiling. Heating of the soxhlet itself is achieved by wrapping with a heating tape regulated by a variable transformer. Both the soxhlet and solution reservoir may require insulation depending upon the solvent-polymer system being used. The solution reservoir should be fitted with approximately 800 ml of solvent initially to allow for filling of the soxhlet. In addition, to prevent solvent or polymer oxidation, the system should be purged well with an inert gas prior to heating. After purging, the flow rate of inert gas can be readily adjusted to allow passage of only a bubble at a time through the sulfuric acid bubbler. This bubbler also scrubs out residual water vapor in the gas. The water cooled condensers are required to prevent loss of solvent and to allow flow of the purging gas. Extracted solution should be removed whenever the polymer solution foams or after about 4 hours initially and thereafter at longer times until the Calorimeter is clean. Note that removal of solution prior to soxhlet dumping results in less solvent required for cleaning.

To prevent disassembly for solution removal, vacuum aspiration of the hot solution was adopted. A trapped water aspirator is used to suck the hot solution through a teflon tube into a cleaned acid bottle. If the solution is to be saved for reuse, it may be advisable to purge the storage bottle with dry nitrogen prior

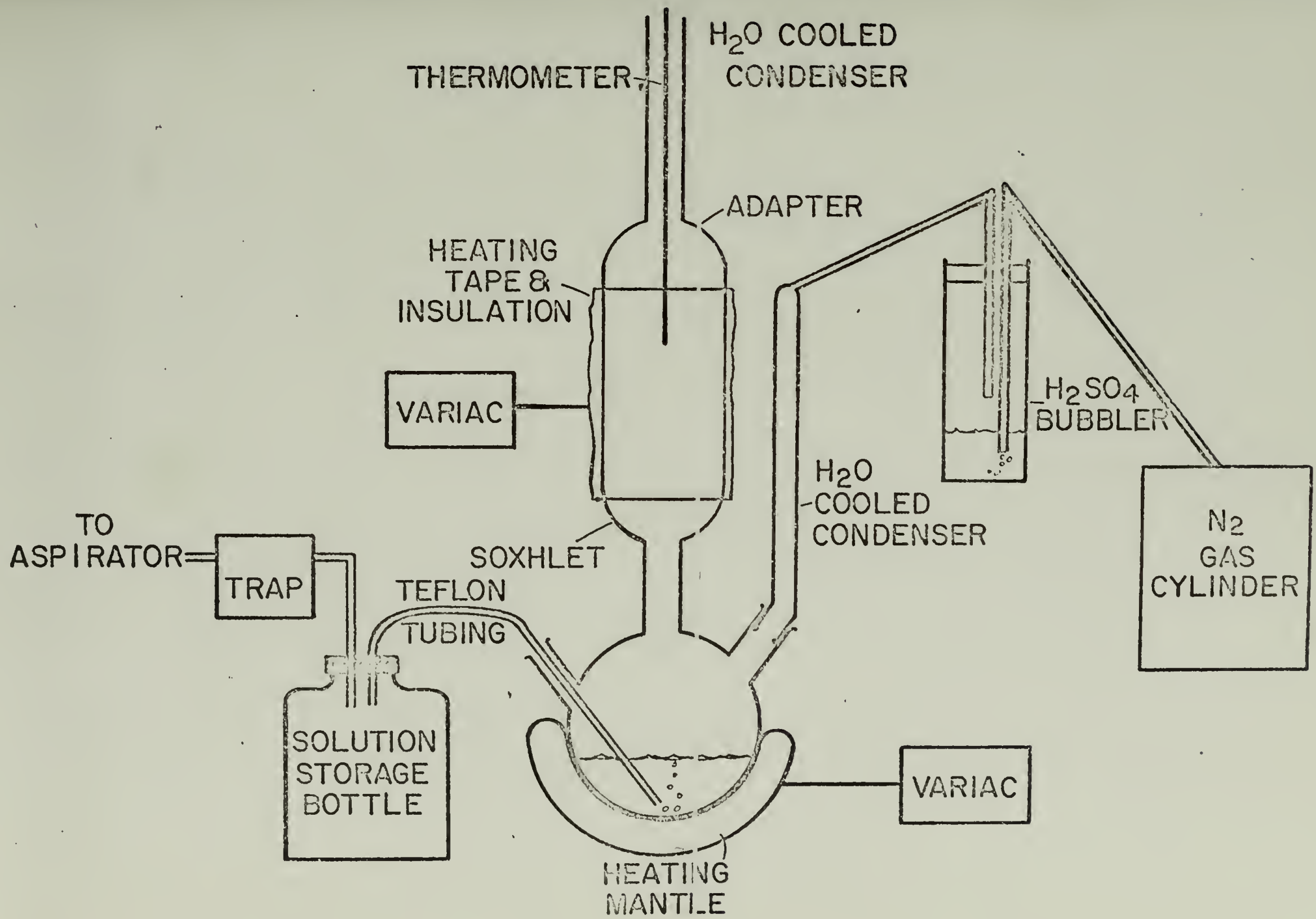

Figure A-2

Schematic Drawing of Apparatus for Extracting Sample from the Calorimeter

to transfer. For direct reprecipitation of the extract polymer, the solution can be aspirated directly into a heated dripping funnel for dropwise addition to an adequately stirred non-solvent.

Soxhlet extraction should proceed until Calorimeter constant weight is achieved. However, in practice it is easier to determine the lack of polymer in the extracted solution by addition of non-solvent. However, after removal from the soxhlet, the outer Calorimeter silver surfaces must be polished with jeweler's rouge and a soft cloth or paper towel. The interior of the Calorimeter and the re-entrant wells need not be polished but should be checked for cleanliness. The weight of the Calorimeter base after extraction and polishing must be less than the previously determined clean weight.

4. Sample Loading

After cleaning, the calorimeter base is weighed and fastened into the plexiglass support block with a ring screw to facilitate sample addition. Powders and liquids are readily added but film specimens require careful cutting to size and packing to achieve the desired sample weight in the range of 35 - 50 grams. It is possible to obtain quality results with a sample weight of less than 10 grams but the larger the weight of sample, the greater the probability of more precise and accurate results. Note that the sample must not protrude far enough above the re-entrant wells and vanes to prevent closure of the vent assembly or sealing of the large teflon coated O-ring.

Needless to say, cleanliness of both the calorimeter and sample is required to obtain meaningful results. Consequently, the sample must contain as little solvent and other unwanted material as possible. Therefore, it is wise to heat all samples prior to loading to above their T_g or T_m in a vacuum oven for about 24 hours or until solvent vapor cannot be detected or polymer constant weight is achieved. If thermal effects upon sample preparation are of interest, prepare the samples as described and then evacuate for approximately 24 hours after thermal treatment. Removal of additives will generally require dissolution and reprecipitation of the polymer of interest. Then the above procedures are required to remove residual solvent.

5. Re-assembly of Calorimeter

The reassembly of the calorimeter proceeds in exactly reverse order to the disassembly procedure. However, note that the lid assembly parts, various screws, etc. are also cleaned prior to reassembly. All weights of parts must be less or equal to previous clean weights.

The vent screw should be oriented so that the punch hole on the outside edge of the screw end is directed towards the "X" scratched on the surface of the lid. Also the vent assembly should be hand tightened to prevent the vent screw from slipping out of its groove. However, the vent assembly should not be tightened excessively as evacuation and helium addition has to be accomplished through the vent.

Also, the lid should be oriented so that the "X" scratched

on its surface lies just to the right of the circular notch on the Calorimeter base lid rim when the calorimeter is viewed from the top. A diagram of this orientation is in the Calorimeter Modifications Log and will not be reproduced here. The screws attaching the lid to the Calorimeter base should be tightened alternately on opposite sides to obtain uniform sealing. Tighten until the lid is flush with the Calorimeter base rim. Note if any screws project below the Calorimeter lower lip surface by scraping the surface with a dissecting needle or spatula. If so, those screws must be removed, ground down and reinserted after the change in weight has been recorded. This is necessary to allow good thermal contact and rapid heat transfer between the Calorimeter and the ring. Care should be taken to insert the Allen wrench properly to prevent undue wear on the screw heads.

6. Evacuation and Helium Addition

The assembled Calorimeter (less heaters and platinum resistance thermometer) is installed in the plexiglass holding block and placed in the evacuation and helium addition apparatus (Figure A3). One ring screw should be sufficient to secure the calorimeter in the block for sealing. During evacuation it is necessary to hold down the vent screw as it will otherwise be lifted - up by the vacuum and will seal the calorimeter. Note that the mechanical vacuum pump is used for evacuation via the calorimeter purge valve located between the mechanical and diffusion pumps. A liquid nitrogen trap is used to enhance the quality of vacuum achievable. In addition, helium when added by the proper manipulation of valves

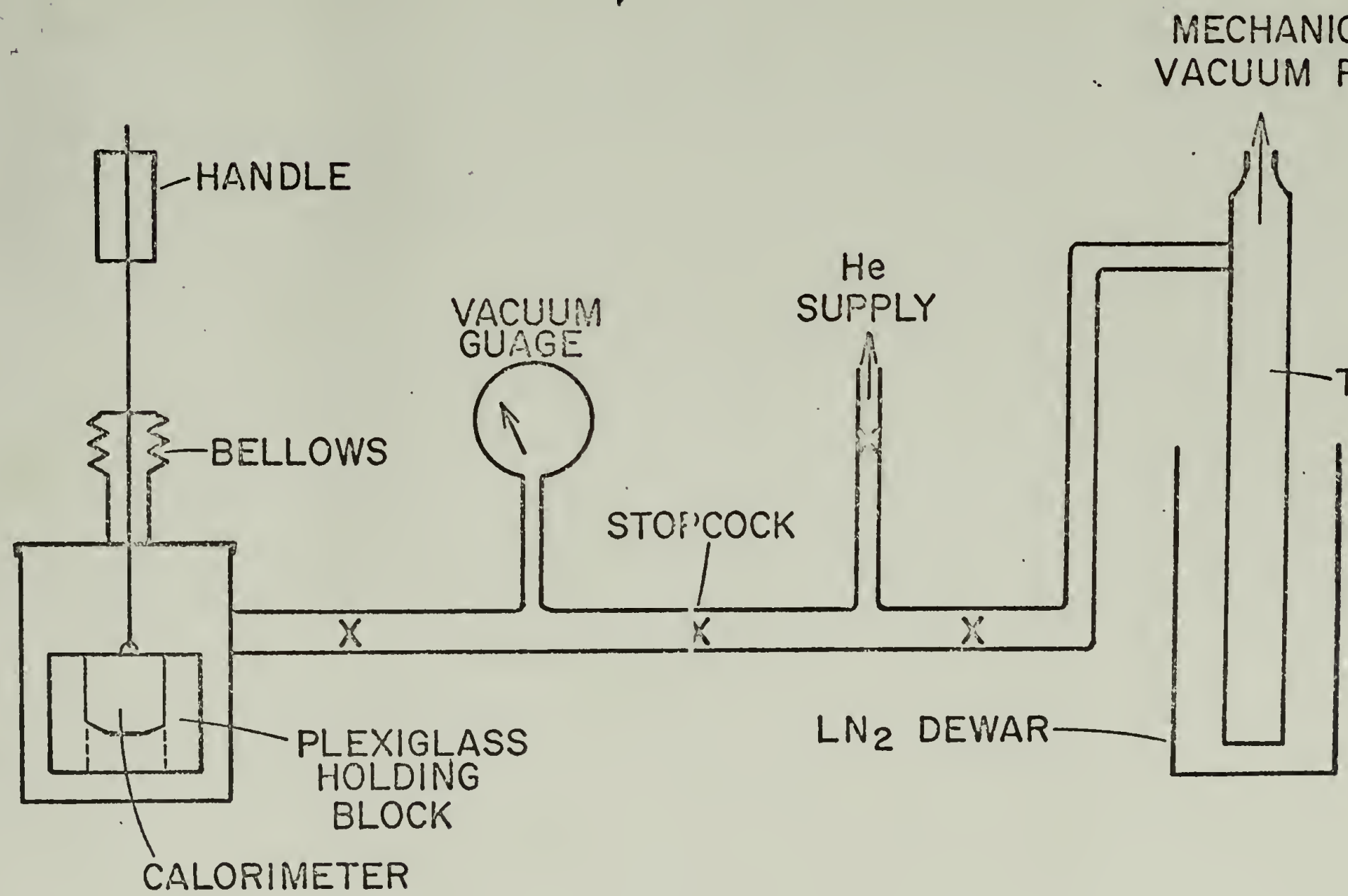

Figure A-3

Schematic Drawing of Apparatus for Evacuating and Sealing Helium Inside the Calorimeter.

is passed through a rubber vacuum hose immersed in liquid nitrogen. This serves as a crude trap to eliminate introduction into the calorimeter of condensibles that may be present in the helium. The standard procedure used for evacuating and filling with helium usually involves preliminary evacuation for about 15 - 30 minutes, then a series of helium purges prior to a long evacuation of at least one hour. The helium purges are repeated prior to sealing at a pressure of 10 - 20 inches of pressure.

7. Leak Testing

As mentioned earlier, helium is added to enhance thermal equilibration and as such must remain inside the calorimeter during the duration of the measurements. Weight gain as air diffuses in and helium diffuses out is the simplest method of leak detection. This technique is not very sensitive unless times on the order of days are allowed for leak testing. However, if no weight gain occurs after a couple of hours, then based on expérience, the leak will not significantly affect the operation of the calorimeter if the series of measurements are completed within a couple of weeks. In other words, experience indicates that if a gross leak is not detectible, then good sealing is generally achieved.

A more exact method of leak testing after assembly requires the use of a helium leak detector. The assembled Calorimeter is placed in a specially constructed aluminum vacuum can and connected to the helium leak detector (in the Physics Department). This is a very sensitive technique but lack of leak detector availability limits its usefulness.

III. OPERATING AND TROUBLE-SHOOTING PROCEDURES

A. MAINTAINING ADIABATIC CONDITIONS

1. Furnace Control

The temperature of the furnace is normally maintained approximately 0.25 degree lower than the shield. This temperature difference is referred to as the Δf and the necessary value for good control varies depending upon temperature of operation, vacuum quality, etc. However, it is advantageous to maintain variables of operation such as vacuum, Δf, etc., as similar as possible between runs so that generalized curves of factors (lumped heat transfer coefficients) and drift rates are applicable.

The Kiethley 150A Microvolt-Ammeter provides proportional control of the furnace-shield side temperatures. Note that control of the current supplied to the furnace top, bottom and side heaters is controlled in two locations. The voltage to the overall furnace and shield is determined by the power supply setting (Dresser-Barnes Corporation, Model 62-119 Regulated Supply) and the on and off controls on the rear of the bottom panel of the power supply rack. The power supply voltage (for both furnace and shield) is normally set at a constant voltage (e.g. 200v) to permit reproducible settings. Therefore, the major control of overall heater current is provided by the on and off controls on the rear bottom panel. The 180 volt dry cell powered relay (located on this bottom shelf) is activated when the main calorimeter on-dummy switch, S1, is operated and simultaneously switches the level of heating for both the shield

and furnace. The on and off current levels for both shield and furnace are adjusted to permit control by their respective potentiometers. This adjustment is easily made by trial and error. The levels of current required (for both shield and furnace) change in a slow smooth manner as the series of measurements proceeds. Trouble can be expected if frequent and/or large adjustments are required. If spiking of shield and/or furnace current occurs during operation, grounding is probably occurring and the power supply should be shut off immediately. Likewise if no current is flowing, the heaters are open-circuited. If adjustment of the either on or off potentiometer has no effect, try the other potentiometer to achieve temporary control as probably the batteries are too weak to activate the relay.

The furnace and shield top, side and bottom temperature differences are sensed by a series of six alumel-chromel thermocouples, TC,bridged between the respective surfaces. Their output is read on a Kiethley 149 Milli-Microvoltmeter as selected by the switches located in the panel above it. The TC Selector Switch determines the surface temperature difference read. The TC Polarity Switch determines the direction of deflection of the Kiethley 149 needle. If the Polarity Switch is negative and the needle defects negative, then the surface temperature difference (i.e. top or bottom) is cold. If the switch is negative and the needle deflects positive, the surface temperature difference is hot. The Instrument Selection Switch has to be turned to Mueller position. Note that if the

top or bottom is hot, the respective shield or furnace top or bottom control (on the front of the bottom power supply panel) would have to be adjusted to a higher value. If cold, the control would be turned to a lower value. Occasionally, top and bottom adjustments will not be sufficient and adjustment of the side control will be necessary. Do not exceed a setting of 9.85 as permanent damage to the potentiometer may result.

The degree of non-adiabaticity is affected by the quality of top and bottom control and the best control possible is desired (i.e. control to < 1 μv). As heat losses generally increase with temperature, the need for stricter control of top and bottom controls becomes greater. When making thermocouple readings, the same absolute value must be obtained when the Polarity Switch is alternated between positive and negative. If this does not occur, adjust zero suppression to achieve equal positive and negative values upon polarity switching. If drifting occurs during surface temperature difference readings, the thermocouple circuit may be open-circuited. Grounding may result in abnormal noise.

The measurement of Δf is accomplished (1) by zeroing the meter with zero suppression on the desired scale, (2) turning off zero suppression to obtain the Δf reading. Return to the normal operating range (normally 10 μv) and rezero if necessary after Δf measurement. Note that the error signal is proportional to the defection of the meter needle from zero. Therefore, fine adjustments can be made by using zero suppression to appropriately position the meter needle.

2. Shield Control

The major difference between furnace and shield control is that a better controller is utilized. Adjustments of the power supply, top, side and bottom controls, thermocouple reading, etc., are identical to those described for the furnace.

A Leeds and Northrup (L&N) Microvolt Indicating Amplifier is used to amplify the ring-shield bridged thermocouple error signal prior to input into the L&N CAT Series 60 Controller - Speedomax H recorder combination. The CAT controller provides proportional-integral-derivative, PID, control of the amplified error signal which is recorded on the Speedomax H recorder. When in operation, the microvolt amplifier is operated on the 50 μv scale in the recorder mode. Scales up to 2000 μv may be required during run on-off cycling. When cooling or grossly out of control, leave the microvolt amplifier in the log mode on the 2000 μv scale. The recorder is normally operated at the $6'' \ hr^{-1}$ (slow) chart speed. The settings for the CAT controller vary slightly with temperature, vacuum, etc., and typical values are recorded as are heater, top, side bottom setting, Δf, etc., in the Run Settings Log Book. Adjustment of the controller settings is well explained in its operating manual. However, remember that patience is a virtue when adjusting the PID controls.

When making runs, the shield-ring temperature difference should be zero on 50 μv scale before, during, and after runs when possible. At the beginning of the run, there may be a short period of loss of control. This should be treated as a non-adiabatic

condition as is the off cycle - the procedure of computing these corrections is described in Section IV B. Note that the pen must be kept on scale and the scale recorded to allow the area of non-adiabacity to be calculated.

Prior to calorimeter shut-off, it may be necessary to cool the shield to prevent unwanted overshoot hot. The amount of cooling required is dependent upon the calorimeter temperature, vacuum, top and bottom control, Δf, size and heat capacity of the sample, etc., and can only be determined by trial and error for the sample and conditions of each run. Generally, more cooling is required at low than high temperatures. It is also worthwhile to note that at low temperatures (< 200°K), it is wise to measure the drift rate (millidegree hour^{-1}) even if out of control on the 2000 μv scale. If the drift rate is low (i.e. near the equilibrium overnight drift rate), as it often is, then another run can be started. This is preferable to waiting until control on the 50 μv scale is achieved as hours may be required for that to occur if the shield overshoots hot at low temperature. Normally, equilibration times range from 5 to 30 minutes depending upon operating conditions with 20 minutes the average time between run end and beginning.

When troubleshooting any of the wiring in the calorimeter (heaters, thermocouples, platinum resistance thermometer, etc.) proceed in a systematic manner to determine the general location of the fault. Then successively narrow the possible sources of breakage, shorting, etc. With the old wiring, it is wise to check

all old breaks for failure or lack of insulation. All thermocouple and heater wires are color-coded at the radiation platform to assist in identification for troubleshooting. Also, diagrams of the lead input into the furnace and shield are drawn in the Calorimetry Maintenance Log Book. The new constant currents circuit diagram and the new vacuum feedthrough design and wiring codes are also included in this log book as are all changes in the instrument.

When making repairs, remember that thermal-free solder must be used for all μv circuits (i.e. thermocouples, etc.) and that this solder is relatively weak and will not withstand fatigue as readily as normal solder. Also note that all heater and thermocouple (especially thermocouple) repairs made in the calorimeter are accomplished by welding. The welder consists of soft lead pencil placed through a glass tee with the tip protruding slightly. The wood is removed from other protruding end of the pencil and one cable to a variable voltage transformer is attached to the bared lead. The electrode attached end of the pencil is sealed to the glass tee with tape and inert gas is allowed to flow through the tee emitting past the sharpened pencil tip. The other lead from the transformer is attached to the broken wires which are twisted together and trimmed to the same length. The pencil tip is touched against the tips of the twisted wires for an instant at about 40 volts for #36 thermocouple wire. Use of a magnifier attached to a headband aids manipulation of the thin wires. After repairing, place a teflon sleeve over the repair and seal the teflon sleeve and the wires in place with insulating resin.

Heater wire connections at the lugs on the top of both the furnace and shield are silver solder joints as are the seams of the silver calorimeter. For silver soldering in either case, clean the surfaces well and use silver solder-flux paste and protect all areas not to be soldered with water-soaked asbestos. After soldering with the micro-torch, remove all flux with preferably hot water. Note that polydimethylsiloxane degradation is enhanced by the presence of unremoved flux.

3. Vacuum Control

Vacuum consistently better than 10^{-5} mm Hg is required for high precision data and reproducible factor and drift values for successive runs and series of runs. Monitoring of vacuum quality is achieved by two thermocouple and two ion gauges. The thermocouple gauges, reading from 2000 μ to 1 μ, are located on the high pressure side (between the mechanical and diffusion pump) and near the manifold (between the diffusion pump and the calofimeter). The ion gauges reading from 10^{-3} to 10^{-11} mm Hg are located near the diffusion pump and near the manifold - both on the low pressure side of the diffusion pump. The thermocouple gauges are normally allowed to remain on whereas the ion gauges (due to their limited life) are used only during run readings. These are normally read at the beginning and end of a run to assure that the vacuum remained good throughout the run. Loss of water pressure, due to main breakage, etc., could result in degradation of the diffusion pump oil and contamination of the system. However, a water switch will shut off the diffusion pump power and will activate a buzzer if water

pressure is drastically reduced. Contamination of the ion gauges with diffusion pump oil will require that they be replaced or rejuvenated.

The liquid nitrogen trap should be used whenever the diffusion pump has been on long enough to evacuate the system to 10^{-4} mm Hg. The dewar, when full, should last 12 hours if the vacuum is 10^{-5} mm Hg or better. If the vacuum is poorer, heat transfer and nitrogen evaporation will occur at a faster rate. Of course, all system evacuation is done in two stages - roughing with the mechanical pump through the by-pass line followed by pumping with the diffusion pump.

Leak testing of the glass components is readily accomplished with a Tesla coil. In fact, with experience, the quality of vacuum can be estimated by the presence and color of the discharge. The higher the pressure, the more pinkish the color until there is no color (i.e. no discharge). As pressure is decreased, the color changes to violet and finally diminishes appreciably in the 10^{-4} - 10^{-5} region. However, the interior of the glass walls will continue to glow even at low pressures due to impurities.

B. MEASUREMENT OF HEAT INPUT, Q

1. Measurement of Current, I and Voltage, E

The energy input to the sample and calorimeter during a measurement is determined by obtaining the value of the integral

$$Q = \int_{t_i}^{t_f} E(t) \qquad \text{(A-4)}$$

as described earlier. In practice E and I change in a smooth linear fashion so the equation can be rewritten,

$$Q = EIt \qquad \text{(A-5)}$$

where E and I are the average current and voltage respectively and t is the time. E and I are determined by measuring the voltage drop across the calorimeter heater and a standard resistor in the heater circuit respectively. Two vernier high precision potentiometers (Croyden Precision Potentiometer) are arranged in each measuring circuit to oppose the major portion of the signals. The remainder of the reading is recorded on a 2500, μv two point printing recorder (G.E. Model 8HG). The final E and I readings are the sum of the potentiometer settings and the chart readings.

The potentiometers need to be rebalanced periodically to ensure that drifting due to thermal fluctuation of constant temperature bath or due to operating battery dischsrge decay. Two 2v lead acid batteries are used as operating batteries. The potentiometers are balanced using standard cells, which along with the standard resistors, etc., are maintained at 28.0 ± 0.05°C in the constant

temperature bath. A setting of 1.01825, when the potentiometers range are set to 1.0v, is required for proper balancing. Note that the standardize test switch is not used and remains in the test position. The Selector Switch for normal recording operation is set at position 3, while position 2 is for direct reading on the galvanometer. This switch must be turned to position 1 for balancing. Actual standardization is accomplished by nulling the galvanometer by successfully adjusting the current regulator resistances by the row of knobs in the right hand side of the potentiometer. These adjustments are initially made on the 10^6, 10^5, 10^4, etc., resistance scales by turning the knob near the galvanometer key on the lower left corner of the instrument. With practice, one can balance both potentiometers in about one minute. This speed is preferred during some periods of operation.

If the potentiometers cannot be balanced, it is due to either an open circuit in the operating battery supply lines or, most probably, the operating batteries need recharging. Noise in E and I are occasionally observed and may be due to loose connections (thermal free solder fatigues easily) and/or poor contact in the panel switches. These switches need to be cleaned periodically and should be resealed with plastic film to minimize contamination. The panel switches, S3 and S4, are used primarily as aids in trouble-shooting. Switching S3 from 1 to 2 and S4 from N1 to N2 results in interchange of signals to the potentiometers. Note that the current regulation settings will also have to be switched. The direct position of S3 allows

for direct measurement of the signal. Switch S4 in the Croyden position allows output of solely I and E on the recorder. The short position of S4 allows a quick check of the recorder by shorting the input. S5 allows switching of galvanometer input from one potentiometer to the other.

A dummy resistor is used to stimulate the calorimeter heaters during the off-on thermal equilibration. This simulation places a nearly constant drain on the power batteries, preventing transient E and I fluctuations when the calorimeter is turned on for a run. The dummy E and I values are adjusted at the end of each run to approximate the calorimeter heater run E and I. The controls for such adjustments are located directly above S4 and S5 for I and E respectively.

2. Measurement of Run Time, t

The time of the run is measured by a electronic timer (Model 522B, Hewlett-Packard Co.). The timer is started and stopped when the main calorimeter on-dummy switch, S1, is turned to on and dummy respectively. The measurement is normally made in units of 0.01 seconds (i.e. time unit set at 0.01 seconds) and requires use of a small low frequency pulse counter to register the thousands of seconds of a run.

It is wise to check the accuracy of the timer daily by the self-check procedure described in the timer manual. In addition, if the run start and stop watch times are noted to the second, erratic timing and subsequent errors in data can be avoided by

simple comparison of timer and watch agreement. All the normal settings are labeled on the timer front panel and will not be reproduced here. However, it is often wise to reset the timer prior to starting a run as, if not reset, occasionally the timer will not start. If the timer does not start, the relay batteries may be faulty as described earlier or the trigger input and/or gate switch may have been accidently switched to the wrong position.

3. Constant Temperature Bath for Standard Resistors and Cells

The standard cells and resistors for the measurement of calorimeter heater current and voltage are maintained at 28.0 ± 0.05°C in a thyratron controlled silicone oil bath. A mercury thermoregulator is used to provide the error signal to the electrically noise-free controller. The bath is maintained at uniform temperature by mixing with a heavy duty stirrer. A forced air fan is used to cool the stirrer motor to prevent overheating. A cooling coil, using tap water, is used to achieve balanced control. The cooling water flow rate is adjustable and requires adjustment periodically as water pressure fluctuates and sticking of the flow meter due to dirt occurs occasionally. Therefore, it is wise to form the habit of checking bath temperature during every run.

A constant current device is used to smooth the current load that the calorimeter uses as lead and heater resistances change with temperature changes. The circuit diagram is drawn in the Instrument Modification Log. This device is also located in the constant temperature bath to eliminate variations due to effect of room temperature fluctuations on transistor performance. This

device is connected between the output of the power batteries and the input to the calorimeter on the rear side of the panel containing the S1, S2 and the fine calorimeter heater current adjust controls.

The current passing through the calorimeter heaters is displayed on the ammeter located in this panel. The level of heating current can be varied from about 20 to 75 ma by adjusting the course current control S2, and the fine (10 turn potentiometer) control current. This corresponds to a variation of the heating rate from about 1 to 15 degrees per hour.

4. Temperature Determination

The sample and calorimeter temperature is measured with a platinum resistance thermometer (type 8164, Leeds and Northrup Co.) and a G-2 Mueller Bridge No. 8069 (Leeds & Northrup Co.). A Kiethley Model 150B microvolt-ammeter is used as the null point detector. Under normal conditions it should be possible to measure the resistance to ± 0.00001 Ω which roughly corresponds to ± 0.0001°K. The calibration at four points with computer interpolation was provided by L&N and is located in the Mueller Bridge table drawer. Also located in this drawer or on the shelf above are all the instrument instruction manuals and warranties, calibration certificates, etc.

The Mueller Bridge operation is adequately described in the L&N manual. However, it is advisable to confirm that the ratio setting (14.9), Bridge temperature (34.9°C), etc., remain unchanged by checking their values every run. Battery supplied DC can be used to heat the bridge during measurements if the AC source is

noisy, but this is generally not required. Noise in null readings may be due to dirty or incompletely filled mercury commutators, dirty resistance contacts, and/or poor contact or loose microvoltmeter or platinum resistance thermometer leads. Pick up and bottle all dirty mercury for reclaimation.

A systematic method of connecting the platinum resistance thermometer leads to the Mueller Bridge is recommended. The connections were made so that the Normal resistance reading was slightly greater than the Reverse resistance reading. Also when readings were made, the Normal was always recorded first and then the Reverse to allow for equal time of temperature drift between successive Normal and Reverse readings.

5. Sequence of Measurements and Run Data Record

The operation of the instrument requires rapid readings and adjustments at the beginning and end of a run. During the run, only adjustments of shield and furnace top and bottom heater current levels are normally required. The following is a stepwise description of the procedures used to make a run (after finishing a previous run).

1. When drift rate appears to be approaching the equilibrium rate, make the following preparatory run readings; ΔF, System Ion Gauge (SIG), bath temperature, Mueller Bridge temperature and ratio, start the G.E. recorder.
2. After the Normal and Reverse resistance recordings prior to start of the run (which are entered as Ni and Ri) are taken, mark the L&N chart as to time, scale and previous

run number. Remove and remark the chart with the new run number, time, etc.

3. Reset the timer and turn on dummy switch, S1, to the on position. Quickly adjust the CAT controller current levels to maintain control on the 50 μv side. Also record exact time on run identification scales, etc., on the G.E. and L&N recorder charts.
4. Record the E and I values prior to and after balancing. Adjust furnace and shield top and bottom controls as required.
5. When approaching the end of the run, cool the appropriate amount depending on conditions as described earlier. Turn off, noting the exact off time, and record the timer reading, E and I and scale settings, etc., on the charts and data sheet. Take Δf and SIG reading and note changes as adjustments may be required. Note if run time calculated from on and off times agree with timer value.
6. After back in control - as evidenced by equilibrium drift rates - start taking drift readings until the equilibrium drift rate is approached sufficiently to allow start of another run. The remaining quantities on the Run Data Sheet (Figure A4) have been found to be useful in calculating a rough estimate of heat capacity as well as drift and non-adiabaticity corrections. For overnight control, adjust Δf to the best appropriate value and balance all tops and bottoms. Also adjust the current output of the CAT

Run #_____ Date_____197_

ON = _____ Δf_i = _____

OFF = _____ SIG_i = _____

t = _____ sec. bath temp. $_i$ = _____

M.B. temp._____°C Δf_f = _____

Ratio _____ SIG_f = _____

N_i = _____ R_i = _____ AVG_i = _____

N_f = _____ R_f = _____ AVG_f = _____

AVG RUN Ω = _____ E = _____

AD_{2000} = _____

C_R = _____

N.A. area = _____ $in.^2$ = _____ μv-min.

Factor = _____ μv-min/m° $\Delta T_{N.A.}$ = _____ m°

Drift Time = _____ min. = _____ hr.

O.N.d.r. = _____ m°/hr. ΔT_d = _____ m°

$DTC = \pm T_{n.a.} \pm T_d$ = _____

Figure A4. Raw Data Sheet Used for Individual Runs

controller to 3.0 ma to allow for the maximum variation of control. Also confirm that the calorimeter on-dummy switch is turned to dummy and that the liquid nitrogen dewars are filled.

IV. COMPUTATION PROCEDURES

A. ROUGH ESTIMATE OF HEAT CAPACITY

Normally it is advisable to compute a pseudo-specific heat from the equation:

$$C_R = \frac{E \cdot I \cdot t}{\Delta R} \qquad (A6)$$

where E = average voltage across the Calorimeter heaters during a run.

I = average current passing through the Calorimeter heaters during a run.

t = the time of the run in seconds

$$\Delta R = \frac{(Ni+Ri)-(Nf+Rf)}{2} \qquad (A7)$$

where N and R are present the normal and reverse platinum resistance thermometer readings and the subscripts "i" and "f" refer to readings taken before and after a run.

This simple calculation can be rapidly performed on an electronic calculator to provide an estimate of the uncorrected results. Plotting of this data will allow for rapid evaluation of the just completed point with respect to the set of points previously obtained. If the new data point deviates from the expected behavior, then a search for possible errors in computation or instrumental difficulties are warranted. To eliminate a false sense of security, it is wise to make expanded plots of this rough data so that changes of 0.1 - 0.2% are observable. One should realize that estimated changes in this rough estimate must include an accounting of the

empty Calorimeter heat capacity calculated in a similar manner. Note that these rough calculations are based on the raw data recorded on the individual run data sheet (Figure A4). In addition, these values are recorded on the run data sheet as well as tabulated for easy reference and plotting using the following format: Date, Run No., Average Run Resistance, C_R, Average Run Δf.

Occasionally a more correct estimate of heat capacity of the sample is desired before drift and adiabatity corrections are finished. This can be achieved by using either the time sharing or batch computer programs described later but without entry of the corrections. These computed results should be labeled as uncorrected - preferably by placing "UC" after the run code prior to data input to the computer.

B. DRIFT AND NON-ADIABATICITY CORRECTIONS

Corrections due to Calorimeter temperature drift ΔT_d, and non-adiabatic conditions, ΔT_{na} result in adjustment of the measured temperature rise, ΔT_m observed during a heating run. Consequently both are lumped into one term, DTC - an acronym for Delta Temperature Correction represented by the following equation:

$$DTC = \pm \Delta T_{na} \pm \Delta T_d \qquad (A8)$$

The sign of the non-aidabatic and drift correction terms depend upon conditions described fully in the following respective sections.

1. Drift Correction

The temperature of the Calorimeter is essentially constant

under "perfect" automatic control conditions. However, heat losses via radiation and conduction combined with the slightly lower (~0.25°) furnace temperature result in a slight downward drift in temperature. The magnitude of this drift is a function of temperature, mass and therefore heat capacity of the combined calorimeter and sample, the quality of vacuum (i.e. conductive losses, the quality of the radiative surfaces of the calorimeter and the interior of the shield and furnace, and the temperature difference, Δ_f, between the shield and furance. Generally under normal operating conditions the latter is the controlling factor in determining the drift rate. Transitional behavior of the sample may result in either positive or negative temperature drifts depending upon the nature of the transition (i.e. exothermic or endothermic).

Positive drift is illustrated in Figure A5, but a negative drift correction is determined in an analogous manner. Referring to Figure A5, note that the initial and final temperature readings (t_{Ti} and t_{Tf} respectively) do not coincide with the time that the calorimeter heaters are turned on and off (t_{ci} and t_{cf} respectively). Consequently, it is not correct to use the run time (i.e. $t_{cf} - t_{ci}$) for drift correction calculation. Instead the time interval, $t_{Tf} - t_{Ti}$, should be used for drift calculations. Although most of the difference between run time and time between initial and final temperature measurements occurs during thermal equilibration after a run (i.e. $t_{Tf} - t_{cf}$).

The measured temperature change (ΔTm) of a run is composed

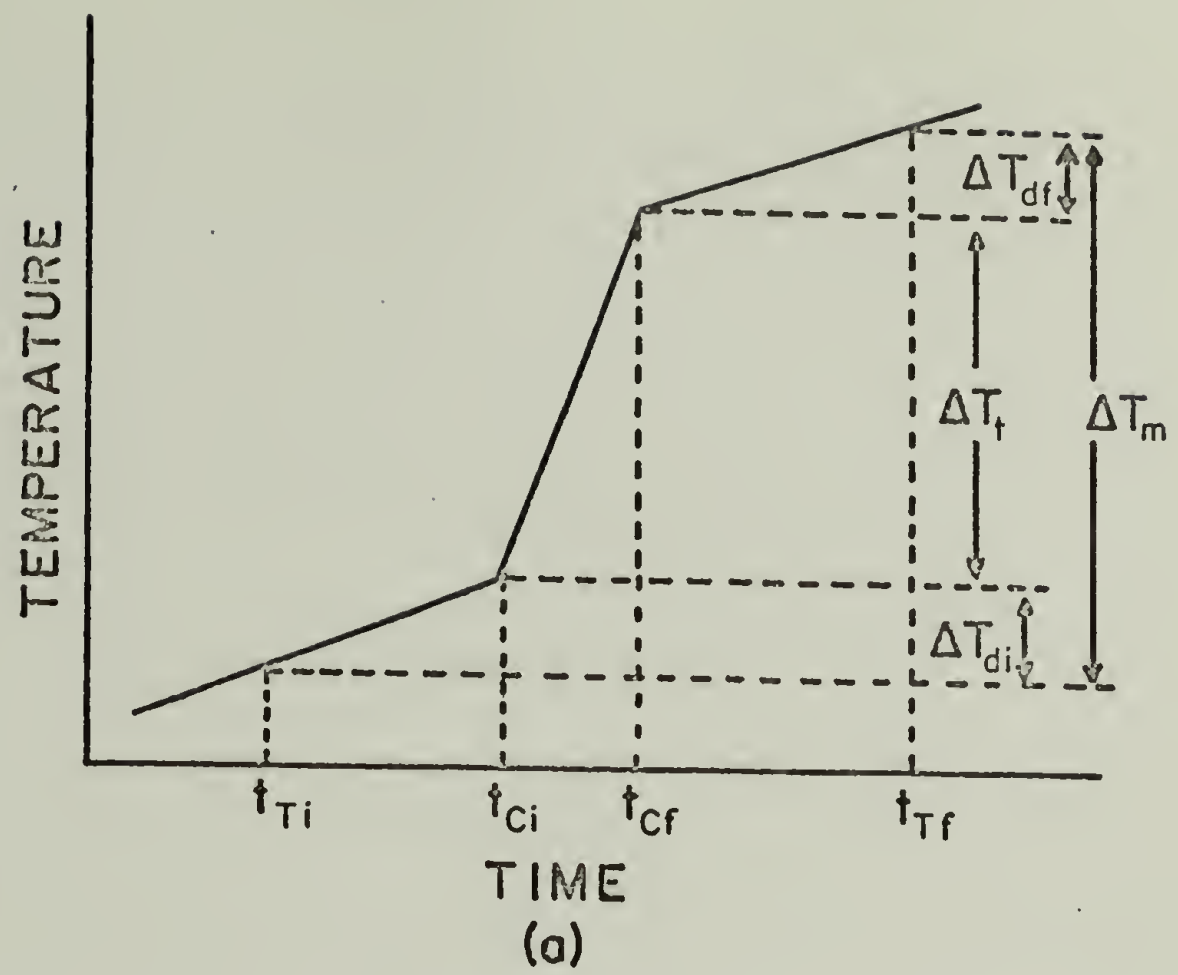

Figure A-5

Schematic Description of (a) Calorimeter Temperature Drift and, (b) Non-Adiabatic Conditions Requiring Correction of the Run Temperature Difference Measured.

of contributions due to drift occurring before Calorimeter heating occurs, (ΔT_{di}) during the run itself, (ΔT_{dm}) and after the run, (ΔT_{df}). The true temperature difference, (ΔT_t) that occurs while the Calorimeter heaters are on and the system is in adiabatic control is represented by the equation:

$$\Delta T_t = \Delta T_m - \Delta T_{di} - \Delta T_{dr} - \Delta T_{df} \qquad (A9)$$

$$\text{or } \Delta T_t = \Delta T_m - (t_{ci} - t_{Tc})d_i - (t_{cf} - t_{ci})dr - (t_{Tf} - t_{cf})d_f \qquad (A10)$$

where d_i, d_r and d_f represent the drift rates before, during, and after the run. Normally the drift rates obtained vary before and after the run as well as between runs. In addition, average run drift rates may be slightly different from the drift rates obtained overnight due to incomplete thermal equilibration. However, unless these differences in overnight and run average drift rates are large or because of some other known reason, overnight drift rates (O.N.d.r.) can generally be used as an average drift rate (d.r.) for all stages of the run. Using this assumption of equal drift rates, Equation (A10) is simplified to:

$$\Delta T_t = \Delta T_m - (t_{Tf} - t_{Ti})\overline{dr} \qquad (A11)$$

Analogous arguments can be used to determine that the equation for negative temperature drift correction is:

$$\Delta T_t = \Delta T_m + (t_{Tf} - t_{Ti})\overline{dr} \qquad (A12)$$

Estimates of drift rate are usually made by adding the decimal position of the normal and reverse platinum resistance thermometer

readings. A suitable interval of time is allowed between readings, preferably an exact fraction of an hour (i.e. 6, 10, 12, 15 min., etc.). The drift rate then can easily be estimated from the equation:

$$dr = [(N_i+R_c) - (N_f+R_f)](10,000)/(2)(\text{hours}) = m^\circ hr^{-1} \qquad (A13)$$

where the factor of two is required to obtain the average resistance instead of the sum. Recall that 0.00001 ohm is roughly equivalent to one millidegree accounting for the factor of 10,000. The N and R are the same as described earlier for the rough estimate of heat capacity.

Both of these equations can be generalized to

$$\Delta T_i = \Delta T_m \pm \Delta Td \qquad (A14)$$

where + is used if negative drift occurs; - is used if positive drift occurs. Also note that units of drift rates are millidegrees per hour, m°/hr, and time is in hours resulting in correction of the run temperature difference in millidegrees.

During transitions, or when equilibrium drift rates are difficult to attain, calculation of data should use the final temperature of the proceeding run as the initial temperature of the current run, etc. By doing this and using the extrapolated overnight drift rate for that particular temperature, the contribution of the sample to the temperature rise of the Calorimeter can be calculated.

Generally, the system is operating under non-adiabatic conditions only when the temperature difference between the Calorimeter (really

the ring) and the shield is non-zero. This results in either a - or + deflection (the shield being hot or cold with respect to the ring respectively) of the Leeds and Northrup (L&N) recorder pen. The net area represents either a gain or loss of energy to the Calorimeter - thereby requiring correction. A prerequisite for making any correction is knowledge of the correlation of deflection area and Calorimeter temperature change.

2. Factor Measurement

The factor correlates the L&N strip chart area in microvolt minutes, μv-min, with the observed decrease in calorimeter temperature. This is achieved by taking a Calorimeter temperature measurement via the platinum resistance thermometer and Mueller Bridge while in control. After the drift rate is determined, shut off the shield, switch the L&N Microvolt Indicating Amplifier to the 2000 μv range and record the μv range, chart speed, Factor No. both on the raw data sheet and the L&N strip chart. Allow the calorimeter to cool to approximately -4 on the L&N chart prior to turning on the shield and bringing back into control eventually on the 50 μv scale. The factor is really a measure of overall thermal loss (both conductive and radiative) so the shield - furnace temperature difference (Δf), the vacuum quality, and top and bottom control of both shield and furnace should be similar to those of a run at that particular temperature. The 0 to -5 distance on the L&N strip chart is 3.25 in. which is equivalent to 100 μv when the L&N Microvolt Recording Amplifier is operated on the

2000 μv range. When slow, the L&N chart speed of 10 in/min is used. The resultant area relationship is $1/in^2=(100)\ (10)/3.25$ μv-min. This relationship is useful as the area measured by the planimeter is in square inches resulting in the following equation for the factor calculation:

$$\text{FACTOR} = (1000/3.25)\ (\text{area 2000 scale})/\Delta R' \qquad \text{(A15)}$$

where $\Delta R' = [(Ni+Ri) - N_f+R_f)](10,000)/2 \qquad = m°$ (A16)

and the N's and R's are described previously. The factor is the strip chart area divided by the calorimeter temperature decrease or μv min/m°.

The value of the factor will smoothly decrease in a curvilinear fashion from a value of approximately 200 μv min/m° at liquid nitrogen temperature to a value of about 30 μv min/m° at 550°K. Unless conditions are changed from sample to sample, factors from successive series of runs will nearly coincide, thereby resulting in fewer factor measurements - only about every 50 degrees. However, if previous data does not exist for the current conditions, factors should be measured about every 20 degrees. Reproducibility is normally on the order of 1% so duplicate measurement of factors is not required except when an unusual value is obtained.

If the liquid nitrogen trap is dirty and allowed to warm up or if for some other reason the vacuum deteriorates, the factor will decrease. Unless these conditions are determined and the factor

measured, the data will be erroneous and even with correction the result will be suspect. Consequently, it is essential to monitor vacuum quality ($<10^{-5}$ mm Hg) and the furnace-shield temperature difference (Δf) constantly to maintain reproducibility acceptable operating conditions.

3. Non-Adiabatic Correction

The process of ending a run results in non-adiabatic transient period until control is achieved (i.e. zero temperature difference between the calorimeter and ring). However, there may be other occasions when non-adiabatic corrections will be applicable. These are handled similar to the off cycle and will not be discussed here.

The shield is normally cooled prior to the calorimeter shut-off (Figure A5b) to accommodate the temperature overshoot of the calorimeter due to its finite equilibration time. The amount of cooling required depends primarily upon the temperature of the system but is also a lesser function of furnace-shield temperature difference (Δf). The required amount of cooling can only be determined from experience at the current operating conditions. However, it is essential that subsequent shield overheating (L&N strip chart pen negative) after calorimeter shut-off be minimized when operating near liquid nitrogen temperatures. If the shield is allowed to overshoot hot, it will take hours to come back into control when near liquid nitrogen temperatures. Often it is possible to start

another run even when out of control under these conditions providing the drift rate is sufficiently low ($\leq 5 m°hr^{-1}$). Normally the shield-ring is allowed to come back into control on the 50 μv scale prior to the final temperature measurement. The resulting + and - areas are measured by a planimeter and the net area in square inches is converted by dividing by the relationship (described in factor section) to obtain μv-min. This quantity in turn is divided by the factor to yield the non-adiabatic temperature correction, ΔT_{na}, in millidegrees.

The sign of ΔT_{na} is determined by the net area of the hot and cold areas. Note in Figure A5b that the solid curve represents the Calorimeter temperature while the dashed line represents the shield temperature. In principle, the cold and hot portions of the cycle of the shield just exactly offsets that of the calorimeter with their respective net area being equal if perfectly balanced. Consequently, a non-zero area results in either a larger or smaller measured temperature rise, ΔT_m, for a run. As is evident from Figure A5b, if A>B or A'>B', then the net area is cold (-) on the L&N strip chart and the sign of ΔT_{na} is negative. Summarized in equation format neglecting drift effects:

$$\Delta T_t = \Delta T_m \pm \Delta T_{na} \qquad (A17)$$

where ΔT_{na} is + when B>A; B'>A'

ΔT_{na} is - when B<A; B'<A'

C. COMPUTER DATA REDUCTION

Efficient reduction of raw data to final finished results would be very time consuming without the use of computer techniques. The calculation of the rough estimate of heat capacity, C_R, requires about two minutes per point on an electronic calculator. Exact calculation similar to that performed via computer requires nearly one half hour on an electronic calculator. However, the Control Data Corporation 3600 used for these calculations requires roughly one minute for 100 such complete calculations.

The computer has been utilized in both time sharing and batch modes to affect data reduction. The advantage of time sharing lies in its rapid return of results but requires rental or purchase of a teletype and data-set. Also the fact that time sharing is only available during specified hours and that data and programs stored in memory are occasionally lost, limits the usefulness of this system. The batch system is relatively slow-with turn-around time in the computer variable from 15 minutes to 4 hours or more, depending on computer usage. However, the major advantage is that data is permanently recorded on punched cards which can easily be reprocessed at will. An example of this advantage is the initial computation of results without inclusion of corrections to determine trends. Later, corrections can be added without retyping the rest of the data. The same procedure with time sharing would require retyping of all the data.

The figures on the following pages contain a selected listing of programs and data to aid in future use, trouble-shooting and modification of these programs. The order of presentation of these programs is based on the relative frequency of use; sample computations, curve fitting and empty calorimeter computation.

1. Sample Computation, Batch

The program called HT CAP is used for point by point calculation of sample heat capacity encraty, enthalpy and entropy as listed in Figures A6, A7, and A8. Note that the initial card is a punched output request card obtainable at the computer center input/output window. If used, punched output of temperature and heat capacity, temperature and enthalpy and temperature and entropy will be obtained for subsequent computer manipulation. Obtaining punched output is very labor and time saving if fitting or further computation is required and should be used to best advantage. Note that for the present program the number of punched output cards will be three times the number of sets of data. Punched output is not printed and will require two passes through the card printer for complete printing. Consult computer center personnel for card printer operating instructions.

If punched output is not desired, remove the 7/8 7/8 Equip card (fourth line from the top) and do not fill out a punched output request card. Note that the first five lines are typed and are not left justified as required. Also the typewriter does not adequately indicate that 7/8 7/8 are two multipunched spaces,

```
      PUNCHED OUTPUT REQUEST CARD
      7/87/8TIME,5
      JOB CARD
      7/87/8EQUIP,7=62.
      7/87/8FTN,L,X
0001  PROGRAM HT CAL
0010  DIMENSION CRT(7,11), R11D(7), R12D(7),RF1D(7), RF2D(7),
     1 NSV(200), STIK(200), STEK(200), STAVK(200), SCPH(200), SCPX(200),
     2 SCPY(200), SCPZ(200) , ABRT(200)
0020  COMMON RC, A, B, C
0030  REAL M, IC, L, LO, IH
0040  INTEGER R11D, R12D, RF1D, RF2D
0050  K = C
0060  PRINT 70
0070  FORMAT (///46X,* RESISTANCE BULB CALIBRATION *//)
0080  DO 100 J = 1,11
0090  READ 95, ( CRT(I,J), I = 1,7 )
0095  FORMAT ( 7(F10.6) )
0100  CONTINUE
0110  READ 120, A, B, C
0111  READ 121, R0, RC, LO, AC
0112  READ 122, C0, C1, C2, C3
0113  READ 123, C4, C5, C6, C7
0114  READ 124, C8, C9, C10, C11
0115  READ 125, WK, XK, RAT, RB, M
0120  FORMAT ( 3(E15.8))
0121  FORMAT (4(F10.5))
0122  FORMAT ( 4(E15.8))
0123  FORMAT ( 4(E15.8))
0124  FORMAT ( 4 (E15.8))
0125  FORMAT ( 2(E15.8), F10.5,F10.2,F10.4)
0160  PRINT 170, A,B,C, R0, RC, LO, AC, C0, C1, C2, C3, C4, C5, C6,
     1 C7, C8, C9, C10, C11, WK, XK, RAT, RB, M
0170  FORMAT (13X,1HA,20X,1HB,21X,1HC,16X,2HR0,13X,2HRC,13X,
     1 2HL0,15X,2HAC//3(5X,E16.9),4(5X,F10.5)///12X,2HC0,19X,2HC1,19X,
     2 2HC2,19X,2HC3,19X,2HC4,19X,2HC5//6(5X,E16.9)///12X,2HC6,19X,
     3 2HC7,19X,2HC8,19X,2HC9,18X,3HC10,18X,3HC11//6(5X,E16.9)///12X,
     4 2HWK,19X,2HXK,16X,5HRATIO,10X,2HRB,13X,4HMASS//2(5X,E16.9),5X,
     5 F10.5,5X,F10.2,5X,F10.4///)
0230  DO 260 J = 1,11
0240  PRINT 250, ( CRT(I,J), I = 1,7 )
0250  FORMAT (1X, 7(F10.6) )
0260  CONTINUE
0290  READ 300, IRUN
0300  FORMAT ( A8)
0302  READ 303, JI
0303  FORMAT ( I3 )
0304  DO 1080 N = 1, JI
0310  K = K + 1
0316  IF ( K . GT. JI) GO TO 1100
0320  READ 330, ( R11D(I), I = 1,7 ), GOOD
0330  FORMAT (7I1, 2X, F4.1 )
0332  ABRT(K) = GOOD
0335  FORMAT ( 2(F10.6) )
0337  IF ( ABRT(K) .EQ. 1.0 ) GO TO 885
0340  READ 330, (R12D(I), I = 1,7 )
0350  READ 330, (RF1D(I), I = 1,7 )
0360  READ 330, (RF2D(I), I = 1,7 )
0370  READ 335, RIC, RFC
0380  READ 390, TIME, ELI, EBF, EC1, ECF, DTC
0390  FORMAT ( F9.2, 5(F10.7) )
```

Figure A-6

First Page of Batch Program Listing
for Sample Thermodynamic Computations.

```
0400    R11 = R12 = RF1 = RF2 = 0
0450    DO 540 I = 1,7
0460    J = R11D(I) + 1
0470    R11 = CRT(I,J) + R11
0480    J = R12D(I) + 1
0490    R12 = CRT(I,J) + R12
0500    J = RF1D(I) + 1
0510    RF1 = CRT(I,J) + RF1
0520    J = RF2D(I) + 1
0530    RF2 = CRT(I,J) + RF2
0540    CONTINUE
0550    R1 = ( R11 + R12 ) * 0.5 + R1C
        RR = ( R1/ R0 ) - 1.0
0551    T = RR / A
0552    RRT = T * ( A + B * T )
0553    RRPT = A + 2.0 * B * T
0554    IF ( RR .GT. 0.0 ) GO TO 560
0555    TSQ = T * T
0556    RRT = RRT + C * ( T - 100.0 ) * T * TSQ
0557    RRPT = RRPT + C * ( 4.0 * T - 300.0 ) * TSQ
0560    TES = ( RR - RRT ) / RRPT
0561    T = T + TES
0562    IF ( TES .GE. 0.0 ) GO TO 565
0563    TES = - TES
0565    IF ( TES .LT. 5.0E-5 ) 570, 552
0570    T1 = T
0580    T1K = T1 + 273.16
0590    RF = ( RF1 + RF2 ) * 0.5 + RFC
        RR = ( RF/ R0 ) - 1.0
        T = RR / A
0593    RRT = T * ( A + B * T )
        RRPT = A + 2.0 * B * T
0595    IF ( RR .GT. 0.0 ) GO TO 599
        TSQ = T * T
        RRT = RRT + C * ( T - 100.0 ) * T * TSQ
        RRPT = RRPT + C * ( 4.0 * T - 300.0 ) * TSQ
0599    TES = ( RR - RRT ) / RRPT
        T = T + TES
0601    IF ( TES .GE. 0.0 ) GO TO 603
        TES = - TES
0603    IF ( TES .LT. 5.0E-5 ) 605, 593
0605    TF = T
0610    TFK = TF + 273.16
0620    TAVK = ( T1K + TFK ) * 0.5
0630    TAV = ( T1 + TF ) * 0.5
0640    TDELTA = ( TF - T1 ) + DTC / 1000
0650    PRINT 659, IRUN, K, R11D, R12D, R1C, RF1D, RF2D, RFC, TIME, EC1,
     1 ECF, EB1, EBF, DTC, R11, R12, R1, T1, T1K, TAVK, TAV, TDELTA,
     2 RF1, RF2, RF, TF, TFK
0659  FORMAT(1H1///X,A8,I4///10X,4HR11D,14X,4HR12D,13X,3HR1C,13X,4HRF1D,
     1 14X,4HRF2D,13X,3HRFC//2(6X,7(I1,1X),4X,7(I1,1X),4X,F10.5)///
     2 10X, 4HTIME,11X,3HEC1,12X,3HECF,12X,3HEB1,12X,3HEBF,12X,
     3 3HDTC//5X,F10.2,5(5X,F10.6)///10X,2HR11,12X,2HR12,13X,2HR1,12X,
     4 2HT1,12X,3HT1K,11X,4HTAVK,12X,3HTAV,12X,3HTDC//8(5X,F10.5)///
     5 10X, 3HRF1, 12X, 3HRF2, 13X, 2HRF, 12X, 2HTF, 12X, 3HTFK, //
     6 5( 5X, F10.5 ) /// )
0720    EC = ( EC1 + ECF ) * 0.5 / RC
0730    L = L0 + A0 * TAVK
0740    EB = ( EB1 + EBF ) *0.5
0750    EH = EB * ( L / RB + RAT )
```

Figure A-7

Second Page of Batch Program Listing
for Sample Thermodynamic Computations

```
0760    1H = 1C - EB / RB
0770    P = 1H * FH * TIME
0780    PK = P / 4.184
0790    CPT = P / TDELTA
0800    CPC = C0+TAV* (C1+TAV* (C2+TAV* (C3+TAV* (C4+TAV* (C5+TAV*
     1 (C6+TAV* (C7+TAV* (C8+TAV* (C9+TAV* (C10+TAV* C11)))))))))))
0810    CPS = CPT - CPC
0820    CPH = CPS / M
0830    CPHC = CPH / 4.184
0840    CPX = CPH / TAVK
0850    CPY = CPH * TDELTA
0860    CPZ = CPY / TAVK
0870    PRINT 880, 1C, L, EH, 1H, P, CPT, CPC, CPS, CPH, CPHC, CPX,
     1 CPY, CPZ
0880    FORMAT (10X,2H1C,15X,1HL,13X,2HEH,12X,2H1H,13X,1HP,14X,3HCPT,12X,
     1 3HCPC,12X,3HCPS//5X,F10.7,5X,F10.4,5X,F10.5,5X,F10.7,
     2 4(5X,F10.5)///11X,2HCP,11X,4HCPHC,10X,7HCP/TAVK,9X,5HCP*TD,
     3 8X,10HCP*TD/TAVK//5X,F10.4,5X,F10.6,4X,F12.8,4X,F9.5,5X,F10.7)
0882    GO TO 1000
0885    PRINT 895, K, K
0895    FORMAT (1H1/////5X,13,2(10X,33HRUN  ABORTED  OR  DATA  DISCARDED)
     1 , 16X, 13)
0902    GO TO 1080
1000    ST1K(K) = T1K
1010    STFK(K) = TFK
1020    STAVK(K) = TAVK
1030    SCPH(K) = CPH
1040    SCPX(K) = CPX
1050    SCPY(K) = CPY
1060    SCPZ(K) = CPZ
1080    CONTINUE
1100    PRINT 1105 , IRUN
1105    FORMAT (1H1 /// 1X, A8 )
1107    PRINT 1110
1110    FORMAT ( /// 5X, 3HRUN, 14X, 3HT1K, 12X, 3HTFK, 12X, 4HTAVK, 12X,
     1 2HCP, 12X, 7HCP/TAVK, 9X, 5HCP*TD, 9X, 10HCP*TD/TAVK ///)
1120    DO 1150 K = 1, J1
1121    IF (ABRT(K) .EQ. 1.0) GO TO 1144
1130    PRINT 1140 , K, ST1K(K), STFK(K),STAVK(K), SCPH(K), SCPX(K),
     1 SCPY(K), SCPZ(K)
1132    WRITE (7, 1141 ) STAVK(K), SCPH(K)
1140    FORMAT (5X, 13, 10X, F10.4, 5X, F10.4, 5X, F10.4, 5X, F10.4, 5X,
     1 F12.8, 5X, F10.4, 5X, F12.8)
1141    FORMAT ( E15.8, 5X, E15.8 )
1142    GO TO 1150
1144    PRINT 1146, K, K
1146    FORMAT (5X, 13, 2(10X, 33HRUN  ABORTED  OR  DATA  DISCARDED),
     1 16X, 13)
1150    CONTINUE
1151    DO 1157 K=.1,J1
1152    WRITE ( 7, 1156 ) STAVK(K), SCPY(K)
1156    FORMAT ( E15.8, 5X, E15.8 )
1157    CONTINUE
1158    DO 1170 K= 1, J1
1159    WRITE ( 7, 1161 ) STAVK(K), SCPZ(K)
1161    FORMAT ( E15.8, 5X, E15.8 )
1170    CONTINUE
2160    END
          SCOPE
@LOAD
```

Figure A-8

Third Page of Batch Program Listing
for Sample Thermodynamic Computations.

with a 7 and 8 punched in both the first and second column of the card. The program ends with the first line of Figure A8 where @ is the lister interpretation of 7/8. The next eleven lines of Figure A9 is the correction table for correcting platinum resistance thermometer values and is referred to in the program as the CRT array. The next two lines are constants of the platinum resistance thermometer and are used in equations to convert from resistances to temperatures. All of the above is permanent data and is changed only if the platinum resistance thermometer is changed or recalibrated or if the Mueller Bridge is recalibrated. The succeeding three lines are coefficients of the orthogonal polynomial used to simulate the empty calorimeter and are represented by the symbols C0 through C11 in Figure A9. The next line or eighteenth line from the top contains two mass calorimeter correction terms, two Mueller Bridge correction terms and the mass of the sample used. The above constants, except for sample mass, only change if a new empty Calorimeter calibration run is made.

The sample mass and the sample code represented by any series of eight alpha - numeric characters on the next line remain unchanged for a particular series of measurements on a sample. The number of individual runs to be computed is listed in the next line and must be right justified in the third column as it I3 formatted. An aborted run can be represented by the next line. These numbers result in proper indexing with the message "RUN ABORTED OR DATA DISCARDED" as illustrated in Figure A10. Also, for an aborted run the computation steps normally required are skipped, saving computer time.

```
@RUN,3,5000
  0.0         0.0         0.0        0.0          0.0        0.0        0.0
9.999645   0.999981   0.099999   0.01       0.001      0.0001     0.00001
19.999255  1.999946   0.199983   0.02       0.002      0.0002     0.00002
29.998660  2.999921   0.299968   0.03       0.003      0.0003     0.00003
39.998345  3.999907   0.399975   0.04       0.004      0.0004     0.00004
49.998024  4.999884    0.499984  0.05       0.005      0.0005     0.00005
59.997623  5.999855   0.599996   0.06       0.006      0.0006     0.00006
70.0       6.999833   0.700008   0.07       0.007      0.0007     0.00007
80.0       7.999803   0.800019   0.08       0.008      0.0008     0.00008
90.0       8.999794   0.900020   0.09       0.009      0.0009     0.00009
100.0      9.999755   1.000011   0.1        0.01       0.001      0.0001
  3.9854599E-3 -5.8089999E-7-4.3119999E-12
25.57180   10.00035   -1.11800   0.03565
   1.1745337E? 7.621[illegible]E-2 -2.4[illegible]E-4   3.60788852E-7
 9.2799080E-11 5.0704627E-11-1.6528976E-13-5.93586140E-16
 5.15624801E-19 6.[illegible]31?7E-21            0.0E0            0.0E0
          0.0E0             0.0E06.00170   10000.00   40.032
PCHMA-A
141
0.00000    1.
 608747
 598156
 68580[illegible]
 675203
0.0        0.0
2560.11   0.773083   0.773083   0.592784   0.592784   -2.362
7/87/8 .                                                           00207
```

Figure A-9

Listing of Batch Program Permanent, Semi-Permanent and Run Data

RESISTANCE BULB CALIBRATION

A	B	C	R0	C	I0	A0
3.98545999E-003	-5.85899998E-007	-4.31199999E-012	25.5718	10.0035	-1.1180	0.03565

C0	C1	C2	C3	C4	C5
1.17453376E+002	7.68127524E-002	-2.40452324E-004	3.60788852E-007	9.27990803E-011	5.07048271E-011

C6	C7	C8	C9	C10	C11
-1.65267620E-013	-5.93586147E-016	5.15524801E-019	6.03503137E-021	0.00000000E+000	0.00000000E+000

AA	XX	RATIO	RB	MASS
1.00000000E+000	0.00000000E+000	6.00170	10000.00	46.3320

0.010000	0.000000	0.000000	0.000000	0.000000	0.000000	0.000000
9.999445	0.999981	0.099999	0.010000	0.001000	0.000100	0.000010
19.999255	1.999942	0.199983	0.020000	0.002000	0.000200	0.000020
29.998860	2.999921	0.299968	0.030000	0.003000	0.000300	0.000030
39.998345	3.999907	0.399975	0.040000	0.004000	0.000400	0.000040
49.998024	4.999864	0.499984	0.050000	0.005000	0.000500	0.000050
59.997623	5.999855	0.599996	0.060000	0.006000	0.000600	0.000060
70.000000	6.999833	0.700008	0.070000	0.007000	0.000700	0.000070
80.000000	7.999833	0.800019	0.080000	0.008000	0.000800	0.000080
90.000000	8.999794	0.900020	0.090000	0.009000	0.000900	0.000090
100.000000	9.999755	1.000011	0.100000	0.010000	0.001000	0.000100

1 RUN ABORTED OR DATA DISCARDED RUN ABORTED OR DATA DISCARDED 1

Figure A-10

Output of Permanent and Semi-Permanent Data and Aborted Run

The next six lines represent the input of run data from a normal run. The first four lines are the Normal, initial; Reverse, initial; Normal, final; and Reverse, final; platinum resistance thermometer readings respectively and are right justified in column seven. Note that this means that the first column is blank for a resistance less than ten ohms. Also note that these are of integer format and decimal insertion will result in a multitude or error statements. The next line contains the resistance correction terms which will normally not vary significantly from zero. The next to last line in Figure A9 is the input of run time, initial voltage, final voltage, initial current, final current and the overall correction term due to drift and non-adiabacity, DTC, in millidegrees as read into the computer by line 300 of Figure A4. The data deck must end with a 7/8 7/8 end-of-file card.

The semi-permanent data and aborted run output are illustrated in Figure A10. The individual run output, although not illustrated, is similar to that obtained via time sharing as shown in Figures A15 and A16. The quantities normally used for thermodynamic interpretation are summarized for ease of comparison and plotting as illustrated in Figure A11. The symbols from left to right are the individual run number, the initial temperature in degree Kalvin (TIK), the final temperature in °K (TFK), the average run temperature in °K (TAVK), the heat capacity (CP), encraty (CP/TAVK), and entropy (CP*TD/TAVK). The appropriate metric units of the thermodynamic quantities are Joules gm^{-1} $°K^{-1}$, Joules gm^{-1} $°K^{-2}$, Joules gm^{-1} and Joules gm^{-1} $°K^{-1}$ respectively. Note that heat capacity and

PCHMA-A

RUN	TIK	TEK	TAVK	CP	CP/TAVK	CP*TD	CP*TD/TAVK
1	RUN ABORTED OR DATA DISCARDED			RUN ABORTED OR DATA DISCARDED			1
2	89.4176	95.3551	91.8863	0.458	0;00499463	3.1928	0.03463807
3	95.4551	100.7663	98.0607	0.480	0;00489652	2.5984	0.02649767
4	101.0216	106.6397	103.7306	0.506	0,00487979	2.9452	0.02839256
5	106.6397	112.1561	109.3979	0.532	0;00486361	2.9345	0.02682436
6	112.1561	117.7461	114.9511	0.554	0;00482402	3.1004	0.02697105
7	117.7461	123.5968	120.6714	0.578	0,00479125	3.3834	0.02803810
8	123.5968	129.3467	126.4818	0.605	0;00478631	3.4920	0.02760904
9	RUN ABORTED OR DATA DISCARDED			RUN ABORTED OR DATA DISCARDED			9
10	RUN ABORTED OR DATA DISCARDED			RUN ABORTED OR DATA DISCARDED			10
11	129.4474	134.6922	132.0098	0.630	0;00477538	3.3058	0.02503040
12	134.6922	139.9391	137.3157	0.654	0,00476268	3.4302	0.02498011
13	139.9391	145.5430	142.7510	0.666	0,00466904	3.7445	0.02624498
14	145.4621	150.6675	148.0648	0.704	0;00475648	3.6643	0.02474778
15	150.6675	155.7278	153.1976	0.723	0,00471919	3.6587	0.02388203
16	155.7278	161.4953	158.6115	0.745	0;00470161	4.3010	0.02711647
17	161.4953	167.3409	164.4281	0.781	0;00475265	4.5745	0.02782072
18	167.3409	172.4711	169.9460	0.790	0;00465128	4.0378	0.02376353
19	172.4711	176.8439	174.6575	0.813	0,00465495	3.5529	0.02034224
20	176.7913	180.8937	178.8425	0.829	0,00463801	3.4008	0.01901566
21	180.8937	185.0159	182.9548	0.848	0,00463561	3.4924	0.01908908
22	185.0215	188.5921	186.7618	0.866	0,00463680	3.0088	0.01611061
23	188.5021	192.0563	190.2792	0.866	0;00455938	3.0820	0.01619747
24	192.0563	195.2014	193.6289	0.878	0,00453420	2.7643	0.01427622
25	195.2014	198.2536	196.7275	0.888	0;00451813	2.7156	0.01380369
26	198.2536	201.2781	199.7659	0.906	0;00453849	2.7427	0.01372946
27	RUN ABORTED OR DATA DISCARDED			RUN ABORTED OR DATA DISCARDED			27
28	201.2824	204.4154	202.8489	0.920	0;00453941	2.8845	0.01421980
29	204.4154	208.7002	206.5578	0.942	0;00456345	4.0341	0.01953022
30	208.7002	212.2241	210.4622	0.957	0;00455094	3.3723	0.01602319
31	212.2241	215.6541	213.9341	0.976	0,00456416	3.3744	0.01577142
32	115.8251	120.1155	117.9708	0.573	0;00486003	2.4569	0.02082518
33	120.1155	123.9336	122.0246	0.584	0;00479242	2.2341	0.01830840
34	123.9336	127.7967	125.8602	0.603	0;00479732	2.3254	0.01847633
35	127.7967	131.6469	129.7168	0.619	0,00477476	2.3903	0.01842737
36	131.6469	135.0831	133.3650	0.634	0,00475549	2.1789	0.01633757
37	135.0831	139.1772	137.1301	0.648	0;00472637	2.6543	0.01935629
38	139.1772	143.3760	141.2776	0.667	0;00472711	2.8048	0.01985342
39	143.3760	147.4234	145.4007	0.686	0;00472429	2.7790	0.01911246
40	147.4234	151.4484	149.4359	0.706	0,00472643	2.8424	0.01902109
41	151.4484	155.3755	153.4119	0.722	0,00471027	2.8377	0.01849724
42	155.3755	159.5150	157.4552	0.740	0;00470517	3.0811	0.01956811
43	159.5623	163.2134	161.3878	0.757	0;00469341	2.7656	0.01713635
44	163.2134	167.0490	165.1312	0.771	0;00466996	2.9581	0.01791334
45	167.0490	170.8478	168.9584	0.791	0;00468569	3.0204	0.01787646
46	170.8478	174.3919	172.6278	0.802	0;00464034	2.8272	0.01637732
47	174.4351	177.9725	176.2038	0.815	0;00462530	2.8831	0.01636244
48	177.9725	181.6256	179.7990	0.836	0;00465442	3.0535	0.01698306
49	181.6256	184.6451	183.1354	0.842	0;00460108	2.5452	0.01389775
50	184.6451	187.8645	186.2548	0.852	0;00457917	2.7469	0.01474795
51	187.8645	191.2005	189.5325	0.874	0;00461558	2.9148	0.01537888

Figure A-11

Output of the Summary of Thermodynamic Data for a Series of Individual Runs.

encraty can be directly plotted versus temperature, whereas the cumulative quantities of enthalpy and entropy are plotted versus temperature using a suitable reference temperature or state. If there is an aborted run or some other discontinuity in the smooth collection of data, the enthalpy and entropy will require appropriate shifts to adjust their cumulative values correctly.

2. Sample Computation, Time Sharing

The sample heat capacity computation program is also stored in computer memory for time sharing usage. The arrangement of the program, permanent and semi-permanent data, run data and output are similar to that of the batch system and will not be discussed here. However, input and output statements are different as is operation. Nevertheless, time sharing program usage and data summary storage and retrieval, being not unique for this program will not be discussed in the section concerning empty calorimeter time sharing computation.

The instructions or questions printed out by the computer on the teletype should be obvious but may require definition. After gaining access to the computer via the appropriate sign - on codes, fetch the desired program (BEATTY 3, for sample heat capacity calculation (Fig. A12, A13, A14) MTCP, for empty calorimeter heat capacity computation or LSCFWOP, for orthogonal polynomial least squares fitting). Input the sample weight by listing program statement 4006 as indicated in the second and third lines from the top in Figure A15. Then retype 4006 exactly replacing the last number by the new sample weight. Next, when required, type

```
LIST MTCP
0001   PROGRAM HI CAP
0010   DIMENSION CRT(7,11), RI1D(7), RI2D(7), RF1D(7), RF2D(7),
0011A NSV(100),STIK(100),STFK(100),STAVK(100),SCPI(100),SCPC(100),
0012A SCPS(100), STDELTA(100)
0020   COMMON RO, A, B, C
0030   REAL M,IC,L,LO,IH
0040   INTEGER RI1D, RI2D, RF1D, RF2D
0050   K = 0
0053A
0080   DO 100 J = 1, 11
0090   READ, ( CRT(I,J), I = 1,7 )
0100   CONTINUE
0110   READ, A, B, C, RO, RC, LO, AO, C0, C1, C2, C3, C4, C5, C6,
0111A C7, C8, C9, C10, C11, WK, KK, RAT, RB, M
0112   PRINT 113
0113   FORMAT ( /// *FOR PERMANENT RUN DATA ENTER 1* /
0114A *FOR INDIVIDUAL RUNS ENTER 2* )
0115   INPUT, NPERM
0116   GO TO ( 120, 320 ), NPERM
0120   PRINT 125
0125   FORMAT ( /// 15X, *RESISTANCE BULB THERMOMETER CALIBRATION*//)
0160   PRINT 170, A , B, C, RO, RC, LO, AO, C0, C1, C2, C3, C4, C5, C6,
0161A C7, C8, C9, C10, C11, WK, KK, RAT, RB, M
0170   FORMAT (9X, 1HA, 17X, 1HB, 17X, 1HC / 3(1X,E16.8,1X) //
0171A 8X, 2HRO, 16X, 2HRC, 16X, 2HLO, 16X, 2HAO / 4(1X,E16.8,1X) //
0172A 8X, 2HC0, 16X, 2HC1, 16X, 2HC2, 16X, 2HC3 / 4(1X,E16.8,1X) //
0173A 8X, 2HC4, 16X, 2HC5, 16X, 2HC6, 16X, 2HC7 / 4(1X,E16.8,1X) //
0174A 8X, 2HC8, 16X, 2HC9, 15X, 2HC10, 15X, 2HC11 / 4(1X,E16.8,1X) //
0175A 8X, 2HWK, 16X, 2HKK, 13X, 5HRATIO, 9X, 2HRB, 9X, 4HMASS /
0176A 2(1X,E16.8,1X), 1X, F10.5, 2X, F10.2, 2X, F10.4 )
0190   PRINT 200
0200   FORMAT ( * IF YOU WANT A LISTING OF THE CRT TABLE ENTER 1 * /
0201A * OTHERWISE ENTER 2 * )
0210   INPUT, NGO
0220   GO TO (230,260), NGO
0230   DO 260 J = 1,11
0240   PRINT 250, ( CRT(I,J), I = 1,7 )
0250 FORMAT (1X,7(F10.6) )
0260   CONTINUE
0280   PRINT 290
0290   FORMAT ( * TO INPUT RUN ENTER 1, OTHERWISE 2 * )
0300   INPUT, NGO
0310   GO TO (320, 1000), NGO
0320   PRINT 330
0330   FORMAT ( * INPUT RUN NAME ( 8 CHARACTERS OR LESS ) IN QUOTES * )
0340   INPUT, NRUN
0350   RI1 = RI2 = RF1 = RF2 = 0
0360   PRINT 370
0370   FORMAT ( ///* INPUT RI1D(1) THRU RI1D(7) * /
0371A *        RI2D(1) THRU RI2D(7) * / *          AND RIC * )
0380   INPUT, RI1D, RI2D, RIC
0390   PRINT 400
0400   FORMAT ( /  * INPUT RF1D(1) THRU RI1D(7) * /
0401A *        RF2D(1) THRU RF2D(7) * / *          AND RFC * )
0410   INPUT, RF1D, RF2D, RFC
0420   PRINT 430
0430   FORMAT ( * INPUT TIME, ECI, ECF, EBI, EBF, AND DTC * )
0440   INPUT, TIME, ECI, ECF, EBI, EBF, DTC
0450   DO 540 I = 1,7
0460   J = RI1D(I) + 1
0470   RI1 = CRT(I,J) + RI1
0480   J = RI2D(I) + 1
0490   RI2 = CRT(I,J) + RI2
0500   J = RF1D(I) + 1
0510   RF1 = CRT(I,J) + RF1
0520   J = RF2D(I) + 1
0530   RF2 = CRT(I,J) + RF2
0540   CONTINUE
```

Figure A-12

Time-Sharing Program for Sample Heat Capacity Calculation

```
0550  R1 = ( R11 + R12 ) * 0.5 + R1C
0551  RRT = RRPT = TES = 0.0
0552  RR = ( R1 / R0 ) - 1.0
0553  T = RR / A
0554  RRT = 1 + ( A + B * T )
0555  RRPT = A + 2.0 * B * T
0556  IF ( RR .GT. 0.0 ) GO TO 560
0557  TSQ = T * T
0558  RRT = RRT + C * (T-100.0) * T * TSQ
0559  RRPT = RRPT + C* ( 4.0 * T - 300.0 ) * TSQ
0560  TES = ( RR - RRT ) / RRPT
0561  T = T + TES
0562  IF ( TES .GE. 0.0 ) GO TO 564
0563  TES = - TES
0564  IF ( TES .LT. 5.0E-5 ) 570, 554
0570  T1 = T
0580  T1K = T1 + 273.16
0590  RF = ( RF1 + RF2 ) * 0.5 + RFC
0591  RRT = RRPT = TES = 0.0
0592  RR = ( RF / R0 ) - 1.0
0593  T = RR / A
0594  RRT = 1 + ( A + B * T )
0595  RRPT = A + 2.0 * B * T
0596  IF ( RR .GT. 0.0 ) GO TO 600
0597  TSQ = T*T
0598  RRT = RRT + C * (T-100.0) * T * TSQ
0599  RRPT = RRPT + C * ( 4.0 * T - 300.0 ) * TSQ
0600  TES = ( RR - RRT ) / RRPT
0601  T = T + TES
0602  IF ( TES .GE. 0.0 ) GO TO 604
0603  TES = - TES
0604  IF ( TES .LT. 5.0E-5 ) 605, 594
0605  TF = T
0610  TFK = TF + 273.16
0620  TAVK = ( T1K + TFK ) * 0.5
0630  TAV = ( T1 + TF ) * 0.5
0640  TDELTA = ( TF - T1 ) * DIC
0650  PRINT 659, KRUN, R11D, R12D, R1C, RF1D, RF2D, RFC, TIME, EC1,
0651A ECF, EB1, EBF, D1C, R11, R12, R1, T1, T1K, RF1, RF2, RF, TF, TFK,
0652A TAVK, TAV, TDELTA
0659  FORMAT ( /// 1X, A8 // 6X, 4HR11D, 15X, 4HR12D, 15X, 3HR1C /
0660A 1X, 2(F12.5X), F10.5 // 6X, 4HRF1D, 15X, 4HRF2D, 15X, 3HRFC /
0661A 1X, 2(F12.5X), F10.5 // 5X, 4HTIME, 9X, 3HEC1, 9X, 3HECF,
0662A 9X,3HEB1,9X,3HEBF,9X,3HD1C / 1X, F10.2, 4(2X,F10.6), 2X,
0663A F10.5 // 5X, 3HR11, 9X, 3HR12, 9X, 2HR1, 10X, 2HT1, 10X, 3HT1K/
0664A 3(1X,F10.5,1X,), 2(1X,F10.4,1X)  // 5X, 3HRF1, 9X, 3HRF2, 9X,
0665A 2HRF, 10X, 2HTF, 10X, 3HTFK / 3(1X,F10.5,1X), 2(1X,F10.4,1X)  //
0666A 6X,4HTAVK, 9X, 3HTAV, 9X, 3HTDC/ 3(1X,F10.4, 1X) )
0680  IF ( TDELTA .EQ. 0.0 ) 690, 720
0690  PRINT 700
0700  FORMAT ( 1X, 10(1H*), * TDELTA = 0.0, RUN IGNORED *, 10(1H*) )
0710  GO TO 260
0720  IC = ( EC1 + ECF ) * 0.5 / RC
0730  L = L0 + A0 * TAVK
0740  EB = ( EB1 + EBF ) * 0.5
0750  EH = EB * ( L / RB * RAT )
0760  IH = IC - EB / RB
0770  P = IH * EH * TIME
0780  PK = P / 4.184
0790  CPT = P / TDELTA
0800  CPC = C0+TAV* (C1+TAV* (C2+TAV* (C3+TAV*
0801A (C4+TAV* (C5+TAV* (C6+TAV* (C7+TAV* (C8+TAV* (C9+TAV*
0802A (C10+TAV* C11))))))))))
0810  CPS = CPT - CPC
0820  CPH = CPS / M
0830  CPHC = CPH / 4.184
0840  CPX = CPH / TAVK
0850  CPY = CPH * TDELTA
0860  CPZ = CPY / TAVK
0870  PRINT 880, IC, L, EH, IH, P, CPT, CPC, CPS, CPH, CPHC, CPX,
0871A CPY, CPZ
0880  FORMAT ( / 7X, 2HIC, 9X, 1HL, 12X, 2HEH, 8X, 2HIH /
0881A 1X, F10.7, 2X, F10.4, 2X, F10.5, 2X, F10.7 // 6X, 1HP, 10X,
0882A 3HCPT, 9X, 3HCPC, 9X, 3HCPS / 4(1X,F10.4,1X) // 7X, 2HCH, 9X,
0883A 4HCPHC, 6X, *CP/TAVK*, 7X, 5HCP*TD, 3X, 10HCP*TD/TAVK /
0884A 1X, F10.4, 2X, F10.6, 2X, F10.6, 2X, F10.5, 2X, F10.7 )
0900  K = K + 1
```

Figure A-13

Time-Sharing Program for Sample Heat Capacity Calculation

```
0910  NSV(K) = NRUN
0920  STIK(K) = TIK
0930  STFK(K) = TFK
0940  STAVK(K) = TAVK
0950  SCPH(K) = CPH
0960  SCPX(K) = CPX
0970  SCPY(K) = CPY
0980  SCPZ(K) = CPZ
0985  CALL FILES ( 2, NRUN, TIK,TFK,TAVK,CPH,CPX,CPY,CPZ )
0990  GO TO 260
1000  CALL FILES ( 3, 0, 0., 0., 0., 0., 0., 0., 0. )
1005  STOP
1010  END
2000  SUBROUTINE TSECT ( R, T )
2010  COMMON R0, A, B, C
2020  RR = ( R / R0 ) - 1.0
2030  T = RR / A
2040  RRT = T * ( A + B * T )
2050  RRPT = A + 2.0 * B* T
2060  IF ( RR .GT. 0.0 ) GO TO 2100
2070  TSQ = T * T
2080  RRT = RRT + C * ( T - 100.0 ) * T * TSQ
2090  RRPT = RRPT + C * ( 4.0 * T - 300.0 ) * TSQ
2100  TES = ( RR - RRT ) / RRPT
2110  T = T + TES
2120  IF ( TES .GE. 0.0 ) GO TO 2140
2130  TES = - TES
2140  IF ( TES .LT. 5.0E-5 ) 2150, 2040
2150  RETURN
2160  END
2210  SUBROUTINE FILES ( NOPT, N1, P1, P2, P3, P4, P5, P6, P7 )
2215  GO TO ( 2220, 2270, 2265 ), NOPT
2220  PRINT 2225
2225  FORMAT ( *-FILE NAME * )
2230  INPUT, NAME
2235  CALL OPEN(1,NAME,-1)
2240  REW IND 1
2245  CALL GETPTR(1,LOC,LEN)
2250  NUM = 0
2252  IF ( LEN .EQ. 0 ) GO TO 2262
2254  READ(1) NUM
2256  CALL SETPTR(1,NUM*6)
2258  READ(1) X
2260  RETURN
2262  WRITE(1) NUM
2265  RETURN
2270  WRITE(1) N1, P1, P2, P3, P4, P5, P6, P7
2275  NUM = NUM + 1
2280  RETURN
2285  PRINT 2290
2290  FORMAT (*-CLOSE FILE * )
2295  INPUT, NDEC
2300  IF ( NDEC .NE. 3HYES ) RETURN
2305  REWIND 1
2310  WRITE(1) NUM
2315  CALL CLOSE(1,NAME)
2320  RETURN
2325  END
2330  ENDPROG
3001  0.0 0.0 0.0 0.0 0.0 0.0 0.0
3002  9.999645 0.999961 0.099999 1.0E-02 1.0E-03 1.0E-04 1.0E-05
3003  19.999255 1.999948 0.199983 2.0E-02 2.0E-03 2.0E-04 2.0E-05
3004  29.998660 2.999921 0.299968 3.0E-02 3.0E-03 3.0E-04 3.0E-05
3005  39.998345 3.999907 0.399975 4.0E-02 4.0E-03 4.0E-04 4.0E-05
3006  49.998024 4.999884 0.499984 5.0E-02 5.0E-03 5.0E-04 5.0E-05
3007  59.997623 5.999855 0.599996 6.0E-02 6.0E-03 6.0E-04 6.0E-05
3008  70.000000 6.999833 0.700008 7.0E-02 7.0E-03 7.0E-04 7.0E-05
3009  80.000000 7.999803 0.800019 8.0E-02 8.0E-03 8.0E-04 8.0E-05
3010  90.000000 8.999794 0.900020 9.0E-02 9.0E-03 9.0E-04 9.0E-05
3011  100.00000 9.999755 1.000011 1.0E-03 1.0E-04 1.0E-05 1.0E-06
4001  3.96545999E-3 -5.65699996E-7 -4.31199999E-12 25.5718C
4002  10.00035 -1.1180 0.03565 1.16668719E2 7.91368798E-2
4003  -1.97739909E-4 -5.97390819E-8 -1.87361699E-9
4004  5.26675476E-11 -1.89696929E-13 -1.81743659E-16
4005  1.70790559E-18 -1.88889478E-21 0.0E0 0.0E0 0.0E0 0.0E0
4006  6.00170 10000.0 83.3350
```

Figure A-14

Time-Sharing Program for Sample Heat Capacity Calculation

```
OK. DATE FILED:  03/29/72.

LIST 4006
4006  6.00170 10000.0 83.3350

RUN
  OK
FILE NAME ?TST


FOR PERMANENT RUN DATA ENTER 1
FOR INDIVIDUAL RUNS ENTER 2
?1

                RESISTANCE BULB THERMOMETER CALIBRATION

          A                    B                    C
 .39854600E-02       -.58590000E-06       -.43120000E-11

         R0          RC           L0           A0
 .25571800E+02        .10000350E+02  -.11180000E+01    .35650000E-01

         C0           C1           C2           C3
 .11666872E+03   .79136880E-01  -.19773991E-03  -.59739082E-07

         C4           C5           C6           C7
-.18736190E-08   .52567548E-10  -.16989693E-12  -.13174386E-15

         C8           C9          C10          C11
 .17079056E-17  -.13563947E-20            0            0

         WR           RR          RATIO          RB          MASS
          0            0         6.00170     10000.00      83.3350
 IF YOU WANT A LISTING OF THE CRT TABLE ENTER 1
 OTHERWISE ENTER 2
 ?1
          0          0          0          0          0          0          0
   9.999645    .999981    .099999    .010000    .001000    .000100    .000010
  19.999255   1.999948    .199983    .020000    .002000    .000200    .000020
  29.998660   2.999921    .299968    .030000    .003000    .000300    .000030
  39.998345   3.999907    .399975    .040000    .004000    .000400    .000040
  49.998024   4.999884    .499984    .050000    .005000    .000500    .000050
  59.997623   5.999855    .599996    .060000    .006000    .000600    .000060
  70.000000   6.999833    .700005    .070000    .007000    .000700    .000070
  80.000000   7.999803    .800019    .080000    .008000    .000800    .000080
  90.000000   8.999794    .900020    .090000    .009000    .000900    .000090
 100.000000   9.999755   1.000011    .001000    .000100    .000010    .000001
 TO INPUT RUN ENTER 1, OTHERWISE 2
 ?1
 INPUT RUN NAME ( 8 CHARACTERS OR LESS ) IN QUOTES
 ?SSA-40


 INPUT R1D(1) THRU R1D(7)
       R2D(1) THRU R2D(7)
       AND RIC
 ?2 4 6 4 3 9 3
 ?2 4 4 6 5 5 8
 ?0

 INPUT RF1D(1) THRU R1D(7)
       RF2D(1) THRU RF2D(7)
       AND RFC
 ?2 5 6 7 1 5 7
 ?2 5 4 9 0 1 3
 ?0
 INPUT TIME, EC1, EC2, EB1, EB2, AND DIC
 ?2700.04 0.855434 0.855434 1.125997 1.125997 0.00129
```

Figure A-15

Permanent and CRT Output and Run Input of Time-Sharing Program

in RUN and the result summary file name. Confirmation of platinum resistance thermometer constants, empty calorimeter fitting constants, and sample weight can be obtained by requesting permanent run data. If requested, then the option of reviewing the CRT table (platinum thermometer resistance to temperature conversion table) is offered. Finally, an individual run request is made which would have been achieved faster by skipping the Resistance Bulb Thermometer Calibration and CRL Table by entering 2 at the permanent run data request. A run code of eight alpha numeric characters is preferable including the individual run number for positive identification required next. Input of initial normal, reverse, and corrective resistance terms in the next request is of integer mode (similar to the batch system) but in addition requires a blank space between numerals as illustrated in Figure A15 for R11D and R12D. The final normal and reverse lead resistances are inputed in a similar fashion. The final data request for an individual run is in floating point format as indicated in Figure A15 with all entries left justified beginning in Column 1, 10, 20, 30, 40 and 50 for time, run data entries of initial current, final current, initial voltage, final voltage and temperature correction term respectively. The individual run output is listed in Figure A16 where TI, TIK and TF, TFK are the initial and final temperatures respectively in °C and °K respectively; P is the symbol for power; CPT, CPC and CPS are the overall heat capacity of the total system, the simulated empty calorimeter and the calculated sample for the average run temperature. The last

```
SSA-40

      RI1D                RI2D                RIC
 2 4 6 4 3 9 3       2 4 4 6 5 5 8                0

      RF1D                RF2D                RFC
 2 5 6 7 1 5 7       2 5 4 9 0 1 3                0

     TIME              ECI               ECF               EBI               EBF               DTC
  2700.04          .855484           .855484          1.125997          1.125997          .00129

      RI1               RI2                RI                TI               TIK
  24.64309          24.46472          24.55390          -9.9729          263.1871

      RF1               RF2                RF                TF               TFK
  25.67071          25.48924          25.57997            .0802          273.2402

     TAVK               TAV               TDC
  268.2136          -4.9464           10.0544

       IC                L                EH                IH
  .0855454          8.4438            6.75885           .0854323

        P               CPT               CPC               CPS
  1559.0767          155.0636          116.2724          38.7912

       CP              CPHC            CP/TAVK           CP*TD          CP*TD/TAVK
    .4655            .111254          .00173550          4.68018           .0174495
TO INPUT RUN ENTER 1, OTHERWISE 2
?2
CLOSE FILE ?YES
 01005, STOP

TIME:     2.684 SEC.
*FETCH TOBCD2
OK.  DATE FILED:  11/10/70.

OUT TOTBCD
OK
RUN
 OK
FILE NAME ?TOT
 00150, STOP

TIME:     0.241 SEC.
NAMES

 1  BEATTY3      1265
 2  TOBCD2         78

 3  TOTBCD         10

LIST TOTBCD
010 SSA-40   263.19 273.24 268.214  .46548  .0017355  4.68018  .0174495

RUN BEATTY3
 OK
FILE NAME ?TOT
```

Figure A-16

Individual Run Printout and Summary Storage for Time-Sharing Program.

five entries are the thermodynamic quantities calculated on a unit mass basis for the average run temperature, where CP is the heat capacity in Joules gm^{-1} $°K^{-1}$, CPHC is the heat capacity in calories/ gm^{-1} $°K^{-1}$, CP/TAVK is the encraty or $(dS/dT)p$ in Joules gm^{-1} $°K^{-2}$, CP*TD is the enthalpy in Joules gm^{-1} and CP*TD/TAVK is the entropy in Joules gm^{-1} $°K^{-1}$.

After completion of a run (Figure A16), the offered choice is that (1.) of entering another individual run or (2.) of filing the calculated results. Entrance of another run is just a repetition of the process just described. Storage of data in a BCD (binary code deck) file requires a YES answer. A NO answer results in exit from the program. To file data, fetch TOBCD2 whose program is listed in Figure A18. After the data filed notation, type OUT file name BCD. Note that the file name is any combination of eight alpha-numeric characters and was previously entered at the beginning of the run. After OUT file name BCD is okayed, type in RUN and file name to accurate data transfer and storage respectively. Retention of data at the teletype can be checked by requesting a listing of programs in use by typing in NAMES. The stored summarized data can be observed by listing file name - BCD as illustrated in Figure A15. Confirmation of summary storage in computer memory can be achieved by requesting a listing of programs in memory by typing in CATALOG. Repetition of an individual run calculation and summarized result storage is demonstrated in Figure A17 to enhance clarity of the summary storage procedure and to illustrate the ease of addition of new data to existing stored data.

```
FOR PERMANENT RUN DATA ENTER 1
FOR INDIVIDUAL RUNS ENTER 2
?2
INPUT RUN NAME ( 8 CHARACTERS OR LESS ) IN QUOTES
?SSA-47


INPUT R11D(1) THRU R11D(7)
      R12D(1) THRU R12D(7)
      AND R1C
?3 1 7 8 9 0 2
?3 1 5 8 8 2 7
?0

INPUT RF1D(1) THRU R11D(7)
      RF2D(1) THRU RF2D(7)
      AND RFC
?3 2 9 1 5 1 0
?3 2 7 1 0 2 2
?0
INPUT TIME, EC1, EC2, EB1, EBF, AND DTC
?3260.10 0.844268 0.844268 1.103140 1.103140 -0.00476
```

SSA-47

R11D	R12D	R1C
3 1 7 8 9 0 2	3 1 5 8 8 2 7	0

RF1D	RF2D	RFC
3 2 9 1 5 1 0	3 2 7 1 0 2 2	0

TIME	EC1	EC2	EB1	EBF	DTC
3260.10	.844268	.844268	1.103140	1.103140	-.00476

R11	R12	RI	T1	TIK
31.78767	31.58689	31.68728	60.5444	333.7044

RF1	RF2	RF	TF	TFK
32.91373	32.70884	32.81128	71.7919	344.9519

TAVK	TAV	TDC
339.3282	66.1682	11.2428

1C	L	EH	1H
.0844258	10.9790	6.65194	.0843150

P	CPT	CPC	CPS
1628.4550	162.6332	121.0368	41.5964

CP	CPHC	CP/TAVK	CP*TD	CP*TD/TAVK
.4991	.119299	.00147099	5.61182	.0165380

```
TO INPUT RUN ENTER 1, OTHERWISE 2
?2
CLOSE FILE ?YES
 01005, STOP

TIME:     2.392 SEC.
FETCH TOTBCD2
NAME ALREADY USED
OUT TOTBCD
OK
RUN
 OK
FILE NAME ?TOT
 00150, STOP

TIME:     0.254 SEC.
LIST TOTBCD
010 SSA-40   263.19 273.24 268.214  .46548  .0017355  4.63013  .0174495
020 SSA-47   333.70 344.95 339.328  .4991   .0014710  5.61182  .0165380
```

Figure A-17

Input, Output and Storage Operations via Time-Sharing

```
FETCH TSBCD2
OK. DATE FILED:  11/10/70.

LIST
0001   PROGRAM TSBCD
0010   NSEQ = 0
0020   PRINT 30
0030   FORMAT ( *-FILE NAME * )
0040   INPUT, NAME
0050   CALL OPEN(1,NAME,-1)
0060   REWIND 1
0070   READ(1) LEN
0090   DO 140 LP = 1,LEN
0100   NSEQ = NSEQ + 10
0110   READ(1) NRUN, P1,P2,P3,P4,P5,P6,P7
0120   WRITE(62,130) NSEQ, NRUN, P1,P2,P3,P4,P5,P6,P7
0130   FORMAT ( S3,1X,A8,2(1X,F6.2),1X,F7.3,1X,F7.5,1X,F9.7,1X,
0131C 1X,F7.5,1X,F9.7)
0140   CONTINUE
0150   STOP
0160   END
0170   ENDPROG
```

Figure A-18

Program for Filing Computed Output Summary

3. Fitting Program

This program will compute by the method of least squares using orthogonal polynomials, a polynomial of degree specifiable up to 100 for as many as 3000 data points after the required constants have been determined. The fitted equation can be used to compare the computed data with the original data. In addition, interpolation or extrapolation can be achieved by reading in new sets of abscissas for ordinate evaluation. The complete procedure can be repeated for several sets of data if so desired. The versatility of this program allows its use for empty calorimeter simulation as well as simulation and extrapolation of sample thermodynamic quantities.

The program, called LSCFWOP, is listed in Figures A19, A20, A21, and A22, and was obtained in unmodified form from the computer center library. Punched output request of output, although not illustrated in this listing, can easily be added as described earlier for the sample heat capacity program.

Format of input data is shown in the first seven lines in Figure A23 and are described in detail below. The first data card contains the run or partial run code of ten alpha-numeric characters. If several sets of data are to be processed at once, the successive run card and data must follow the last data card of the previous run. A blank card will terminate the program. The second input card contains the input data format left justified in Column 1 for ordinates, abscissas, XBAR, GAMMA, and TOL. Note that the

```
      7/8TIME,5
      JOB CARD
      7/8EOCARD,23800
      7/8FTN,L,X
      PROGRAM LSCFWOP
      DIMENSION VEC(3000,6),S(101),ALP(101),BETA(101),RHOSQ(101),XP(101)
      DIMENSION INFMT(10),ID(10)
      COMMON VEC,S,ALP,BETA,XP
      IHLT=3H
 1327 READ 3000,ID
      DO 1337 I=1,10
      IF(ID(I)-IHLT) 1400,1337,1400
 1337 CONTINUE
      GO TO 411
 1400 PRINT 2
    2 FORMAT(1H1)
      PRINT 8000,ID
      READ 8000,INFMT
 8000 FORMAT(10A8)
      PRINT 1500,INFMT
 1500 FORMAT(//14H INPUT FORMAT 10A8/)
      READ 21,MM,KK,KOT,KIP,KAP,KOP,NOP,NIP,MTI
   21 FORMAT(10I5)
      READ INFMT,XBAR,GAMMA,TOL
      PRINT 4
    4 FORMAT(/44H  MM   KK  KOT  KIP  KAP  KOP  NOP  NIP  MTI)
      PRINT 21,MM,KK,KOT,KIP,KAP,KOP,NOP,NIP,MTI
      PRINT 1
    1 FORMAT(//23H XBAR      GAMMA      TOL)
      PRINT INFMT,XBAR,GAMMA,TOL
      READ INFMT,((VEC(J,1),VEC(J,2),J=1,MM)
      CALL SHIFT(XBAR,GAMMA,MM)
      S1 = MM
      DO 31 J = 1,MM
      VEC(J,3) = 0.0
   31 VEC(J,4) = 1.0
      BETA(1) = 0.0
      S3 = 0.0
      DO 32 L = 1,MM
   32 S3 = S3 + VEC(L,2)**2
      K2 = KK + 1
      DO 303 I = 1,K2
      S4 = 0.0
      DO 33 J = 1,MM
   33 S4 = S4 + VEC(J,2)*VEC(J,4)
      S(I) = S4/S1
      S5 = S3-S(I)**2*S1
      IF(MM-I-1)305,305,301
  301 RHOSQ(I) = S5/FLOATF(MM-I-1)
      GO TO 303
  305 RHOSQ(I) = S5
  303 K1 = I -1
      DO 34 K = 1,K1
      IF(ABSF(RHOSQ(K)-RHOSQ(I))-TOL) 71,71,34
   34 CONTINUE
      IF(I - K2)35,72,72
   35 DO 36 N = 1,MM
   36 VEC(N,5) = VEC(N,1)*VEC(N,4)
      T1 = 0.0
      DO 37 JJJ = 1,MM
```

Figure A-19

Least Squares Orthogonal Polynomial Fitting Program

```
   37 T1 = T1 + VEC(JJJ,5)*VEC(JJJ,4)
      ALP(I+1) = T1/S1
      T2 = 0.0
      DO 38 M = 1,MM
      VEC(M,5) = (VEC(M,1)-ALP(I+1))*VEC(M,4)-BETA(I)*VEC(M,3)
      T2 = T2+VEC(M,5)**2
      VEC(M,3) = VEC(M,4)
   38 VEC(M,4) = VEC(M,5)
      BETA(I+1) = T2/S1
      S3 = S5
      S1 = T2
  302 CONTINUE
   72 K3 = K2
      GO TO 40
   71 K3 = 1
   40 CALL UNSHIFT(XBAR,GAMMA,MM)
      KGL= 2
      IF(KIP) 718,718,717
  717 CALL POLM(K3,KAP)
  718 IF(NOP) 420,719,719
  719 DO 7000 J=1,MM
 7000 VEC(J,5) = VEC(J,2)
      IF(NOP)420,405,407
  407 PRINT 1001
 1001 FORMAT(1H2/50H THE ORDINATE VALUES USING THE RECURRENCE FORMULAS)
      PRINT 2
      MC = MM
      GO TO 1002
  405 CALL SHIFT(XBAR,GAMMA,MM)
      DO 406 N =1,MM
      VEC(N,2) = XP(1)
      K4 = K3 - 1
      DO 406 K=1,K4
  406 VEC(N,2) = VEC(N,2)*VEC(N,1) + XP(K+1)
      CALL UNSHIFT(XBAR,GAMMA,MM)
      IF(MM1-K4) 4760,4760,420
 4760 PRINT 5,K4
    5 FORMAT(1H2/73H THE ORDINATE VALUES AS EVALUATED BY GENERATING THE
     1POLYNOMIAL OF DEGREE I4/1H1)
      CALL MPRINT(MM,KGF)
  420 IF(KOT) 1527,1527,402
  402 READ 21,MC
      PRINT 821
  821 FORMAT(1H2/50H THE FOLLOWING ORDINATES ARE CALCULATED FOR THE NEW
     1ABSCISSAS)
      KGL = 1
      KOT = KOT - 1
      READ INPUT,(VEC(J,1),J=1,MC)
 1002 K2 = K3 - 1
      NOP = 0
      CALL SHIFT(XBAR,GAMMA,MC)
      DO 51 J = 1,MC
      VEC(J,2) = 0.0
      VEC(J,3) = 0.0
   51 VEC(J,4) = 1.0
      DO 502 I = 1,K3
      DO 52 J = 1,MC
      VEC(J,2) = VEC(J,2) + A(I)*VEC(J,4)
      IF(I -K3)503,502,502
  503 B2 = (VEC(J,1)-ALP(I+1))*VEC(J,4) - BETA(I)*VEC(J,3)
```

Figure A-20

Least Squares Orthogonal Polynomial Fitting Program

```
      VEC(J,3) = VEC(J,4)
      VEC(J,4) = P2
   52 CONTINUE
      CALL UNSHIFT(XBAR,GAMMA,MC)
      JJ2 = 1 - 1
      IF(NIP)1003,1003,1004
 1004 IF(1-KO)502,1003,502
 1003 IF(MT1-JJ2) 5436,5436,502
 5436 PRINT 643,JJ2
  643 FORMAT(////66H THE FOLLOWING VALUES WERE CALCULATED USING A POLYNO
     1MIAL OF DEGREE 14)
      GO TO (705,799), KGL
  799 CALL XPRINT(MC,KOP)
      GO TO 502
  705 PRINT 707
  707 FORMAT(/3(8X,29H ABSCISSA              ORDINATE    ))
      MC1 = MC - 2
      DO 701 K = 1,MC1,3
      L = K
  701 PRINT 23,VEC(K,1),VEC(K,2),VEC(K+1,1),VEC(K+1,2),VEC(K+2,1),
     1  VEC(K+2,2)
      IF(L+1-MC1)703,702,502
  702 PRINT 23,VEC(MC,1),VEC(MC,2)
      GO TO 502
  703 PRINT 23,VEC(MC-1,1),VEC(MC-1,2),VEC(MC,1),VEC(MC,2)
  502 CALL SHIFT(XBAR,GAMMA,MC)
 5002 CONTINUE
   23 FORMAT(3(5X,E14.4,3X,E14.4))
      IF(KOT) 1327,1327,402
  411 CONTINUE
      END
      SUBROUTINE POLK(KO,KR)
      DIMENSION COEF(100,100),ALP(101),BETA(101),S(101),XP(101),
     1 DUM(3000)
      COMMON DUM,COEF,S,ALP,BETA,XP
      DO 31 I = 1,KO
      COEF(1,1) = 1.0
   31 COEF(1,1+1) = 0.0
      DO 32 I = 2,KO
   32 COEF(1,2) = COEF(1-1,2) - ALP(1)
      DO 33 J = 3,KO
      DO 33 I = J,KO
   33 COEF(I,J) = COEF(I-1,J) - ALP(I)*COEF(I-1,J-1)  -
     1  BETA(I-1)*COEF(I-2,J-2)
      DO 34 I = 1,KO
      DO 34 J = 1,I
   34 COEF(I,J) = COEF(I,J)*S(I)
   17 FORMAT(///46H THE COEFFICIENTS FOR THE POLYNOMIAL OF DEGREE 14/(/
     1 6E20.10))
      DO 26 N = 1,KO
      MKM = N - 1
      XP(N) = 0.0
      DO 531 I=1,N
  531 XP(N) = COEF(I,I) + XP(N)
      IF(MKM) 400,350,400
  400 DO 35 J=1,MKM
      XP(N-J) = 0.0
      M = J + 1
      DO 35 I = M,N
   35 XP(N-J) = COEF(I,I-J) + XP(N-J)
```

Figure A-21

Least Squares Orthogonal Polynomial Figging Program

```
350 IF(KR) 21,26,23
 21 MN1 = N - 1                                                          177
    PRINT 17,MN1,(XP(L),L=1,N)                                           178
    GO TO 26                                                             179
 23 IF(N-KO)26,21,26                                                     180
 26 CONTINUE                                                             181
    END                                                                  182
    SUBROUTINE SHIFT(X,Y,MQ)                                             183
    DIMENSION VEC(3000,6),S(101),ALP(101),BETA(101),XP(101)              184
    COMMON VEC,S,ALP,BETA,XP                                             185
    DO 31 I=1,MQ                                                        186
 31 VEC(I,1)=(VEC(I,1)-X)/(1.0-Y)                                        187
    END                                                                  188
    SUBROUTINE UNSHIFT(X,Y,MQ)                                           189
    DIMENSION VEC(3000,6),S(101),ALP(101),BETA(101),XP(101)              190
    COMMON VEC,S,ALP,BETA,XP                                             191
    DO 31 I=1,MQ                                                        192
 31 VEC(I,1)=VEC(I,1)*(1.0-Y) + X                                        193
    END                                                                  194
    SUBROUTINE XPRINT(NUM,KOP)                                           195
    DIMENSION VEC(3000,6),S(101),ALP(101),BETA(101),XP(101)              196
    COMMON VEC,S,ALP,BETA,XP                                             197
    YSQ = 0.0                                                            198
    YMAX = 0.0                                                           199
    YBAR = 0.0                                                           200
    YAV  = 0.0                                                           201
    DO 950 J=1,NUM                                                       202
    VEC(J,6)= VEC(J,2)-VEC(J,5)                                          203
    T = ABSF(VEC(J,6))                                                   204
    YBAR = YBAR + T                                                      205
    YSQ = YSQ + T*T                                                      206
    IF(YMAX-T) 970,950,950                                               207
 970 YMAX = T                                                            208
 950 YAV = YAV + VEC(J,6)                                                209
    YBAR = YBAR/FLOATF(NUM)                                              210
    YSQ = SQRTF(YSQ/FLOATF(NUM))                                         211
    GO TO (900,902,904,905),KOP                                          212
 904 PRINT 966                                                           213
 966 FORMAT(////9X,8HORIGINAL,11X,8HCOMPUTED,10X,9HHEAT CAP./9X,         214
   111HTEMPERATURE,10X,9HHEAT CAP.,9X,11HDIFFERENCES//)
    PRINT 965,(VEC(J,1),VEC(J,2),VEC(J,6),J=1,NUM)                       217
 965 FORMAT(3(5X,E15.8))                                                 218
    GO TO 900                                                            219
 902 PRINT 964                                                           220
 964 FORMAT(////9X,8HORIGINAL,11X,8HORIGINAL,10X,9HHEAT CAP./8X,         221
   111HTEMPERATURE,9X,9HHEAT CAP.,10X,11HDIFFERENCES//)
    PRINT 965,(VEC(J,1),VEC(J,5),VEC(J,6),J=1,NUM)                       223
    GO TO 900                                                            224
 905 PRINT 962                                                           225
 962 FORMAT(////9X,8HORIGINAL,12X,8HORIGINAL,12X,8HCOMPUTED,12X,9HHEAT   226
   1CAP./8X,11HTEMPERATURE,10X,9HHEAT CAP.,11X,9HHEAT CAP.,10X,
   211HDIFFERENCES//)
    PRINT 961,(VEC(J,1),VEC(J,5),VEC(J,2),VEC(J,6),J=1,NUM)              229
 961 FORMAT(4(5X,E15.8))                                                 230
 900 PRINT 960, YAV, YBAR , YSQ , YMAX                                   231
 960 FORMAT(///53HSUM OF (COMPUTED HEAT CAP. MINUS ORIGINAL HEAT CAP.)=  232
   1 E16.8//17H ERROR NORM L1 = E16.8//17H ERROR NORM L2 = E16.8//       233
   229H ERROR NORM L-INFINITY = E16.8 )                                  234
    GO TO (1900,2000,2000,2000),KOP                                      235
1900 PRINT 4                                                             236
```

Figure A-22

Least Squares Orthogonal Polynomial Fitting Program

SE

INPUT FORMAT (2E15,8)

MM	KK	KOT	KIP	KAP	KOP	NOP	NIP	MTI
39	9	0	1	1	4	1	1	9

XBAR	GAMMA	TOL
0,00000000+000	0.00000000+000	
1,00000000-007		

THE COEFFICIENTS FOR THE POLYNOMIAL OF DEGREE 9

-1.6011888216-019	-2.3164336447-017	9.4283029833-015	1.0656786685-012	-1.5392625557-010	-1.9582990286-008
1.9628389495-006	-1.4262166950-004	7.2939790796-002	1.1736580780+002		

THE ORDINATE VALUES USING THE RECURRENCE FORMULAS

Figure A-23

Empty Calorimeter Calibration Coefficients Obtained From the Fitting Program

format (2E15.8) shown in Figure A23 illustrates that the data is read into the program in pairs. More than one pair of data can be located on each card if space permits as long as the input format is adjusted. For example, three sets of data pairs could be entered on one card if the input format uses 6F10.5.

The third input card contains a series of numbers which control operation of the program and are listed below:

MM - the number of data sets of points (an integer) right justified in Column 5.

KK - the maximum degree of fitting polynomial desired (an integer) right justified in Column 10. To assure reacting this degree, assign the value 0 to TOL later.

KOT - the number of new temperatures (an integer) after the fitting polynomial has been determined right justified in Column 15.

KIP - control parameter in Column 20 to determine whether the fitting polynomial coefficients should be computed (KIP - 1) or not computed (KIP - 0).

KAP - control parameter in Column 25 to determine (1) if all the polynomial coefficients will be printed (KAP - 1), (2) if none of the coefficients will be printed (KAP - 0), or (3) if only the highest order coefficients are to be printed (KAP - 1).

KOP - control parameter determining output of original data as indicated below:

KOP

1. (a) sum of computed and calculated heat capacity differences
   (b) error norms
2. (a) original temperatures
   (b) original heat capacities
   (c) computed minus original heat capacities
   (d) (a) and (b) as for KOP - 1
3. (a) original temperatures
   (b) original heat capacities
   (c) computed minus original heat capacities
   (d) (a) and (b) as for KOP - 1
4. (a) original temperatures
   (b) original heat capacities
   (c) computed heat capacities
   (d) computed minus original heat capacities
   (e) (a) and (b) as for KOP - 1

NOP - control parameter in Column 35

NOP

0 - new heat capacity values determined from fitting polynomial using original values

1 - original temperatures used to calculate new heat capacities using fitting equation

-1 - no heat capacities will be computed (occupies Column 34 and 35)

NIP - control parameter in Column 40

NIP

0 - printed output of each order of polynomial

1 - printed output only of highest order of polynomial

MTI - printing control parameter in column right justified in column right justified in Columns 41 - 45. Printout will occur only for degrees equal to or greater than MTI.

XBAR and GAMMA are parameters for shifting along the temperature scale according to the equation

$$T_i = (T-\overline{T})/(1-TOL) \qquad (A13)$$

T_i - is the final shifted temperature

T - is the original temperature

$\overline{T}$ - is for shifting average temperature used is a weighing function

TOL - the error tolerance (normally 10^{-7}). If the maximum degree polynomial is desired, the TOL should be 0.

If a new set of temperatures is to be read in for extrapolation or interpolation, the number of new values, right-justified in Column 5, must follow the end of the original data set.

The output of run code, input format, control parameters and orthogonal polynomial of degree nine is illustrated in Figure A23. Note that C_o is the last coefficient printed and C_9 is the first coefficient printed. The original computed and differences in heat capacities of an empty calorimeter calibration is illustrated in Figure A24. Note that the temperatures are in °C and the heat capacities are in Joules gm^{-1} $°K^{-1}$.

THE FOLLOWING VALUES WERE CALCULATED USING A POLYNOMIAL OF DEGREE 9

ORIGINAL TEMPERATURE	ORIGINAL HEAT CAP.	COMPUTED HEAT CAP.	HEAT CAP. DIFFERENCES
-1.63820859+002	8.91364760+001	8.93513262+001	2.14850202-001
-1.53726361+002	9.33972030+001	9.33186429+001	-7.85601307-002
-1.46127440+002	9.60371620+001	9.58743041+001	-1.62857931-001
-1.92344765+002	7.42462570+001	7.42456074+001	-6.49556518-004
-1.74735062+002	8.43080110+001	8.42359671+001	-7.20438547-002
-1.70204340+002	8.64714730+001	8.64674498+001	-4.02320921-003
-1.64384625+002	8.90970640+001	8.91087202+001	1.16561744-002
-1.47239102+002	9.55381370+001	9.55213355+001	-1.68014504-002
-1.41448500+002	9.71832600+001	9.72879953+001	1.04735272-001
-1.35138340+002	9.91309630+001	9.90270343+001	-1.03928698-001
-1.28526488+002	1.00581141+002	1.00671415+002	9.02741402-002
-1.22040339+002	1.02056621+002	1.02136528+002	7.97069166-002
-1.15688911+002	1.03611717+002	1.03452402+002	-1.59314644-001
-1.08465077+002	1.05019584+002	1.04831188+002	-1.88395536-001
-1.00437346+002	1.05897428+002	1.06241472+002	3.44044209-001
-9.30251630+001	1.07432577+002	1.07447917+002	1.53395738-002
-8.61196090+001	1.08420669+002	1.08499925+002	7.92558752-002
-7.96678340+001	1.09423988+002	1.09509221+002	8.52330998-002
-7.11795170+001	1.10556069+002	1.10565649+002	9.58026387-003
-6.33170660+001	1.11572217+002	1.11546100+002	-2.60367841-002
-5.66282790+001	1.12696040+002	1.12325862+002	-3.70177830-001
-2.53899010+001	1.15452354+002	1.15383510+002	-6.88437745-002
-1.66033270+001	1.15863116+002	1.16105169+002	2.42072908-001
-9.37491000+000	1.16466478+002	1.16667712+002	2.01234197-001
-2.10167200+000	1.17183128+002	1.17211864+002	2.87357159-002
3.21775300+001	1.19679174+002	1.19605739+002	-7.34353382-002
3.83203740+001	1.20123457+002	1.20011342+002	-1.12115033-001
4.46495670+001	1.20710693+002	1.20419002+002	-2.91611040-001
5.11500090+001	1.20854305+002	1.20824521+002	-2.97838654-002
5.78304050+001	1.21184500+002	1.21224200+002	3.97000890-002
6.47149670+001	1.21436499+002	1.21615376+002	1.78876584-001
7.19100070+001	1.21878695+002	1.21999970+002	1.21274617-001
7.90799930+001	1.22290659+002	1.22358966+002	6.83074109-002
8.69519170+001	1.22671976+002	1.22729337+002	5.73610198-002
9.60519280+001	1.23232873+002	1.23138852+002	-9.40210056-002
1.25439723+002	1.24789075+002	1.24624262+002	-1.64793320-001
1.44768267+002	1.25745886+002	1.25935825+002	1.89938782-001
1.54764491+002	1.26607115+002	1.26527056+002	-8.00589658-002

UM OF (COMPUTED HEAT CAP. MINUS ORIGINAL HEAT CAP.)= 5.87430191-007

ERROR NORM L1 = 1.10880864-001

ERROR NORM L2 = 1.43136282-001

ERROR NORM L-INFINITY = 3.70177830-001

Figure A-24

Comparison of Original and Simulated Empty Calorimeter Heat Capacities

An example of fitting program utilization for fitting and extrapolation of sample heat capacities is demonstrated in Figures A25, A26, A27, and A28. In this particular example, temperature-heat capacity data were fitted in one temperature region and was found to the linear. Then heat capacities were simulated at temperatures of experimentally obtained data in a lower temperature region. By doing this, the heat capacity difference, ΔCp, between experimental and computer extrapolated heat capacities could be obtained with a high degree of precision and accuracy enabling better and more confident interpretation of the experimental results.

Note that the new set of temperatures used for heat capacity simulation is preceded by the number of sets of temperatures right justified in Column 5 (Figure A25) as indicated earlier in the program description section. The original set of temperature heat capacity data in Figure A25 is the punched output obtained from the batch sample heat capacity program.

Figure A26 illustrates the fitting programs ability to determine the coefficients of fitting polynomials of various degrees. The variation of simulated heat capacity for these polynomials of different degrees can be observed by comparison of simulated heat capacities (Figures A27 and A28) enabling proper solution of the true fitting equation. As for the empty calorimeter calibration, comparison of original and simulated heat capacities is the best method for determination of the quality of fit. Note that heat capacity has been used as an ordinate in all of these examples.

```
    4 FORMAT(1H2)
      RETURN
 2000 PRINT 5
    5 FORMAT(1H1)
      END
         SCOPE
@RUN,5,5000
PCHMA-I
(E15.8,5X,E15.8)
   25    3     1     1    -1     4     1     0     1
          0.0E0                0.0E0
        1.0E-07
 1.99765867+002       9.06634497-001
 2.02848877+002       9.20815134-001
 2.06557789+002       9.42616629-001
 2.10462158+002       9.57800031-001
 2.13954120+002       9.76947866-001
 1.99180980+002       9.06444[illegible]-001
 2.02379186+002       9.22137436-001
 2.05529810+002       9.40979914-001
 2.08504832+002       9.47184779-001
 2.11581896+002       9.71018495-001
 2.14609931+002       9.76233569-001
 2.17491971+002       9.94416264-001
 2.20553544+002       9.98761299-001
 2.24009082+002       1.00367655+000
 2.28128650+002       1.03556766+000
 2.29623432+002       1.03218482+000
 2.35341429+002       1.0[illegible]+000
 2.40283935+002       1.23694411+000
 2.45036547+002       1.10216568+000
 2.51439650+002       1.12652316+000
 2.60141742+002       1.16118743+000
 2.66882224+002       1.19437430+000
 2.70695349+002       1.21439432+000
 2.74748189+002       1.23064672+000
 2.79239825+002       1.2466[illegible]+000
   22
 9.18863476+001       [illegible]
 1.03730610+002       1.0[illegible]+002
 1.14951[illegible]83+002       1.20671437+002
 1.26481752+002       1.37069803+002
 1.37315657+002       1.42751042+002
 1.48064792+002       1.5[illegible]11+002
 1.58611545+002       1.644[illegible]1+002
 1.69916003+002       1.74657[illegible]03+002
 1.78842532+002       1.82094820+002
 1.86761787+002       1.9[illegible]+002
 1.[illegible]+002       1.[illegible]+002
 1.17[illegible]+002       1.[illegible]+002
 1.[illegible]+002       1.[illegible]+002
 1.[illegible]+002       1.[illegible]+002
 1.41277603+0[illegible]       1.4[illegible]+002
 1.45435935+0[illegible]       1.[illegible]+002
 1.[illegible]+002       1.[illegible]+002
 1.[illegible]+002       1.[illegible]+002
 1.[illegible]+002       1.[illegible]+002
 1.[illegible]       1.[illegible]
 1.[illegible]       1.[illegible]
 1.[illegible]       1.[illegible]
7/87/8
```

Figure A-25

Sample Heat Capacity Punched Output as Input to Fitting Program and Extrapolation Temperatures Input.

```
PCHMA-1

 INPUT FORMAT (E15,8,5X,E15,8)

  MM    KK   KOT   KIP   KAP   KOP   NOP   NIP   MTI
   25     3     1     1    -1     4     1     0     1

 XBAR       GAMMA      TOL
 0,00000000+000        0,00000000+000
 1,00000000-007

 THE COEFFICIENTS FOR THE POLYNOMIAL OF DEGREE    0

    1,0412200000+000

 THE COEFFICIENTS FOR THE POLYNOMIAL OF DEGREE    1

    4,3382973470-003     4,8802933801-002

 THE COEFFICIENTS FOR THE POLYNOMIAL OF DEGREE    2

   -1,8108773213-005     1,2932716108-002    -9,5829606110-001

 THE COEFFICIENTS FOR THE POLYNOMIAL OF DEGREE    3

   -2,8114208836-007     1,8204403745-004    -3,4250209476-002     2,7251700807+000
 THE ORDINATE VALUES USING THE RECURRENCE FORMULAS
```

Figure A-26

Coefficients for Three Powers of the Orthogonal Fitting Polynomial.

THE FOLLOWING ORDINATES ARE CALCULATED FOR THE NEW ABSCISSAS

THE FOLLOWING VALUES WERE CALCULATED USING A POLYNOMIAL OF DEGREE 1

ABSCISSA	ORDINATE	ABSCISSA	ORDINATE	ABSCISSA	ORDINATE
2,0000+002	9,1646-001	2,0500+002	9,3815-001	2,1000+002	9,5985-001
2,1500+002	9,8154-001	2,2000+002	1,0032+000	2,2500+002	1,0249+000
2,3000+002	1,0466+000	2,3500+002	1,0683+000	2,4000+002	1,0900+000
2,4500+002	1,1117+000	2,5000+002	1,1334+000	2,5500+002	1,1551+000
2,6000+002	1,1768+000	2,6500+002	1,1985+000	2,7000+002	1,2201+000
2,7500+002	1,2418+000	2,8000+002	1,2635+000		

THE FOLLOWING VALUES WERE CALCULATED USING A POLYNOMIAL OF DEGREE 2

ABSCISSA	ORDINATE	ABSCISSA	ORDINATE	ABSCISSA	ORDINATE
2,0000+002	9,0390-001	2,0500+002	9,3189-001	2,1000+002	9,5898-001
2,1500+002	9,8516-001	2,2000+002	1,0104+000	2,2500+002	1,0348+000
2,3000+002	1,0583+000	2,3500+002	1,0808+000	2,4000+002	1,1025+000
2,4500+002	1,1232+000	2,5000+002	1,1431+000	2,5500+002	1,1620+000
2,6000+002	1,1801+000	2,6500+002	1,1972+000	2,7000+002	1,2134+000
2,7500+002	1,2287+000	2,8000+002	1,2431+000		

THE FOLLOWING VALUES WERE CALCULATED USING A POLYNOMIAL OF DEGREE 3

ABSCISSA	ORDINATE	ABSCISSA	ORDINATE	ABSCISSA	ORDINATE
2,0000+002	9,0775-001	2,0500+002	9,3220-001	2,1000+002	9,5711-001
2,1500+002	9,8227-001	2,2000+002	1,0075+000	2,2500+002	1,0325+000
2,3000+002	1,0571+000	2,3500+002	1,0811+000	2,4000+002	1,1043+000
2,4500+002	1,1266+000	2,5000+002	1,1475+000	2,5500+002	1,1671+000
2,6000+002	1,1849+000	2,6500+002	1,2010+000	2,7000+002	1,2149+000
2,7500+002	1,2266+000	2,8000+002	1,2357+000		

Figure A-27

Simulation of Heat Capacities for Extrapolated Temperatures Using the Computed Coefficients for each Polynomial.

THE FOLLOWING VALUES WERE CALCULATED USING A POLYNOMIAL OF DEGREE 2

ORIGINAL TEMPERATURE	ORIGINAL HEAT CAP.	COMPUTED HEAT CAP.	HEAT CAP. DIFFERENCES
1.99765900+002	9.09200000-001	9.02563396-001	-6.63660382-003
2.02948900+002	9.22100000-001	9.19957238-001	-2.14276176-003
2.06557800+002	9.40500000-001	9.40426149-001	-7.38506933-005
2.10462200+002	9.56700000-001	9.61435708-001	4.73570813-003
2.13954100+002	9.73000000-001	9.79757909-001	6.75790854-003
1.99181000+002	9.08500000-001	8.99224625-001	-9.27537514-003
2.02379200+002	9.22600000-001	9.17329486-001	-5.27051340-003
2.05529800+002	9.38500000-001	9.34832665-001	-3.66733473-003
2.08504600+002	9.47900000-001	9.50971961-001	3.07196111-003
2.11581900+002	9.66700000-001	9.67358938-001	6.58938152-004
2.14600900+002	9.75300000-001	9.83103230-001	7.80322979-003
2.17492000+002	9.90700000-001	9.97871095-001	7.17109513-003
2.20503500+002	1.00140000+000	1.01293207+000	1.15320732-002
2.24009100+002	1.01070000+000	1.03015040+000	1.93504026-002
2.28128700+002	1.03770000+000	1.04959813+000	1.18981322-002
2.29623400+002	1.03510000+000	1.05653860+000	2.14386029-002
2.33341400+002	1.07710000+000	1.08234264+000	5.24264461-003
2.40203900+002	1.23970000+000	1.10339269+000	-1.36007113-001
2.45036500+002	1.10150000+000	1.12338842+000	2.18884178-002
2.51439600+002	1.12800000+000	1.14863035+000	2.06303530-002
2.60141700+002	1.16300000+000	1.18015493+000	1.75549331-002
2.66862200+002	1.19390000+000	1.20339822+000	9.49821679-003
2.70695300+002	1.21280000+000	1.21559193+000	2.79192746-003
2.74748200+002	1.22970000+000	1.22797517+000	-1.72482783-003
2.79239800+002	1.24820000+000	1.24100384+000	-7.19616472-003

UM OF (COMPUTED HEAT CAP, MINUS ORIGINAL HEAT CAP,)= 3.05590220+010

ERROR NORM L1 = 1.37619636-002

ERROR NORM L2 = 2.92342693-002

ERROR NORM L+INFINITY = 1.36007113+001

Figure A-28

Comparison of Original and Heat Capacities Simulated by a Two Degree Polynomial.

However, encraty, enthalpy, entropy or some other thermodynamic function could have been substituted just as readily.

4. Empty Calorimeter, Batch Program

As for sample computation, both batch and time sharing programs were written. The batch program is listed in Figures A29, A30, and A31 and is identical to the sample program except for the differences outlined below. Note that a punched output and equip card are not among the control cards at the beginning of the program. Neither are the other statements that provide for punched output. Of course, punched output by modifying this program using the sample batch program as a model, another series of differences result from the measurement of an empty Calorimeter. That is, only overall heat capacity can be calculated. For ease of comparison, the previous empty calibration run (CPC) is simulated using the old polynomial constants. Subsequently, this value is substracted from the current value of empty Calorimeter heat capacity (CPT) to determine the degree of deviation (CPS). Note that the quantities in parenthesis are the symbols used in the program and output headings. An individual run output is shown in Figure A32. A summary of these quantities and the run initial, final and average temperature is listed at the end of individual run computation singular to the sample batch program. Input of data is illustrated by the last nine lines of Figure A31.

5. Empty Calorimeter, Time Sharing Program

This program has the combination of features just described

```
      7/8TDE,1
      JOB CARD
      7/8FTN,L,X
0001  PROGRAM MT CAL
0010  DIMENSION CRT(7,11), RI1D(7), RI2D(7),RF1D(7), RF2D(7),
    1 NSV(100), ATIC(100), ATFC(100), STAVC(100), SCPT(100), SCPC(100),
    2 SCPS(100), ABRT(100)
0020  COMMON RC, A, B, C
0030  REAL M, IC, L, LO, IH
0040  INTEGER RI1D, RI2D, RF1D, RF2D
0050  K = 0
0060  PRINT 70
0070  FORMAT (///46X,* RESISTANCE BULB CALIBRATION *//)
0080  DO 100 J = 1,11
0090  READ 95, ( CRT(I,J), I = 1,7 )
0095  FORMAT ( 7(F10.6) )
0100  CONTINUE
0110  READ 120, A, B, C
0111  READ 121, RC, RC, LO, AO
0112  READ 122, C0, C1, C2, C3
0113  READ 123, C4, C5, C6, C7
0114  READ 124, C8, C9, C10, C11
0115  READ 125, WK, XK, RAT, RB, M
0120  FORMAT ( 3(E15.8))
0121  FORMAT (4(F10.5))
0122  FORMAT ( 4(E15.8))
0123  FORMAT ( 4(E15.8))
0124  FORMAT ( 4 (E15.8))
0125  FORMAT ( 2(E15.8), F10.5,F10.2,F10.4)
0160  PRINT 170, A, B, C, RC, RC, LO, AO, C0, C1, C2, C3, C4, C5, C6,
    1 C7, C8, C9, C10, C11, WK, XK, RAT, RB, M
0170  FORMAT (13X,1HA,20X,1HB,21X,1HC,16X,2HRC,13X,2HRC,15X,
    1 2HLO,15X,2HAO//3(5X,E16.9),4(5X,F10.5)///12X,2HC0,19X,2HC1,19X,
    2 2HC2,19X,2HC3,19X,2HC4,19X,2HC5//6(5X,E16.9)///12X,2HC6,19X,
    3 2HC7,19X,2HC8,19X,2HC9,18X,3HC10,18X,3HC11//6(5X,E16.9)///12X,
    4 2HWK,19X,2HXK,16X,5HRATIO,13X,2HRB,13X,4HMASS//2(5X,E16.9),5X,
    5 F10.5,5X,F10.2,5X,F10.4///)
0230  DO 260 J = 1,11
0240  PRINT 250, ( CRT(I,J), I = 1,7 )
0250  FORMAT (1X, 7(F10.6) )
0260  CONTINUE
0290  READ 300, IRUN
0300  FORMAT ( A8)
0302  READ 303, J1
0303  FORMAT ( I3 )
0304  DO 1000 N = 1, J1
0310  K = K + 1
0316  IF ( K . GT. J1) GO TO 1100
0320  READ 330, ( RI1D(I), I = 1,7 ), CURD
0330  FORMAT (7I1, 2X, F4.1 )
0332  ABRT(K) = CURD
0335  FORMAT ( 2(F10.6) )
0337  IF ( ABRT(K) .EQ. 1.0 ) GO TO 800
0340  READ 33 , (RI2D(I), I = 1,7 )
0350  READ 33 , (RF1D(I), I = 1,7 )
0360  READ 330, (RF2D(I), I = 1,7 )
0370  READ 335, RIC, RFC
0380  READ 37 , TIME, TCI, TCF, ERI, ERF , ETC
0390  FORMAT (F10.2, 5(F10.6) )
0400  RI1 = RI2 = RF1 = RF2 = 0
```

Figure A-29

Empty Calorimeter Calibration Program.

```
0450    DO 540 I = 1,7
0460    J = R11D(I) + 1
0470    R11 = CRT(I,J) + R11
0480    J = R12D(I) + 1
0490    R12 = CRT(I,J) + R12
0500    J = RF1D(I) + 1
0510    RF1 = CRT(I,J) + RF1
0520    J = RF2D(I) + 1
0530    RF2 = CRT(I,J) + RF2
0540    CONTINUE
0550    RI = ( R11 + R12 ) * 0.5 + RIC
        RR = ( RI/ R0 ) - 1.0
0551    T = RR / A
0552    RRT = T * ( A + B * T )
0553    RRPT = A + 2.0 * B * T
0554    IF ( RR .GT. 0.0 ) GO TO 560
0555    TSQ = T * T
0556    RRT = RRT + C * ( T - 100.0 ) * T * TSQ
0557    RRPT = RRPT + C * ( 4.0 * T - 300.0 ) * TSQ
0560    TES = ( RR - RRT ) / RRPT
0561    T = T + TES
0562    IF ( TES .GE. 0.0 ) GO TO 565
0563    TES = - TES
0565    IF ( TES .LT. 5.0E-5 ) 570, 552
0570    TI = T
0580    TIK = TI + 273.16
0590    RF = ( RF1 + RF2 ) * 0.5 + RFC
        RR = ( RF/ R0 ) - 1.0
        T = RR / A
0593    RRT = T * ( A + B * T )
        RRPT = A + 2.0 * B * T
0595    IF ( RR .GT. 0.0 ) GO TO 599
        TSQ = T * T
        RRT = RRT + C * ( T - 100.0 ) * T * TSQ
        RRPT = RRPT + C * ( 4.0 * T - 300.0 ) * TSQ
0599    TES = ( RR - RRT ) / RRPT
        T = T + TES
0601    IF ( TES .GE. 0.0 ) GO TO 603
        TES = - TES
0603    IF ( TES .LT. 5.0E-5 ) 605, 593
0605    TF = T
0610    TFK = TF + 273.16
0620    TAVK = ( TIK + TFK ) * 0.5
0630    TAV = ( TI + TF ) * 0.5
640     TDELTA = ( TF - TI ) + ( DTC / 1000 )
0650    PRINT 659, IRUN, K, R11D, R12D, RIC, RF1D, RF2D, RFC, TIME, ECI,
      1 ECF, EBI, EBF, DTC, R11, R12, RI, TI, TIK, TAVK, TAV, TDELTA,
      2 RF1, RF2, RF, TF, TFK
0659    FORMAT(1H1///X,A8,I4///10X,4HR11D,14X,4HR12D,13X,3HRIC,13X,4HRF1D,
      1 14X,4HRF2D,13X,3HRFC//2(5X,7(I1,1X),4X,7(I1,1X),4X,F10.5)///
      2 10X, 4HTIME,11X,3HECI,12X,3HECF,12X,3HEBI,12X,3HEBF,12X,
      3 3HDTC//5X,F10.2,5(5X,F10.6)///10X,3HR11,12X,3HR12,13X,2HRI,12X,
      4 2HTI,12X,3HTIK,11X,4HTAVK,12X,3HTAV,12X,3HTDC//8(5X,F10.5)///
      5 10X, 3HRF1, 12X, 3HRF2, 13X, 2HRF, 12X, 2HTF, 12X, 3HTFK, //
      6 5 ( 5X, F10.5 ) /// )
0720    IC = ( ECI + ECF ) * 0.5 / RC
0730    L = LO + AC * TAVK
0740    EB = ( EBI + EBF ) *0.5
0750    EH = EB * ( L / RB + RAT )
0760    IH = IC - EB / RB
```

Figure A-30

Empty Calorimeter Calibration Program

```
0770    P = 1H * EH * TIML / 1.011
0780    PK = P / 4.184
0790    CPT = P / TDELTA
0800    CPC = C0+TAV* (C1+TAV* (C2+TAV* (C3+TAV* (C4+TAV* (C5+TAV*
     1 (C6+TAV* (C7+TAV* (C8+TAV* (C9+TAV* (C10+TAV* C11)))))))))))
0810    CPS = CPT - CPC
0870    PRINT 880, IC, L, EH, IH, P, CPT, CPC, CPS
0880    FORMAT (10X,2HIC,15X,1HL,13X,2HLH,12X,2HIH,13X,1HP,14X,3HCPT,12X,
     1 3HCPC,12X,3HCPS//5X,F10.7,5X,F10.4,5X,F10.5,5X,F10.7,
     2 4(5X,F10.5))
0882    GO TO 1000
0885    PRINT 895, K, K
0895    FORMAT (1H1/////5X,13,2(10X,33HRUN  ABORTED  OR  DATA  DISCARDED)
     1 , 16X, 13)
0902    GO TO 1080
1000    STIC(K) = TI
1010    STFC(K) = TF
1020    STAVC(K) = TAV
1030    SCPT(K) = CPT
1040    SCPC(K) = CPC
1050    SCPS(K) = CPS
1080    CONTINUE
1100    PRINT 1105 , IRUN
1105    FORMAT (1H1 /// 1X, A8 )
1107    PRINT 1110
1110    FORMAT ( /// 5X, 3HRUN, 14X, 3HTIC, 12X, 3HTFC, 12X, 4HTAVC, 12X,
     1 3HCPT, 15X, 3HCPC, 12X, 3HCPS)
1120    DO 1150 K = 1, J1
1125    IF (ABRT(K) .EQ. 1.0 ) GO TO 1144
1130    PRINT 1140 , K, STIC(K), STFC(K),STAVC(K), SCPT(K), SCPC(K),
     1 SCPS(K), K
1140    FORMAT (5X, 13, 10X, 4(F11.6, 5X), F12.8, 5X, F11.6, 5X, 13)
1142    GO TO 1150
1144    PRINT 1146, K, K
1146    FORMAT (5X, 13, 2(10X, 33HRUN  ABORTED  OR  DATA  DISCARDED),
     1 16X, 13)
1150    CONTINUE
2160    END
          SCOPE
@LOAD
@RUN,3,5000
       0.0         0.0         0.0         0.0         0.0         0.0         0.0
9.999645   0.999981   0.099999   0.01        0.001       0.0001      0.00001
19.999255  1.999948   0.199983   0.02        0.002       0.0002      0.00002
29.998660  2.999921   0.299968   0.03        0.003       0.0003      0.00003
39.998345  3.999907   0.399975   0.04        0.004       0.0004      0.00004
49.998024  4.999884   0.499984   0.05        0.005       0.0005      0.00005
59.997623  5.999859   0.599996   0.06        0.006       0.0006      0.00006
70.0       6.999833   0.700008   0.07        0.007       0.0007      0.00007
80.0       7.999803   0.800019   0.08        0.008       0.0008      0.00008
90.0       8.999794   0.900020   0.09        0.009       0.0009      0.00009
100.0      9.999755   1.000011   0.1         0.01        0.001       0.0001
  3.98545999E-3 -5.85899996E-7-4.31199999E-12
25.57180   10.00035   -1.11800   0.03565
  1.16668719E-4  7.91366798E-2 -1.97733909E-4 -5.96390617E-8
 -1.87361899E-9  5.28675478E-11-1.69696929E-13-1.61743659E-16
  1.70790559E-18-1.08689479E-21          0.0E0          0.0E0
          0.0E0          0.0E06.00176   10000.00   42.4879
5E-CORR
 70
0000000   1.0
 733975
 735012
0934155
0934063
0.0         0.0
5670.51    3.6048[illegible]  3.6048[illegible]  0.797036   0.797036   -1.532
7/87/8
```

Figure A-31

Empty Calorimeter Calibration Program

SE-CORR 46

RI1D	RI2D	RIC	RF1D	RF2D	RFC
3 0 4 6 3 6 5	3 0 3 4 8 1 7	0.00000	3 1 1 1 7 3 4	3 1 0 2 7 9 0	0.00000

TIME	ECI	ECF	EBI	EBF	DTC
4300.04	0.562698	0.562698	0.745515	0.745515	7.803000

RI1	RI2	RI	II	IIK	TAVK	TAV	TDC
30.46728	30.34680	30.40454	47.75441	320.91441	324.31001	51.15001	6.79196

RF1	RF2	RF	IF	IFK
31.14593	31.02654	31.08626	54.54561	327.70561

IC	L	EH	IH	P	CPT	CPC	CPS
0.0562678	10.4437	4.47514	0.0501933	820.84028	120.85430	120.19340	0.66090

Figure A-32

Individual Run Printout for Empty Calorimeter Calibration

for the batch empty program and those described earlier for the sample time sharing program. Consequently, program usage input and output formats should be understandable without further description. However, listing of this program (Figures A33, A34, and A35) is included to facilitate user understanding.

```
FETCH BEATTY3
SR. DATE FILED:  03/29/72.

LIST
0001   PROGRAM FT CAP
0010   DIMENSION CRT(7,11), RI1D(7), RI2D(7), RF1D(7), RF2D(7),
0011A ASW(100),STIF(100),STFF(100),STAR(100),SORT(100),SORF(100),
0012A SORT(100), SORZ(100)
0020   COMMON R0, A, B, C
0030   REAL R,IC,L,LO,IR
0040   INTEGER RI1D, RI2D, RF1D, RF2D
0045   CALL FILES ( 1, 0, 0.,0.,0.,0.,0.,0.,0.)
0050   K = 0
0053A
0080   DO 100 J = 1, 11
0090   READ, ( CRT(I,J), I = 1,7 )
0100   CONTINUE
0110   READ, A, B, C, R0, RC, LO, AO, CO, C1, C2, C3, C4, C5, C6,
0111A C7,C8,C9,C10,C11,WR,XK,RAT,RB,R
0112   PRINT 113
0113   FORMAT ( /// *FOR PERMANENT RUN DATA ENTER 1* /
0114A *FOR INDIVIDUAL RUNS ENTER 2* )
0115   INPUT, NPERM
0116   GO TO ( 120, 320 ), NPERM
0120   PRINT 125
0125   FORMAT ( /// 15X, *RESISTANCE BULB THERMOMETER CALIBRATION*//)
0160   PRINT 170, A , B,C,R0,RC,LO,AO,CO,C1,C2,C3,C4,C5,C6,
0161A C7, C8, C9, C10, C11, WR, XR, RAT, RB, R
0170   FORMAT (9X,1HA,17X,1HB,17X,1HC / 3(1X,E16.8,1X) //
0171A 7X, 2HR0,9X, 2HRC, 9X, 2HLO, 9X, 2HAO / 4(1X,E16.8,1X) //
0172A 8X, 2HC0, 16X, 2HC1, 16X, 2HC2, 16X, 2HC3 / 4(1X,E1 . ,1X)
0173A 8X, 2HC4, 16X, 2HC5,  ,2HC6, 16X, 2HC7 / 4(1X,E16.8,1X) //
0174A 8X, 2HC8, 16X, 2HC9, 15X, 2HC10, 15X, 2HC11 / 4(1X,E16.8,1X) //
0175A 8X, 2HWR, 16X, 2HXR, 13X, 5HRATIO, 9X, 2HRB, 9X, 4HMASS /
0176A 2(1X,E16.8,1X), 1X, F10.5, 2X, F10.2, 2X, F10.4 )
0190   PRINT 200
0200   FORMAT ( * IF YOU WANT A LISTING OF THE CRT TABLE ENTER 1 * /
0201A * OTHERWISE ENTER 2 * )
0210   INPUT, NGO
0220   GO TO (230,280), NGO
0230   DO 260 J = 1,11
0240   PRINT 250, ( CRT(I,J), I = 1,7 )
0250  FORMAT (1X,7(F10.6) )
0260   CONTINUE
0280   PRINT 290
0290   FORMAT ( * TO INPUT RUN ENTER 1, OTHERWISE 2 * )
0300   INPUT, NGO
0310   GO TO (320, 1000), NGO
0320   PRINT 330
0330   FORMAT ( * INPUT RUN NAME ( 6 CHARACTERS OR LESS ) IN QUOTES * )
0340   INPUT, NRUN
0350   RI1 = RI2 = RF1 = RF2 = 0
0360   PRINT 370
0370   FORMAT ( ///* INPUT RI1D(1) THRU RI1D(7) * /
0371A *          RI2D(1) THRU RI2D(7) * / *         AND RIC * )
0380   INPUT, RI1D, RI2D, RIC
0390   PRINT 400
0400   FORMAT (./  * INPUT RF1D(1) THRU RI1D(7) * /
0401A *          RF2D(1) THRU RF2D(7) * / *         AND RFC * )
0410   INPUT, RF1D, RF2D, RFC
0420   PRINT 430
0430   FORMAT ( * INPUT TIME, ECI, ECF, EBI, EBF, AND DTC * )
0440   INPUT, TIME, ECI, ECF, EBI, EBF, DTC
0450   DO 540 I = 1,7
0460   J = RI1D(I) + 1
0470   RI1 = CRT(I,J) + RI1
0480   J = RI2D(I) + 1
0490   RI2 = CRT(I,J) + RI2
0500   J = RF1D(I) + 1
0510   RF1 = CRT(I,J) + RF1
0520   J = RF2D(I) + 1
0530   RF2 = CRT(I,J) + RF2
0540   CONTINUE
```

Figure A-33

Empty Calorimeter Time-Sharing Program

```
0550   A1 = ( A11 + A12 ) * 0.5 + A1C
0551   AA1 = AAPT = TES = 0.0
0552   AA = ( A1 / A0 ) - 1.0
0553   T = AA / A
0554   AAT = T * ( A + B * T )
0555   AAPT = A + 2.0 * B * T
0556   IF ( AA .GT. 0.0 ) GO TO 560
0557   TSQ = T * T
0558   AAT = AA1 + C * (T-100.0) * T * TSQ
0559   AAPT = AAPT + C* ( 4.0 * T - 300.0 ) * TSQ
0560   TES = ( AA - AA1 ) / AAPT
0561   T = T + TES
0562   IF ( TES .GE. 0.0 ) GO TO 564
0563   TES = - TES
0564   IF ( TES .LT. 5.0E-5 ) 570, 554
0570   T1 = T
0580   T1K = T1 + 273.16
0590   AF = ( AF1 + AF2 ) * 0.5 + AFC
0591   AA1 = AAP1 = TES = 0.0
0592   AA = ( AF / A0 ) - 1.0
0593   T = AA / A
0594   AA1 = T * ( A + B * T )
0595   AAPT = A + 2.0 * B * T
0596   IF ( AA .GT. 0.0 ) GO TO 600
0597   TSQ = T*T
0598   AA1 = AA1 + C * (T-100.0) * T * TSQ
0599   AAPT = AAPT + C * ( 4.0 * T - 300.0 ) * TSQ
0600   TES = ( AA - AA1 ) / AAPT
0601   T = T + TES
0602   IF ( TES .GE. 0.0 ) GO TO 604
0603   TES = - TES
0604   IF ( TES .LT. 5.0E-5 ) 605, 594
0605   TF = T
0610   TFK = TF + 273.16
0620   TAVK = ( T1K + TFK ) * 0.5
0630   TAV = ( T1 + TF ) * 0.5
0640   TDELTA = ( TF - T1 ) + DTC
0650   PRINT 659, NRUN, A11D, A12D, A1C, AF1D, AF2D, AFC, TIME, ECI,
0651A ECF, EBI, EBF, DTC, A11, A12, A1, T1, T1K, AF1, AF2, AF, TF, TFK,
0652A TAVK, TAV, TDELTA
0659   FORMAT ( /// 1X, A8 // 6X, 4HA11D, 15X, 4HA12D, 15X, 3HA1C /
0660A 1X, 2(7I2,5X), F10.5 // 6X, 4HAF1D, 15X, 4HAF2D, 15X, 3HAFC /
0661A 1X, 2(7I2,5X), F10.5 // 5X, 4HTIME, 9X, 3HECI, 9X, 3HECF,
0662A 9X, 3HEBI, 9X, 3HEBF, 9X, 3HDTC / 1X, F10.2, 4(2X,F10.6), 2X,
0663A F10.5 // 5X, 3HA11, 9X, 3HA12, 9X, 2HA1, 10X, 2HT1, 10X, 3HT1K/
0664A 3(1X,F10.5,1X,), 2(1X,F10.4,1X)  // 5X, 3HAF1, 9X, 3HAF2, 9X,
0665A 2HAF, 10X, 2HTF, 10X, 3HTFK / 3(1X,F10.5,1X), 2(1X,F10.4,1X)  //
0666A 6X, 4HTAVK, 9X, 3HTAV, 9X, 3HTDC/ 3(1X,F10.4, 1X) )
0680   IF ( TDELTA .EQ. 0.0 ) 690, 720
0690   PRINT 700
0700   FORMAT ( 1X, 10(1H*), * TDELTA = 0.0, RUN IGNORED *, 10(1H*) )
0710   GO TO 280
0720   IC = ( ECI + ECF ) * 0.5 / AC
0730   L = L0 + A0 * TAVK
0740   EB = ( EBI + EBF ) * 0.5
0750   EH = EB * ( L / RB + RAT )
0760   IH = IC - EB / RB
0770   P = IH * EH * TIME
0780   PK = P / 4.184
0790   CPI = P / TDELTA
0800   CPC = C0+TAV* (C1+TAV* (C2+TAV* (C3+TAV*
0801A (C4+TAV* (C5+TAV* (C6+TAV* (C7+TAV* (C8+TAV* (C9+TAV*
0802A (C10+TAV* C11))))))))))
0810   CPS = CPI - CPC
0870   PRINT 880, IC, L, EH, IH, P, CPI, CPC, CPS
0871A
0880   FORMAT ( / 7X, 2HIC, 9X, 1HL, 12X, 2HEH, 8X, 2HIH /
0881A 1X, F10.7, 2X, F10.4, 2X, F10.5, 2X,F10.7 // 6X, 1HP, 10X,
0882A 3HCPI, 9X, 3HCPC, 9X, 3HCPS / 4( 1X, F10.5,1X) // )
0883A
```

Figure A-34

Empty Calorimeter Time-Sharing Program

```
0884A
0900   K = K + 1
0910   NSV(K) = NRUN
0912   STDELTA(K) = TDELTA
0913   IF (STDELTA(K) .EQ. 0.0 ) 914, 920
0914   PRINT 916
0916   FORMAT (' 1K, 10(1H*), * RUN ABORTED OR DAT DISCARDED*, 10(1H*))
0918   GO TO 280
0920   STIK(K) = TIK
0930   STFK(K) = TFK
0940   STAVK(K) = TAVK
0950   SCPT(K) = CPT
0960   SCPC(K) = CPC
0970   SCPS(K) = CPS
0990   GO TO 280
1000   STOP
1010   END
2000   SUBROUTINE TSECT ( R, T )
2010   COMMON R0, A, B, C
2020   RR = ( R / R0 ) - 1.0
2030   T = RR / A
2040   RRT = T * ( A + B * T )
2050   RRPT = A + 2.0 * B* T
2060   IF ( RR .GT. 0.0 ) GO TO 2100
2070   TSQ = T * T
2080   RRT = RRT + C * ( T - 100.0 ) * T * TSQ
2090   RRPT = RRPT + C * ( 4.0 * T - 300.0 ) * TSQ
2100   TES = ( RR - RRT ) / RRPT
2110   T = T + TES
2120   IF ( TES .GE. 0.0 ) GO TO 2140
2130   TES = - TES
2140   IF ( TES .LT. 5.0E-5 ) 2150, 2040
2150   RETURN
2160   END
2170   ENDPROG
3001   0.0 0.0 0.0 0.0 0.0 0.0 0.0
3002   9.999645 0.999981 0.099999 1.0E-02 1.0E-03 1.0E-04 1.0E-05
3003   19.999255 1.999948 0.199983 2.0E-02 2.0E-03 2.0E-04 2.0E-05
3004   29.998660 2.999921 0.299968 3.0E-02 3.0E-03 3.0E-04 3.0E-05
3005   39.998345 3.999907 0.399975 4.0E-02 4.0E-03 4.0E-04 4.0E-05
3006   49.998024 4.999884 0.499984 5.0E-02 5.0E-03 5.0E-04 5.0E-05
3007   59.997623 5.999855 0.599996 6.0E-02 6.0E-03 6.0E-04 6.0E-05
3008   70.000000 6.999833 0.700008 7.0E-02 7.0E-03 7.0E-04 7.0E-05
3009   80.000000 7.999803 0.800019 8.0E-02 8.0E-03 8.0E-04 8.0E-05
3010   90.000000 8.999794 0.900020 9.0E-02 9.0E-03 9.0E-04 9.0E-05
3011   100.00000 9.999755 1.000011 1.0E-03 1.0E-04 1.0E-05 1.0E-06
4001   3.98545999E-3 -5.85899998E-7 -4.31199999E-12 25.57180
4002   10.00035 -1.1180 0.03565 1.16668719E2 7.91368798E-2
4003   -1.97739909E-4 -5.97390819E-8 -1.87361899E-9
4004   5.23675478E-11 -1.89896929E-13 -1.81743859E-16
4005   1.70790559E-18 -1.8868947E-21 0.0E0 0.0E0 0.0E0 0.0E0
4006   6.00170 10000.0 30.6370
```

Figure A-35

Empty Time-Sharing Program